FREEWAY TRAFFIC STATE DETECTION USING CCTV STATIONARY IMAGES

By

Kaixin Yang

A dissertation submitted in partial fulfillment of

the requirements for the degree of

Doctor of Philosophy

(Civil and Environmental Engineering)

at the

UNIVERSITY OF WISCONSIN-MADISON

2012

Date of final oral examination: 05/30/12

The dissertation is approved by the following members of the Final Oral Committee:

Bin Ran, Professor, Civil and Environmental Engineering
Jeffrey Russell, Professor, Civil and Environmental Engineering
David Noyce, Professor, Civil and Environmental Engineering
Chin Wu, Professor, Civil and Environmental Engineering
Zhiguang Qian, Assistant Professor, Statistics

ABSTRACT

Freeway Traffic State Detection Using CCTV Stationary Images

Kaixin Yang

Under the supervision of Professor Bin Ran

At the University of Wisconsin-Madison

Traffic detection and data collection are essential to transportation planning and management. The CCTV (Closed Circuit Television) traffic cameras have been increasingly deployed for traffic surveillance on major roadways by DOT (Department of Transportation) in the U.S. However, the real-time traffic video data is still very limited to be published online because of the large load to the video servers and internet connections. As a result, the traffic snapshots which are clipped from the video data are widely used as an effective approach to publish the real-time traffic conditions through internet. Currently, almost all U.S. states can provide traffic snapshots via DOT or traveler information websites (511 System).

These traffic snapshots are published and updated every 1 minute to 5 minutes in different states. They are potential new traffic data source that can be obtained free from internet without additional equipment and instruction cost. They can provide valuable traffic information to analyze traffic flow patterns and congestion status, where no other detectors are available. How to utilize these online CCTV snapshots effectively for traffic detection and

data collection would be of practical significance. In this research, a novel traffic state detection model is developed, which could contribute to both academic and industry fields. The primary contribution of this study is to provide an effective solution to detect the traffic state using the CCTV stationary images. Traffic space occupancy is used as a reliable measure for quantitative traffic analysis and congestion estimation. The practical value of the proposed approach is that it turns widely freely available video source from internet into useful traffic information, and this could be done without interfering the existing CCTV system in DOT.

The traffic image data used in this study were collected from I-894 freeway corridor in Milwaukee, Wisconsin. I proposed a model to measure the traffic space occupancy, which could not be measured directly in the field. In addition, a perspective transformation method is provided to estimate the traffic parameters without accurate camera calibration. The proposed algorithms and image processing were implemented in MATLAB. The model validation is performed with field loop detector data collected from the same roadway segments. The model performance was evaluated under different traffic status, illumination conditions, and roadway geometry. The validation and evaluation results indicate that the proposed model has a robust detecting capability for traffic status.

Thesis Supervisor: Professor Bin Ran

ACKNOWLEDGEMENTS

At the moment of accomplishment of my Ph.D. research, I would like to thank all those people who made this possible and an unforgettable experience for me. First and foremost I wish to thank my advisor, Professor Bin Ran. I appreciate all his contributions of time, support and encouragement during tough times in my Ph.D. pursuit. This work would not be completed without his guidance throughout the years. I would like to express my gratitude to my thesis committee, Dr. David Noyce, Dr. Jeffrey Russell, Dr. Chin Wu and Dr. Zhiguang Qian. Their constructive advices, criticisms and reviews are of great value not only to this study but also to my future work.

It is a pleasant to express my thanks to my friends and Tops lab members who contribute in many ways to the success of this work. My time at Madison was enriched by their friendship as well as collaboration and advice. I would cherish the time spent with them as good memories and a part of my life. I am especially grateful to Dr. Jing Jin and Dr. Steven Parker for their inspirations and suggestion.

There are no words that can express my gratitude and regards to my family. I would like to dedicate this dissertation to my mom and brother. Thank you for your encouragement and unconditional love that carry me through always. I could not have completed this journey and lifted up without you by my side. This dissertation is the end of a long journey in pursuing my Ph.D. It is also the start to a new future and my academic career.

TABLE OF CONTENTS

LIST OF FIGURES

LIST OF TABLES

CHAPTER 1 INTRODUCTION

1.1 Background

Traffic detection and data collection are essential to transportation planning and management. Intelligent Transportation System (ITS) has been considered as an effective technology to solve the traffic problems and improve the safety. ITS technologies have been introduced since early 1990's by integrating advanced information technologies, communications, electronics, and management strategies. It includes Advanced Traveler Information System (ATIS), Advanced Traffic Management System (ATMS), Advanced Public Transportation System (APTS), and Advanced Vehicle and Highway System (AVHS). The ATIS and ATMS technologies attempt to improve mobility by implementing traffic management and traveler guidance strategies using data collected through advanced traffic surveillance and vehicle detection technologies.

A recent progress in ATMS is the deployment of the 511 travel information systems in Department of Transportation (DOTs) in the United States. The 511 system utilizes information and communications technologies to collect, process, and publish real time traffic condition to travelers. It assists travelers with pre-trip and en route driving information to improve the convenience, safety and efficiency of a travel. The 511 system has been implemented via telephone, radio, internet, and mobile services throughout the U.S.

The Closed-Circuit Television (CCTV) traffic system plays an important role in traffic

surveillance, operation and management, from the traditional manual monitoring to prevailing video-based traffic detection. The camera can cover a wider area than other traffic detectors, and is less intrusive and cost to install. However, a critical issue with the CCTV system is that it is still limited to publish the live video data through internet due to the bandwidth and communication capacity. It also requires huge storage to archive historical video data for a long duration. As a result, although video data contains significant amount of visual information regarding traffic conditions, they are only kept at Traffic Management Centers for a short period of time (e.g. 3 days in Wisconsin) unless specially requested. Meanwhile, only low-frequency video snapshots are available to the public through DOT/511 websites.

Figure 1.1 shows 511 Deployment in U.S. and camera distributions in some states and cities. For now, there are more than 35 states have deployed 511 service. The stationary traffic images of major highway segments and intersections could be published and updated every 1 to 5 minutes through 511 website. Most of other states without 511 systems also provide the traffic still images via DOT website. Currently, only few states do not have such traffic information service online or under construction (Arkansas, Hawaii, Illinois, North Carolina and South Dakota). Table A-1 in appendix summarizes the traffic online cameras information including the camera number statewide, update time and websites to public in most U.S. states.

Comparing with traffic video data, the stationary images could be stored for a long time to study historical traffic flow pattern. From a practical perspective, the existing numerous

CCTV stationary images in Departments of transportation agencies could be a new data source for traffic quantitative analysis, operation and management. In this research, I will utilize the CCTV snapshots published on DOT/511 websites to detect traffic status and congestion information.

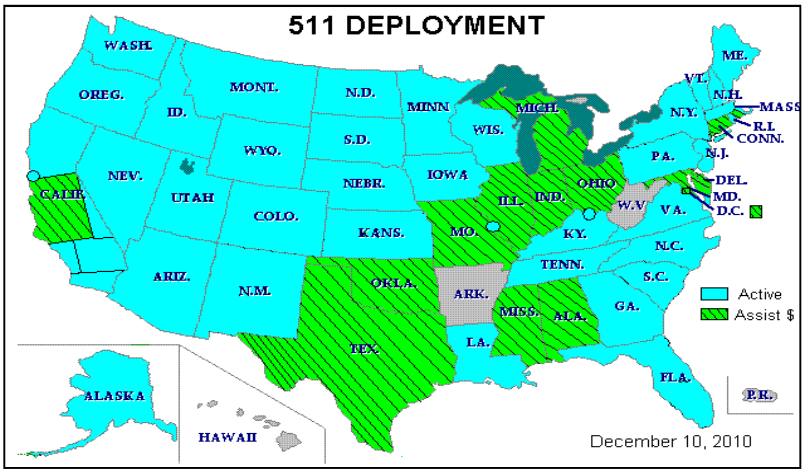

(Source: http://www.deploy511.org/deployment-stats.html)

Wisconsin

Virginia

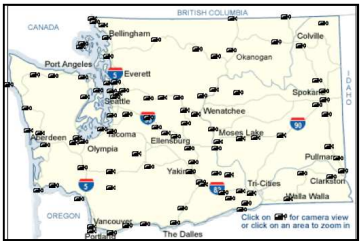

Washington

Minneapolis, MN

New York, NY

Phoenix, AZ

Figure 1.1 511 System Deployment in U.S

1.2 Problem Statement

CCTV (Closed Circuit Television) traffic cameras have been increasingly deployed for traffic surveillance on major roadways by DOT (Department of Transportation) in U.S. They are the most popular form of traffic monitor and record massive traffic video data every day. Figure 1.2 shows a typical video-based traffic monitor and control center. To reduce the human burden of watching numerous monitors, many commercial video-based traffic detection systems are available. However, in the practical application, DOT only use CCTV video for traffic surveillance not for traffic detection (traffic volume, speed, occupancy). Since video-based traffic detection system needs higher requirement for camera resolution (720p or 1080p) and installation, which are very expensive in both equipment and maintenance costs comparing with the already installed CCTV cameras. Generally, the resolution of existing CCTV video data is only 352*260 pixels.

Figure 1.2 A Typical Video-based Traffic Monitor and Control Center

On the other hand, the commercial systems require camera calibration when to detect the traffic flow parameters. Camera calibration is the process to obtain the camera focal length,

installation height, and tilt angles through field data measurement. Most of the Traffic Management Center (TMC) uses the video data to monitor the traffic congestion and incident. The CCTV cameras can be adjusted to different angle, zoom in and zoom out if any traffic incidents occurred. While video-based detection system requires camera calibration and fixed position.

Another difficulty is that the demand for storage capacity to support video surveillance applications is huge. CCTV traffic cameras generate millions of hours of traffic video every day world-wide. Unless special request, such precious video data will be deleted from the video buffer maintained at Traffic Management Centers due to the huge size. Meanwhile, the real-time video stream is still very limited to be published online due to the large load to the video servers and internet connections. As a result, low-frequency traffic snapshots have been widely used as an effective approach to publish traffic conditions through DOT or 511 traveler information websites.

The traffic snapshots are published and updated every 1 minute to 5 minutes in different states. They are potential new traffic data source if traffic information can be obtained from these snapshots. Most of the current traffic detectors are only installed on major freeway, no traffic data available on most arterials and local streets. These traffic snapshots distribute broadly on major freeways, arterials and local roadways. They are clipped from existing CCTV video data, can be obtained free from internet without additional equipment and instruction cost. They can provide valuable traffic information to analyze traffic flow patterns and congestion

status where no other detectors available. If existing traffic detecting system has quality issues (e.g. sensitivity issues, calibration, communication, electronic breakdown and etc.), they could be compensation and provide information to validate the detectors with problem. Moreover, these traffic snapshots can be stored for a long time for historical traffic analysis and incidents reconstruction evidence. If properly labeled (e.g. incident, congestion, and etc.), they can even be used to index and identify video data of interests.

Table 1.1 Video vs. Stationary Image based Traffic Detection

	Video Based	Stationary Image Based
Storage	Could not be stored for long term due to the huge size	Can be stored for a long time
Published via internet	Limited to be published due to the upload & bandwidth limitations	Can be updated every 1 or 3 minutes
Computer system	Requires powerful video data processing capability	Lower
Camera Calibration	Requires camera calibration and needs recalibration if moved	No need
Camera installation	Higher requirements for install height, angle & stability	Utilize existing CCTV camera
Detected traffic variables	Traffic volume, speed and occupancy	Traffic occupancy

How to utilize these online CCTV snapshots effectively for traffic detection and data collection would be practical significance. Table 1.1 summarizes the characteristics of video and stationary image based traffic detection. Traffic video data are essentially image sequence with high temporal frequency, e.g. 20 frames per sec. Intensive temporal information can be

derived from such high-frequency image sequence which significantly facilitates the detection of moving objects. Such temporal information is not available for traffic images, e.g. 1-5 min snapshots commonly available from DOT/511 websites. Therefore, the traffic snapshots clipped from the CCTV video data are stationary traffic images with relative low frequency and low resolution. Processing these stationary images is difficult to use the existing video-based traffic detection methods.

1.3 Research Objectives and Scope of Work

The primary objective of this research is to develop a traffic state detection model using the stationary traffic images obtained from internet. To achieve this, a new approach is proposed combining multi-segmentation and feature extraction for vehicle detection. The traffic space occupancy is calculated as the measure to estimate the traffic status. The traffic image data used in this study were captured from I894 freeway in Milwaukee, Wisconsin. The model calibration and validation are performed using loop detector data collected from the same roadway segments. The research scope and assumptions are as follows:

- Focus on the freeway mainline segment, later may extend to arterial
- Work on daytime images, later may extend to night time data
- Assume no system or communication error with CCTV
- Assume fixed camera position and angle with respect to the road, no vertical deviation, no zoom in or rotation for traffic incidents monitor.

1.4 Contributions of the Research

In this research, a novel traffic state detection model is developed, which could contribute to both academic and industry fields. The primary contribution of this study is to provide an effective solution to detect the traffic state using the CCTV stationary images. Traffic space occupancy is used as a reliable measure for quantitative traffic analysis and congestion estimation. The practical value of the proposed approach is that it turns widely freely available video source from internet into useful traffic information, and this could be done without interfering the existing CCTV system in DOT.

The specific contributions of this research are as follows:

- Propose a novel traffic state detection model to estimate the traffic occupancy using CCTV traffic images.
- Develop a new image processing algorithm combining multi-segmentation and feature extraction to conduct vehicle detection from the CCTV images.
- Instead of using field data to perform camera calibration, a projection transformation method is applied to calculate the traffic parameter while the camera parameters are not available.
- Provide an approach to measure space occupancy through the stationary images which is difficult to measure directly in the field.

1.5 Organization of the Thesis

The flowchart of this research work is illustrated in Figure 1.3. In Chapter 1, I introduce the research background, problems, research scope and contribution. Chapter 2 will conducts literature review including the previous studies using traffic video stream data to detect the traffic flow information. The generic image segmentation methods are also reviewed in this section, especially the algorithms for roadway and object detection.

In Chapter 3, I propose a traffic state detection model and the image processing algorithms. The model is consisted of three major modules, roadway detection module, vehicle extraction module and projection transformation module. The traffic space occupancy is calculated based on the roadway length and total vehicle length extracted from the image. Then, the traffic state and congestion information could be estimated.

I present the experimental design and model validation in Chapter 4. The traffic data acquisition, model calibration and validation are described in detail in this section. The experimental data is collected from Lincoln avenue segment on I-894 freeway corridor in Milwaukee, WI. The experiment results will be analyzed and compared with loop detector data obtained from the same roadway locations, In Chapter 5, more image data collected from other four sites on I-894 freeway will be processed, to evaluate the performance and effectiveness of the proposed model. Chapter 6 is the conclusion section to summarize this research and offer suggestions to the future work.

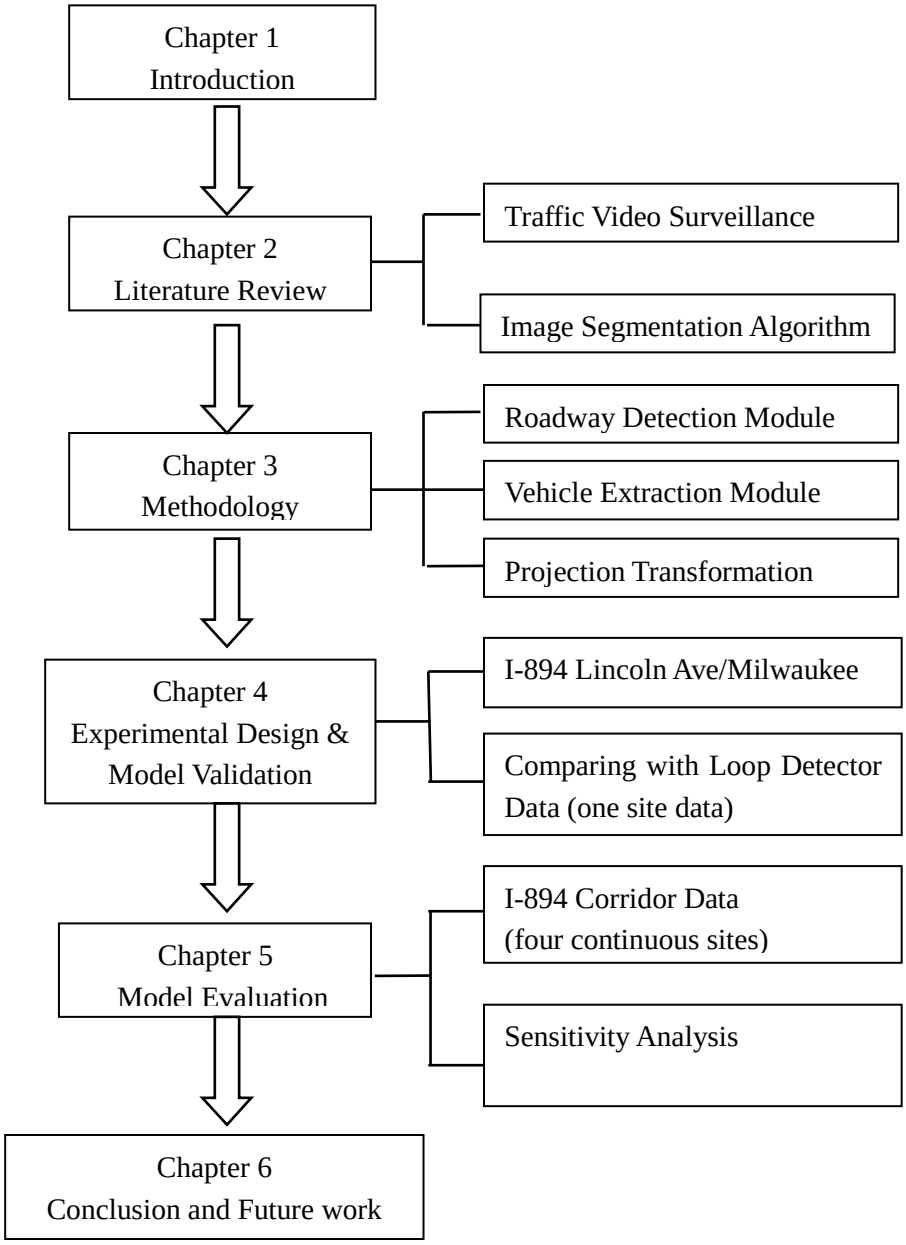

Figure 1.3 Flowchart of the Dissertation Research

CHAPTER 2 LITERATURE REVIEW

2.1 Overview of Video-Based Traffic State Detection

Increasing number of vehicles would enter the existing transportation network annually, and the new road construction could not keep up with the growth of the traffic demand. Therefore, the effectiveness of traffic operation and management are becoming more crucial. The key to better traffic management is access to real time traffic data, and the capability for quick response and processing of these data for traffic analysis and operation. Hence, the new traffic sensors that can provide large volumes of real-time data are steadily growing. Currently, loop detectors produce the largest amount of traffic data. Although, this detector technology is well established, the installation and maintenance are not simple, and the associated cost can be very high. Recently, more and more video-based systems (CCTV) have been introduced. These pole or bridge mounted camera sensors have shown significant performance. The trend of switching toward imaging technologies is expected to increase.

Comparing with current available traffic detection techniques, such as the inductive loop detector, infrared (IR), lasers, radar, ultrasonic sensors etc, vision-based traffic detection offer more advantages over other devices (Table 2.1). Since 1990s, traffic video surveillance system has been widely deployed by DOT to monitor the traffic status and incidents, due to its visual information, low maintenance costs and little impact to the road infrastructure. Various video-based traffic detection methods have been proposed and advanced significantly in both research and technology fields.

Table 2.1 Advantage &disadvantage of current traffic detectors

Detector	Advantages	Disadvantages
Loop detector	• Mature technology & standard electronics units • Excellent counting accuracy	• Require lane closure for installation and maintenance • Decrease road life • Susceptible to damage by heavy vehicles, road repair and utilities
Radar	• Good performance in inclement weather	• Cannot detect stopped or very slow moving vehicles
Infrared	• Collect traffic data during day and night	• Performance degradation under diverse weather condition like heavy rain, fog or snow • Maintenance require lane closure
Commercial video system	• Single camera and processor can cover multiple lanes • Visual traffic information • Low maintenance costs and little impact to the road infrastructure	• Occlusion & shadows affect the detection accuracy • Require stable camera installation and calibration

The video-based traffic detection uses video stream data to extract the traffic information of freeway and major intersection. Vehicles are detected and tracked via video image processing, which can yield traditional traffic variables such as traffic flow, speed and occupancy. The key algorithms for background subtraction, vehicle detection and tracking have been introduced, improved, and tested by several studies (Koller, D., 1993, Klausmann, P. et al., 1999, Badenas, J. M. & Bober, F. Pla, 2001, Bose B. & Grimson, E., 2004, Gupte, S. et al, 2004, O'Kelly, et al., 2005, Kanhere, N.K and Birchfield, S.T., 2008). Common video-based traffic detection model includes three major modules: background generation, vehicle tracking and camera calibration.

At the industry side, a number of commercial systems have been developed and implemented for traffic surveillance and detection, such as AUTOSCOPE, CCATS, TAS, TraCam, CCATS, and IMPACTS etc. (Kastrinaki, V., 2003). However, even a number of commercial systems for traffic detection have existed, many requirements still cannot be met. Such as operation in real-time, function under a wide range of traffic conditions, weather, illumination and traffic congestion. These issues will result in the change of the background condition, and further, limit the vehicle detection result (Coifman, B. et al., 1998). In addition, most of the commercial system are expensive (hardware & software) and require high angle camera installation and large store devices.

2.1.1 Background Generation

For video-based traffic detection, the cameras are static and installed above the ground to obtain the traffic video data. The detection principle is essentially based on the fact that the vehicles to be detected are the in motion among the video sequences. Therefore, if the background could be generated and compared with current frame, the moving vehicles could be extracted. Traditional background generation approach includes frame averaging algorithm and background frame differencing method.

2.1.1.1 Frame Averaging Method

The frame averaging algorithm is based on the statistical information of pixel value to generate a background image, and then use it to separate the moving vehicles from the

background. The background image is specified either manually by selecting an image without vehicles, or is detected in real-time by forming a mathematical average of successive images. The detection is then achieved by means of subtracting the reference image from the current image. Threshold is usually performed in order to obtain presence/absence information of vehicle motion.

Zhang, G. et al. (2007) proposed a traffic detection and classification system which constructs a background image using the median value of each pixel from the video frames. The color values of the pixel at (i, j) in the extracted background image BG_{ij} can be obtained as follows:

$$BG_{ij} = \begin{cases} R_{bg} = \text{median}\ \{R_1, R_2, \ldots R_t\} \\ G_{bg} = \text{median}\ \{G_1, G_2, \ldots G_t\} \\ B_{bg} = \text{median}\ \{B_1, B_2, \ldots B_t\} \end{cases} \quad (2.1)$$

Where,

R_{bg}, G_{bg}, B_{bg} represent the red, green and blue channel of the background image in the RGB color space.

$R_1, R_2, \ldots R_t$ is the red channel value of the pixel (i, j) in the frame sequence from the 1^{th} frame to the t^{th} frame, similar to the green channel G_i, and blue channel B_i.

This method often combines with other vehicle tracking approach to extract the traffic parameters. A virtual loop detector was applied by Zhang, G., et al. (2007), which comprises three parts, a registration line, a detection line and a longitudinal line. The virtual loop

detector is analogous to the loop detector that it records the vehicles passing through it. The vehicle length could be calculated along the longitudinal line that is occupied by the vehicle region. The performance results show that the overall accuracy for vehicle count is 97.73%, and the truck count accuracy is 91.53%.

Pumrin, S. (2002) provided a traffic detection approach applying background extraction using median value of each pixel from 100 image sequence. Then recognize the moving blobs and their centroids to estimate the mean speed followed by Sobel edge detector.

2.1.1.2 Background Frame Differencing Method

The background frame differencing method generates a background image from the successive video frames. The differences between two successive frames are computed pixel-by pixel to detect motionless objects in the video frames.

$$BG_i(x, y) = \begin{cases} 0 & if \quad |f_{i+1}(x, y) - f_i(x, y)| > T \\ f_{i+1}(x, y) & if \quad |f_{i+1}(x, y) - f_i(x, y)| <= T \end{cases} \tag{2.2}$$

$$\mathrm{BG}(x, y) = \frac{1}{m(x, y)} \sum_{i=1}^{n} \mathrm{BG}_i(x, y) \tag{2.3}$$

Where,

$f_i(x, y)$: the intensity at pixel (x,y) in the i^{th} video frame

$BG_i(x, y)$: i= 1,2 …n, background sequence at pixel (x, y)

T: threshold

BG (x, y): final background image

m (x, y): number of $BG_i(x, y)$ is not zero at pixel (x, y)

Fathy, M. & Siyal, M.Y. (1995) used the background differencing and morphological edge detection technique for real-time traffic analysis. In Woochul Lee's work (2006), he applied the background frame differencing method followed by vehicle tracking through a virtual detection line to estimate the traffic flow and speed. Cheung, S.C. and Kamath, C. (2004) proposed a robust technique for background subtraction using urban traffic video. The drawback of this method is the background can change significantly with shadows cast by buildings and clouds, or due to changes in lighting conditions. The background frame is required to be updated regularly under these changing environmental conditions. The most commonly used background updating techniques are averaging and selective updating.

2.1.2 Vehicle Tracking

More video-based detection approaches consider the spatial and temporal characteristics of video sequences, and deal mainly with the analysis of variations in time of the same pixel rather than with the pixel given by the environment in a frame (Bensrhair, M. et al., 2001). Other methods focus on using object modeling and tracking to match with the observed vehicles and estimate the traffic variables.

2.1.2.1 Inter-frame Differences Method

Inter-frame differencing is the most direct method for motion objects detection between two consecutive frames. Dailey et al. (2000) used the inter-frame differencing method to estimate the traffic speed from un-calibrated cameras. The differences between two successive frames are computed pixel-by pixel to track the moving vehicles between the sequential images. Then an edge detector is operated to find the movement of the vehicle centroid. The mean speed could be estimated from the inter-frame distance and time interval. Figure 2.1 presented the algorithm of the inter-frame differencing method.

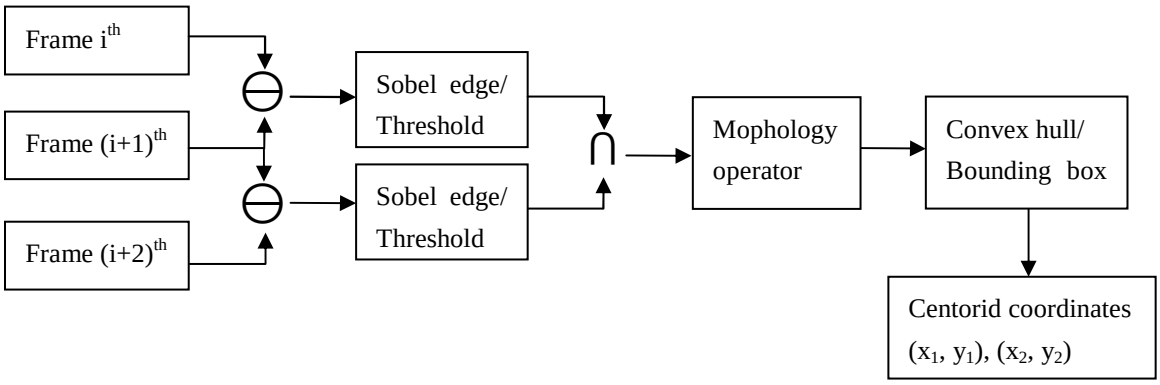

Figure 2.1 Inter-frame Differencing Method

Differencing the i^{th} and the $(i+1)^{th}$ frames as well as the $(i+1)^{th}$ and the $(i+2)^{th}$ frames to get two difference frames. Sobel edge detector and a threshold are applied to extract the moving edges. Two morphological operations, dilation and erosion are used to close and fill the edge curves to create moving blobs which represent the moving vehicles. The centroids coordinates of the blobs are calculated as the vehicle trajectory between the successive frames.

$$S = \frac{d}{\Delta t} \tag{2.4}$$

Where,

d: inter-frame distance

⊿t: time between the successive frames.

To identify and track the correlation vehicles, a minimum value of 0.90 of the linear regression correlation coefficient is used. With an estimation of the traveled distance, the vehicle speed is estimated from the equation (2.4). This approach is very fast and works well when the motion changes are significant. However, it not succeeds in detecting stopped or slow-moving vehicles.

2.1.2.2 Model-based Method

The work in N. Buch (2010) builds a 3-D vehicle modeling to match with the motion objects under calibrated cameras. Figure 2.2 shows the diagram of the 3-D model based detection and classification system. A Gaussian mixture models (GMM) is used to generate the initial foreground mask. The vehicle contours $\{S_m\}$ are extracted from the foreground mask and compared with a projected model profile to detect the vehicle class. The classifier uses 3D wire frame models to find the corresponding class label for every contours $\{S_m\}$ generated by the detector. The camera requires calibration to convert ground plane coordinates (3D model) to the image coordinate (2D projection).

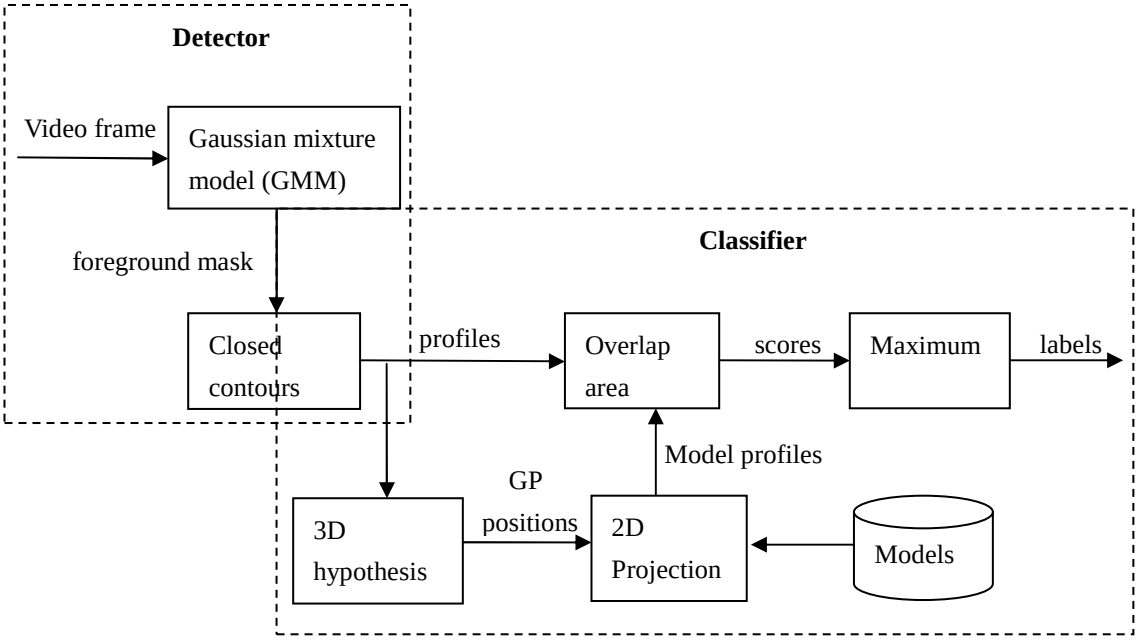

Figure 2.2: 3-D Model based Detection and Classification Algorithm

The measure of quality of fit between the vehicle contours $\{S_m\}$ and model masks $\{M_{x,y,i,k}\}$ is defined by the area operator A( ) ∈ pixels, and the overlap ratio operator O( ) ∈ [0, 1].

$$O\left(M_{x,y,i,k}, S_k\right) = \frac{A(M_{x,y,i,k} \cap S_k)}{A(M_{x,y,i,k} \cup S_k)} \quad (2.5)$$

A maximum operation is performed to find the highest quality of fit $P_k \in [0, 1]$ for every counter S_k:

$$P_k = Max\ O(M_{x,y,I,k}, S_k) \quad (2.6)$$

A threshold T= 0.48 is applied to $\{P_k\}$ to detect vehicle set $\{D_L\}$ with L<k is given by

$$\{D_L\} = \{P_k | P_k > T\} \quad (2.7)$$

The classification precision of the method could achieve 87%. Another work in C Mallikarjuna et al (2009) selected around 400 image samples that contain vehicles, and 1,200

image samples that do not contain vehicles as input to train the classifier. The classification result could achieve 88.25%. The weakness of the model-based approach is that it is unrealistic to build various geometric models or templates for all vehicles that captured from the traffic video data.

2.1.2.3 Feature Tracking-based Method

The feature tracking-based method tracks objects as a whole or characteristic points such as corners or lines of the object. Coifman et al. (1998) developed a corner feature tracking algorithm to detect the traffic velocity, flow and density. The vehicle tracking algorithm is shown in the Figure 2.3, which includes several modules: sub-feature detection, feature tracking & grouping, vehicle trajectory and camera calibration.

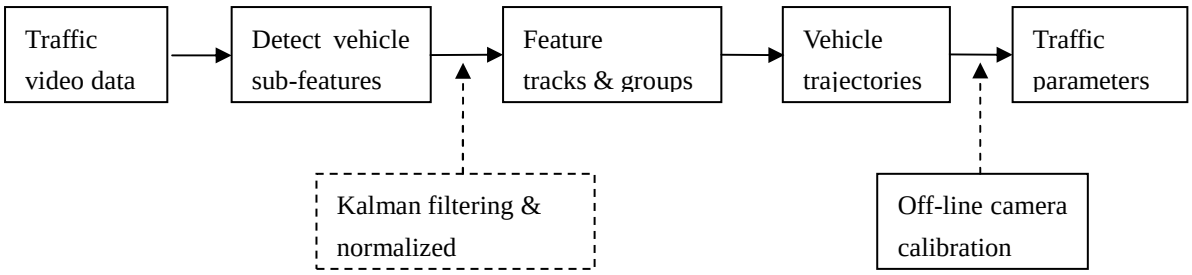

Figure 2.3 Feature Tracking-based Method

Instead of tracking the whole vehicles, vehicle corner features are tracked over time and grouped into discrete vehicles using a motion constraint. Features that are seen rigidly moving together belong to the same vehicle and grouped together. Kalman filtering and normalized

correlation are used to find the corner's locations in the sequential video frames. By monitoring the vehicle feature trajectory, the vehicle moving distance *d* could be measured. Off-line camera calibration is performed to obtain the depth scaling factor due to perspective projection. Ideally, the camera calibration requires the field survey and measurement.

Consider a region *A*, in the time-space plane with *m* vehicle passing through it. Let *d(A)* be the sum of the distance traveled by all vehicles in region *A*, *t(A)* be the sum of the time spent by all vehicles in region *A*, and |*A*| is the region area. The traffic flow *q(A)*, density *k(A)* and velocity *v(A)* could be calculated by following equations:

$$q(A) = \frac{d(A)}{|A|} \tag{2.8}$$

$$k(A) = \frac{t(A)}{|A|} \tag{2.9}$$

$$v(A) = \frac{q(A)}{k(A)} = \frac{d(A)}{t(A)} \tag{2.10}$$

The experimental results show that the detection rate for speed could reach 90%, the flow and density accuracies are 75%.

In the work of Todd N. Schoepflin (2003), he proposed a cross correlation of vehicle features (horizontal lines) by using a standard technique to detect the mean speed. Image binarization by automatic threshold and morphological operators were used to generate the background.

Broggi (1995) used the parallel and local feature extraction to detect the road boundary. Jung, Y.K. and Ho, Y.S. performed a feature-based vehicle tracking system based on the congested traffic video sequences in 2001. In the work of Kim, Z. (2003), a probabilistic feature groping approach was used to fast vehicle detection and tracking. The advantage of the feature tracking-based is that the features of the moving object could be visible even under the occlusion or night-time conditions. It is a relatively robust and reliable method to improve the detection rate.

2.1.2.4 Optical Flow Field Method

This approach utilizes the relative temporal displacement of the pixels as well as the spatial structure to generate an optical flow field within the image sequences. The algorithm does not detect and track the individual vehicles. Instead, it creates an intensity profile of the traffic flow in time order which is similar to the time-space trajectory diagram. Young Chou (2006) proposed an optical flow field method to estimate the mean traffic speed. Principle component analysis (PCA) was used to generate the intensity profile for the background (road surface). For each frame, he creates a mask and stacks the maximum intensity profile in time order to obtain the intensity flow.

To estimate the local speed at (t,x) in the time-space domain, let I (t,x) denote the intensity at location (t,x) in the time-space domain. Fix a local window size, $w_t * w_x$. At location (t,x) and for Δt= 0.5,….1,2 sec, d=0,…m, compute D by equation 2.11.

$$D(d) = \sum_{t=t_0-w_t}^{t_0+w_t} \sum_{x=x_0-w_x}^{x_0+w_x} |I(t + \Delta t, x + d) - I(t - \Delta t, x - d)| \quad (2.11)$$

Find d_0 which minimizes D (d). The tentative speed is: $v_k(t,x) = d_0/\Delta t$. Estimate v_0 and σ_0 by the mean and standard of $v_k(t,x)$ for all locations (t,x) and all k's. The speed is estimated in equation 2.12.

$$v(t,x) = \frac{\sum_k \exp\left[-\frac{(v_k(t,x)-v_0)^2}{2\sigma_0^2}\right] v_k(t,x)}{\sum_k \exp\left[-\frac{(v_k(t,x)-v_0)^2}{2\sigma_0^2}\right]} \quad (2.12)$$

The experimental results show that the average standard deviation of the error between the estimated speed and the loop data is 3.4 mph.

2.1.3 Camera Calibration

Camera calibration is the process of finding the true parameters of the camera that produced a given image. When the camera parameters are known, we can compute the traffic speed under the real world coordinate. The camera parameters can be represented in a 3 * 4 matrix called the camera matrix. Let (X,Y,Z) represent a 3D point position in the real world coordinates and(x,y,1) represent the 2D point position in the image coordinates (Kanhere, N. et al., 2008). The relationship between the two is captured by the matrix P:

$$\begin{pmatrix} x \\ y \\ 1 \end{pmatrix} = P * \begin{pmatrix} X \\ Y \\ Z \\ 1 \end{pmatrix} = \begin{bmatrix} f & 0 & 0 & 0 \\ 0 & -f\sin a & -f\cos a & fh\cos a \\ 0 & \cos a / s & -\sin a / s & h\sin a / s \end{bmatrix} * \begin{pmatrix} X \\ Y \\ Z \\ 1 \end{pmatrix} \quad (2.13)$$

Where,

h: camera height

f: camera focal length

a: camera tilt angle

s: image scale

In order to find the true parameters of the camera, the field measurements are necessary. Figure 2.4 shows the field detection region, capital ABCD and the image corresponding region abcd. If we know the coordinates of points A, B, C, D under camera coordinate system, and the coordinates of points a, b, c, d under real world coordinate system , the camera parameters could be calculated based on the camera matrix P.

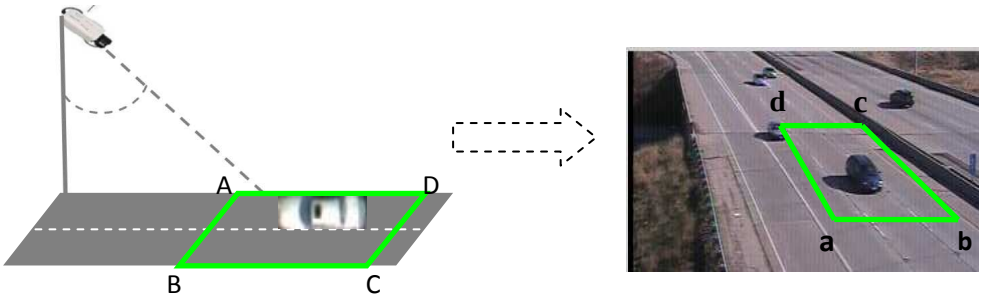

Figure 2.4 Camera Calibration

Many scholars try to conduct the camera calibration without the field measurement. Fung et al. (2003) developed a novel camera calibration technique using the geometry properties of road

lane markings. Road lane marking is the most common structured pattern and is readily found in a typical traffic scene. They accurately determined camera parameters, including pan angle, tilt angle, swing angle, focal length, and camera distance, using the appropriate camera model. However, the effectiveness of their method is potentially reduced where the geometry of road segment is not straight. Damaged or unclear road lane markings can also generate significant errors in the camera calibration process. Many recent studies focus on the algorithms for estimating traffic variables using un-calibrated traffic cameras (Schoepflin, Todd Nelson, 2003).

2.1.4 State of the Art in Industry Field

The video-based traffic state detection methods have been reviewed and categorized above. In this section, I attempt a brief review of the representative traffic monitoring systems in the industry field. There are typically two categorizations, tripwire-based and track-based systems (Beymer, D., et al., 1997). The tripwire-based traffic monitoring systems do not track vehicle, instead, they simulate the loop detectors and record the vehicles passing through a virtual loop detector. The track-based systems do track vehicles and follow their movements. Generally, vehicles are segmented and tracked by region based tracking software.

The representative commercial tripwire-based systems include AUTOSCOPE, CCATS, TAS, IMPACTS and TraCam. These systems typically detect vehicles within several detection regions (roughly the size of each detection region is a rectangle zone of a vehicle) in the video images The system indicates vehicle presence by detecting the image intensity

changes and integrates their spatial and temporal signatures to measure the traffic speed. In terms of the track-based monitor systems, the representative examples are CMS Mobilizer, Eliop EVA, PEEK VideoTrak, Nestor TracVision, and Sumitomo IDET (Kastrinaki, V., 2003). These systems either track moving vehicles by estimating optical flow vectors or extract individual vehicle features, aggregating and track them.

The challenges of the traffic monitor systems include the shadow, occlusion, congestion, lighting transitions and weather condition changes. An effective traffic surveillance system should meet several requirements as follows (Coifman, B., 1998).

- Automatic detection and tracking each vehicle under shadow and occlusion.
- Function under a wide range of traffic conditions such as the light traffic and congestion state.
- Function under variety of lighting condition like sunny, overcast, twilight, night and rainy etc.
- Fast computation and operation in real-time.

Even though a number of commercial monitoring systems have been created, many of these requirements still cannot be met. This result in research in more advanced video-based vehicle detection technology. The representative video-based traffic monitoring systems were summarized in terms of their fundamental processing techniques and estimation of traffic parameters in Table 2.1.

Table 2.1 Representative Traffic Monitor Systems

System	Method	Traffic parameters
AUTOSCOPE	Background frame differencing with edge detection based on the spatial and temporal gradients	Volume Speed Occupancy
CCATS	Background removal and model of time signature for vehicle detection	Volume Speed
TAS	Background frame differencing combines with virtual loop detectors	Volume Speed
IMPACTS	Tripwire based method	Volume Speed
ACTIONS	Optical flow field and cluster method to detect moving vehicles	Volume Speed Occupancy
IDSC	Background frame differencing	Volume Speed
MORIO	Optical flow field and 3D modeling	Volume Speed
TITAN	Background frame differencing and morphological processing for vehicle segmentation and features extraction	Volume Speed Occupancy
TRIP II	Spatial signature with neural nets for object detection	Volume Speed
TULIP	Thresholding for object detection	Volume Speed
TRANSVISION	Background frame differencing and lane region detection	Volume Speed
VISATRAM	Background frame differencing and tracking the spatial-temporal cube	Volume Speed
CMS Mobilizer	Optical flow field and feature tracking	Volume Speed
PEEK VideoTrak	Background frame differencing and vehicle tracking	Volume Speed Occupancy

2.2 Overview of Stationary Image Segmentation Algorithms

The video-based traffic detection approaches are not suitable to process the stationary traffic image, as the vehicles are in motion among video sequences. In this research, I will apply static image segmentation and object detection methods. This section conducts a review of the existing image segmentation algorithms especially for roadway and object detection.

Image segmentation is the foundation of pattern recognition and image processing. Image segmentation is to subdivide an image into a set of continuous and disconnect regions that are homogeneous and meaningful with respect to some characteristics for image analysis. Let *R* represent the entire image region and segment *R* into n partitions, R_1, R_2, …R_n, such that:

1. $\bigcup_{i=1}^{n} R_i = R$
2. R_i is a connected region, I =1,2,…n
3. $R_i \cap R_j = \emptyset$ for i and j, $i \neq j$
4. P (R_i) = True for i = 1,2,…n
5. P ($R_i \cup R_j$) = False for $i \neq j$

Where, P (R_i) is a logical predicate defined by the pixels in partition R_i, $\emptyset$ is the null set. Condition 1 indicates the segmentation must be complete. Condition 2 requires that pixels in a sub-region R_i must be connected. Condition 3 denotes that all partitions must be disjoint. Condition 4 states that pixels in a segmented region should share same property. Condition 5 indicates that regions are different in the sense of predicate P (Rafael C. Gonzalez, 2002).

Broadly speaking, there are two types of images segmentation methods, pixel based and

object/region based techniques. Pixel-based image segmentation is based on pixel properties, means that the pixel is the minimum analysis unit, without considering the relationship of neighboring pixels (Kang, W. et al., 2009). Traditional pixel-based image segmentation methods include threshold segmentation approach, edge/gradient based detection, feature/clustering based algorithm.

Table 2.2 Summary of image segmentation techniques

Segmentation	Method description	Common approaches
Threshold	Compare the image pixel values with predefined threshold T based on the gray level histogram	Global, Local and Dynamic thresholds
Edge/gradient based	Partition an image via detecting the image discontinuous or abrupt changes in gray level.	Sobel, Rroberts, Prewitt, Canny, Laplacian of Gaussian (LoG)
Feature/clustering based	Categorize the pixels into clusters according to the feature space, and then back to the spatial domain to form separate regions.	Utilizing different kinds of features such as spectral information, color, texture and variation of gray level etc.
Region based	Group pixels into homogeneous regions according to given criteria, such as gray value, color and texture characters.	Region growing, splitting, merging or their combination
Special theory based	Apply fuzzy set theory, neural networks, wavelet approaches to perform classification into image segmentation.	Fuzzy set theory, Neural networks, Genetic algorithm, Wavelet, Markov random field (MRF), Level set etc.

The principle of object-based image segmentation is to group the pixels into homogeneous regions as the minimum image processing unit according to the spatially contiguous characteristics. Each region is consisted of a number of adjacent pixels and contains their spectral and spatial features. The subsequent image analysis is based on the segmented

regions (Techmer, A., 200, Chi, Hongbo, 2009). Current image segmentation algorithms combine certain special theory to improve the partition results, such as fuzzy set theory, neural networks, wavelet approaches and so on. The existing image segmentation techniques are summarized in Table 2.2.

Traffic detection is to extract the traffic variables and provide the real time traffic flow information for transportation management. Therefore, the roadway segments and vehicles have to be detected from the image plane under the camera coordinate system. Lots of image segmentation algorithms have been proposed to generate different rules for object recognition in previous studies. Following context will review and discuss the existing image segmentation methods especially for roadway and vehicle detection.

2.2.1 Threshold Method

Threshold segmentation method partition an image through the gray level histogram to compare each pixel value with the predefined threshold T. Let I (i, j) be an image, I (i, j) =0 when p (i, j) < T, I (i, j) =1 when p (i, j) >= T. Where p (i, j) refers to the pixel value at the pixel (i, j). The threshold selection requires that the gray level histogram of an image has a number of peaks, which corresponds to different structure or properties (Liu, Ping, 2004). The threshold selection schemes may be implemented globally, locally or dynamically.

The image would be partitioned into two classes under global threshold. Global threshold T

depends only on gray level values and the predefined threshold value T. There have been many algorithms developed to generate better threshold image segmentation research, such as minimum threshold, Otsu, optimal threshold, histogram concave analysis, iterative threshold and entropy-based threshold etc. (Cheriet, Said & Suen, 1998, Hu, Hoffman & Reinhardt, 2001).

In terms of the local threshold, the original image is divided into several sub regions by various thresholds Ts, which are derived from the pixels properties of the local region. Main local threshold techniques include statistical threshold, 2-D entropy-based threshold and histogram-transformation threshold etc. If there are several objects taking different gray level in an image, the dynamic thresholds (T1、T2、…Tn) should be performed depending on f (x, y), p(x, y) and the spatial coordinates x and y. In general, dynamic threshold includes watershed and interpolatory threshold.

Threshold techniques can work very well and fast with low computation for an image which has obvious contrast. However, if the image has noisy background or low peaks, this method would usually fail to find the most suitable threshold value (Rekik, Zribi, Hamida & Benjelloun, 2009). Other problems might emanate without considering the neighbor spatial relationship and result in unconnected sub regions, over or under-segmentation etc.

2.2.2 Edge/ Gradient based Detection

Edge/gradient-based approach is to extract the dominant edges by detecting the intensity discontinuities or abrupt changes in the image. In general, gradient operators are defined by function g(x) to identify the edge/boundary. There are several commonly used gradient operators, Sobel, Rroberts, Prewitt and Canny method are based on the first derivative of image f (x, y). The Laplacian of Gaussian (LoG) is based on second derivative. Among them Canny technique is the most representative one (Rafael C., Gonzalez, 2007). The detected edge segments could be aggregated together by Hough Transform into long straight lines. For roadway detection, a realistic assumption is often used, which requires the horizontal and vertical roadway curvature are insignificant, the road boundaries or lane marking width does not change drastically.

Bertozzi, M. et al. (1998) detects lane markings through a horizontal edge detector and enhances vertical edges via a morphological operator. For each horizontal line, it then forms correspondences of edge points to a two-lane road model and identifies the most frequent lane width along the image through a histogram analysis. To detect the possible road markings or boundaries, In the work of Enkelmann, W. (1995), he emploied a contour algorithm based on the range of acceptable gradient directions. This range is adapted in real-time to the current state variables of the road model.

Edge/gradient based detection works well for images having significant contrast between sub

regions. The technique can be efficiently performed followed by morphological operators and Kalman filters. Prior knowledge of the road geometry could be useful to identify the roadway boundaries and lane markings. However, the limitation of this method is that it could not produce a closed curve or boundary. In addition, the method could suffer from noise effects, edge less and irrelevant feature structures, thus produces undesirable results (Fathy, M. & Siyal, M.Y., 1998, Chan & Vese, 2001). For instance, the vehicle shadow might be appeared quite strong, highly affects the edge tracking and vehicle recognition.

2.2.3 Feature/Clustering based Method

Feature/clustering techniques label the image pixels into different clusters utilizing various features, such as color, texture, spectral information and variation of gray. In general, two features are often performed for road segmentation, namely color and texture. For each pixel, the color value is defined by the spectral response at the red, green and blue bands (R, G, B). The R and B planes can be used to distinct the road and non-road pixels, while green band contributes very little in the road detection. The color feature requires special treatment to ensure the consistency, due to the impact from illumination, shadow, season and weather factors (Buluswar, S.D. 1998). The texture of the road is normally more regular and smoother than that of the background environment. The road segments can be discriminated from the image through the texture by calculating the gradient amplitude.

C-means, Kohonnen self-organizing maps and K means are unsupervised clustering methods

that can be employed for feature clustering. Kim, J. (2001) used the adaptive thresholding and K-means clustering for a real-time region-based motion segmentation. The K means algorithm is an iterative method which needs to run several times but very fast to return the clusters found. Each pixel in the image is assigned to a certain cluster that minimizes the variance between the pixel and the cluster center. The solution quality of K means algorithm depends largely on the value of K and initial set of clusters. K means could guarantee to converge, but may not return the optimal results.

The template or a deformable model defining the shape features to match the road edges or lane markings is used, especially in remote sensing image processing (Hickman, A. et al, 2003). Kluge, K. and Lakshmanan, S. applied a deformable template approach to lane detection in 1995. Kreucher, C. and Lakshmanan, S. (1999) conducted a lane extraction algorithm that used frequency domain features. Y. Wang (1994) uses a spline-based model to describe the parallel borders of the road lane. A.L. Yuille (2000) uses snakes to model the roadway segments. Once a set of candidate lane markers has been detected, Hough transformation is often used to track and convert them into connected straight lines.

The application of the feature/clustering algorithm are straightforward for classification and easy for implementation. But there are certain drawbacks such as the inefficiency in selecting the number of clusters and appropriate features, to match the complex road geometry or vehicle model. Bayesian optimization and Kalman filtering algorithm are often employed to improve the features matching for the observed images. This requires the probability

distributions of roadway positions which can be derived from test data using edge detector.

2.2.4 Region based Segmentation

The region based approach is a process to group a set of pixels together into sub regions based on the predefined criteria. The candidate pixels in a region should share similar characteristics with respect to the color, texture and intensity etc. The most commonly procedures for region based segmentation are thresholding, region growing, splitting, merging and classifying (Wang et al, 2007).

Palubinskas, G., (2010) used a model and region approach to detection the traffic congestion in optical remote sensing imagery. The region growing can be processed like this: set a group of seeds points firstly, grow regions by appending each seed to the neighboring pixels that fit similarity criteria, stop when match with the stopping rule. The region splitting and merging approach rather than choosing seed points, they can divide an image into a set of arbitrary, unconnected regions and then merge or split the regions in an attempt to satisfy the conditions of reasonable image segmentation (Jung, C. 2003).

This type of segmentation technique performs well when the region homogeneity criterion is easy to define. However, it is a kind of iterative approach, the major drawback is that it requires lots of computation time and memory (Kang, W., 2009). In addition, the segmented region might be fragmented, over or under-segmentation of the image.

2.2.5 Other Special Theory-based Methods

Numerous special theory-based segmentation algorithms derive from other fields of knowledge such as fuzzy mathematics, genetic algorithm, wavelet transformation, morphology, artificial intelligence and so on. In image segmentation, recognition uncertainty is a key factor that leads to unsatisfied partition results for fixed algorithms. And further, the result will influence the performance of subsequent image processing. Application of fuzzy operators could handle the uncertainty inherent. Fuzzy set theory can allow certain degree of flexibility and generate fuzzy boundaries between different clusters in image segmentation (Kang, W., 2009). But the main drawback of the fuzzy theory is that it is difficult to determine the attributes of fuzzy membership and the computation could be intensive to calculate the fuzzy factor (Gao, X., 2004).

In terms of neural network-based method, it is a totally different approach comparing with other image segmentation algorithms. The image is firstly mapped into a neural network where every neuron stands for a pixel. Then, detect the image edges by using dynamic equations to direct the state of every neuron towards minimum energy defined by neural network (Wang Q., 1998, Bullock, D., et al.,1993). Jin, X. et al. (2007) proposed a vehicle detection technique from high-resolution satellite imagery using morphological shared-weight neural networks. Neural network based segmentation is suitable for real-time application due to the highly parallel ability, robustness to noise and fast computing capability. However, there are some limitations of this method either, such as the training time is very long and

need to avoid overtraining, initialization may influence the segmentation result (Jung, C., 2003). Other theory-based methods were also proposed for image segmentation (Zhang, X. and u, Forshaw, M.R.B., 1997). Wang, J. and Miller, R. (2005) used a dynamic and quasi-static background modeling for vehicle detection. In the work of Paragios, N. and Deriche, R. (2000), they applied a geodesic active contours and level sets for the detection and tracking of moving objects.

2.3 Chapter Summary

Video-based traffic monitor system has been widely used in traffic management areas. In this section, a review of the previous research on video-based traffic detection methods was given. The generic model for estimating traffic parameters includes the crucial steps of image acquisition, background generation, vehicle tracking and traffic parameter calculation. Each step can be performed with a variety of techniques and algorithms. Various commercial traffic monitoring systems are reviewed and classified based on the detection method. However, even though a number of commercial monitoring systems have been created, they still cannot meet the practical application for traffic state detection. The performance challenges of the traffic monitor systems include the shadow, occlusion, congestion, lighting transitions and weather condition changes.

The existing video-based processing methods developed for dynamic video data can not fit to the stationary images. For stationary image processing, the image segmentation algorithms and object detection methods were discussed in detail. Roadway and vehicle detection are

the fundamental process to estimate the traffic parameters. In the past decades, numerous image segmentation algorithms were proposed to generate different rules to conduct object detection. However, so far, there is not universal method for the object detection especially for images with complex background. More advanced image processing techniques could be developed following the ongoing computer vision research.

CHAPTER 3 METHODOLOGY

3.1 Model Framework

A new traffic state detection model is proposed in this study to estimate the traffic condition using CCTV stationary images. Figure 3.1 shows the overview of the traffic state detection model. The model contains three primary modules: roadway detection module, vehicle detection module and projection transformation module.

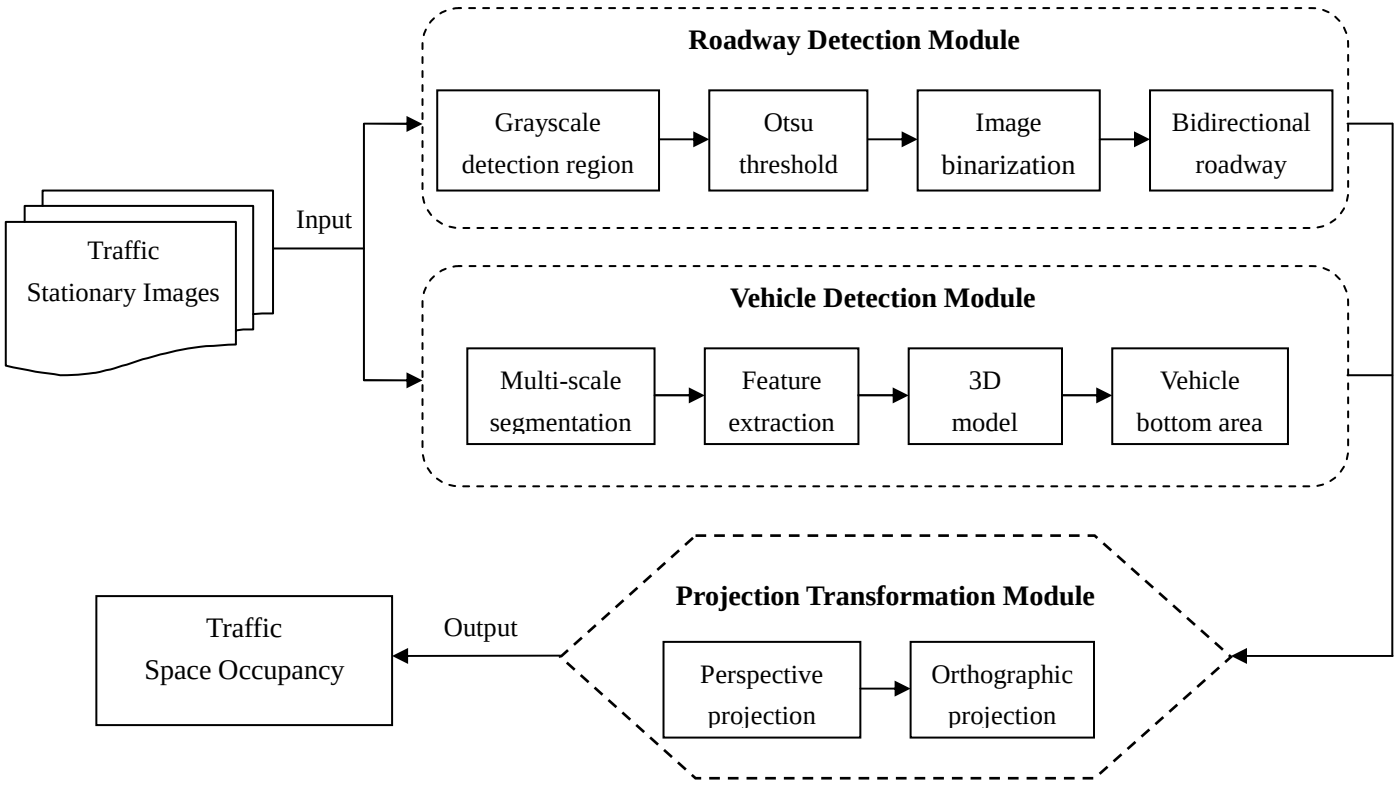

Figure 3.1 Proposed Model Framework

The roadway detection module aims to generate the bidirectional roadway area, and calculate

the left and right roadway distance respectively. The vehicle detection module is to extract the vehicles from the stationary traffic image, especially the vehicle bottom area to estimate the vehicle length. Instead of performing camera calibration, a projection transformation method is proposed in this study to eliminate the impact caused by perspective projection. Once the roadway distance and the vehicle length are obtained, the traffic space occupancy could be derived from the ratio of the roadway distance and the total vehicle length. And further, provides the traffic state and congestion information.

3.2 Roadway Detection Module

The road detection module has three major components, ROI & grayscale image generation, image binarization and roadway generation. The road assumptions define the freeway segment is a general highway scene, where the ground plane is flat, the road boundaries are parallel with constant width, the horizontal road curvature changes slowly and the vertical curvature is insignificant.

3.2.1 ROI & Grayscale Image Generation

In the original traffic image, the vehicles beyond the camera's field of view are not clear to be detected. So the original image is cropped into a ROI (region of interest) image first. In general, there are two types of images, the color image and the gray image. A typical color image is the RGB image. The RGB image is a 24-bit image which is composed of the red, green, and blue color channels. The color of each pixel is depended on the combination of the

red, green, and blue intensities stored in each color channel. In terms of the gray image, known as black-and-white image, it is a 8-bit image and the pixel intensity vary from black to white. The range of the gray value is from 0 to 255. The RGB color image can be converted to the grayscale image by calculating the effective brightness of the color. Equation (3.1) shows how to convert the color image to the grayscale image (Gonzalez, R., 2002).

$$Y = 0.299 * R + 0.587 * G + 0.114 * B \quad (3.1)$$

Where, *Y* is the grayscale value; *R, G, B* indicates the pixel intensity value in the red, green, and blue channels. Figure 3.2 shows the roadway detection algorithm and procedure. The figure 3.2a is the original input image, and 3.2b has been cropped and converted into detection region (ROI) with grayscale image.

3.2.2 Image Binarization

Image binarization is a common method in image processing to convert a grayscale image to monochrome. The optimum binarization threshold was obtained using the maximum between-class variance method. Figure 3.2c shows the histogram shape-based image threshold performing Otsu's algorithm. Otsu assumes that the image to be thresholded by two classes of pixels (foreground and background). Otsu computes the histogram and probabilities of each intensity level, then calculates the optimum threshold separating those two classes to make the sum of foreground and background spreads is at its minimum. The between-class variance is expressed in terms of the class probabilities and their means in equation 3.2.

$$\sigma^2 B(t) = \sigma^2 - \sigma^2 w(t) = w_f\,(t) w_b\,(t)\,[\mu_b(t) - \mu_f\,(t)]^2 \quad (3.2)$$

$\sigma^2 w(t)$ is the within-class variance defined as the sum of the two classes variances multiplied by their associated weights.

$$\sigma^2 w(t) = w_f\,(t)\sigma^2 f(t) + w_b\,(t)\sigma^2\,b(t) \quad (3.3)$$

Where,

σ²w(t): Within-class Variance

σ²f(t): foreground variance

σ²b(t): background variance

t: threshold

$w_f\,(t)$: probability of the foreground class

$w_b\,(t)$: probability of the background class

σ²B(t): between class variance

$\mu_b(t)$: background class mean

$\mu_f\,(t)$: foreground class mean

σ²: combined variance

In figure 3.2, the binary image 3.2d is created according to the Otsu's threshold, and the roadway area (white color) is almost detected from the image. The vehicles and noise on the roadway could be removed through mathematical morphology operation discussed in the next context. Image binarization is a simple and fast method which can fit the requirement to process the real-time traffic images.

3.2.3 Roadway Generation

The morphology operation is an image processing technique based on the set theory, topology and lattice theory. I conduct mathematical morphology operation to obtain the bidirectional roadway area. Basic operators in binary morphology include erosion, dilation, opening and closing. I perform a closing operation using a 2*2 structuring element to merge the fragmented pieces in Figure 3.2d.

The binary morphology is to probe an image A with a pre-defined shape, drawing conclusions on how this shape fits or misses the shapes in the image. This probe is called structuring element, denoted by B. The closing of A by B is obtained by the dilation of A by B, followed by erosion of the resulting structure by B (Gonzalez, R., 2002). The dilation of A by the structuring element B is defined by equation 3.4:

$$A \oplus B = \bigcup_{b \in B} A_b \tag{3.4}$$

If B has a center on the origin, then the dilation of A by B can be understood as the locus of the points covered by B when the center of B moves inside A. The erosion of the binary image A by the structuring element B is given by the expression:

$$A \ominus B = \bigcap_{b \in B} A_{-b} \tag{3.5}$$

When the structuring element B has a center (e.g., B is a disk or a square), the erosion of A by B can be understood as the locus of points reached by the center of B when B moves inside A.

The closing of an image by a structuring element is obtained by the dilation, followed by erosion of the resulting structure by the structuring element. The closing is the complement of

the locus of translations of the symmetric of the structuring element outside the image A which defined in equation 3.6.

$$A \bullet B = (A \oplus B) \ominus B \qquad (3.6)$$

Figure 3.2e shows the final bidirectional roadway area. To calculate the roadway segment length, a projective transformation was applied subsequently to calibrate the roadway geometric distortion caused by the perspective projection.

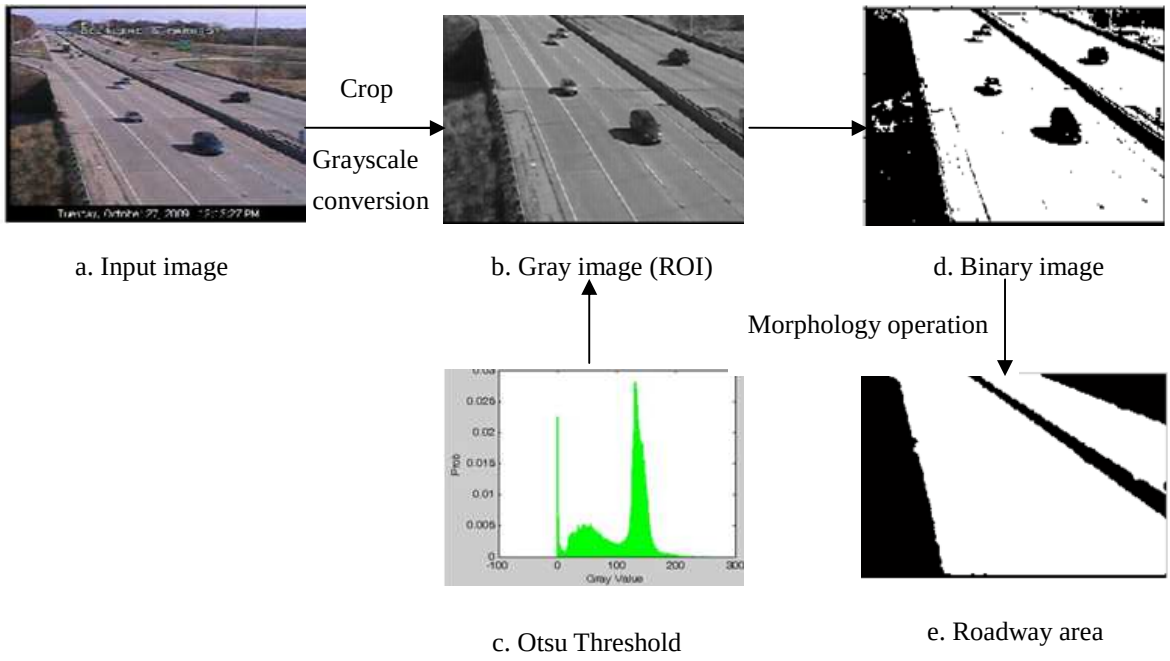

Figure 3.2 Roadway Detection Algorithm and Procedure

3.3 Vehicle Extraction Module

The aim of the vehicle detection is to recognize the vehicles from the stationary image and estimate the vehicle size. There are many algorithms available for object detection in the research area of image processing and computer vision. However, detecting objects from the

general and uncontrolled environments is still an open issue. In this research, I use multi-scale segmentation and feature extraction algorithm to detect the vehicles.

3.3.1 Multi-scale Segmentation

The multi-scale segmentation is a kind of object-based image segmentation which is contrast to pixel-based image segmentation. Human beings perform image recognition on an object level. For example, we can identify the road, vehicles and background environment from the entire image directly (Figure 3.3). And further, we can distinguish the vehicle types such as truck or car, as well as the number of vehicles and lanes. It is so called top-down strategy pattern recognition.

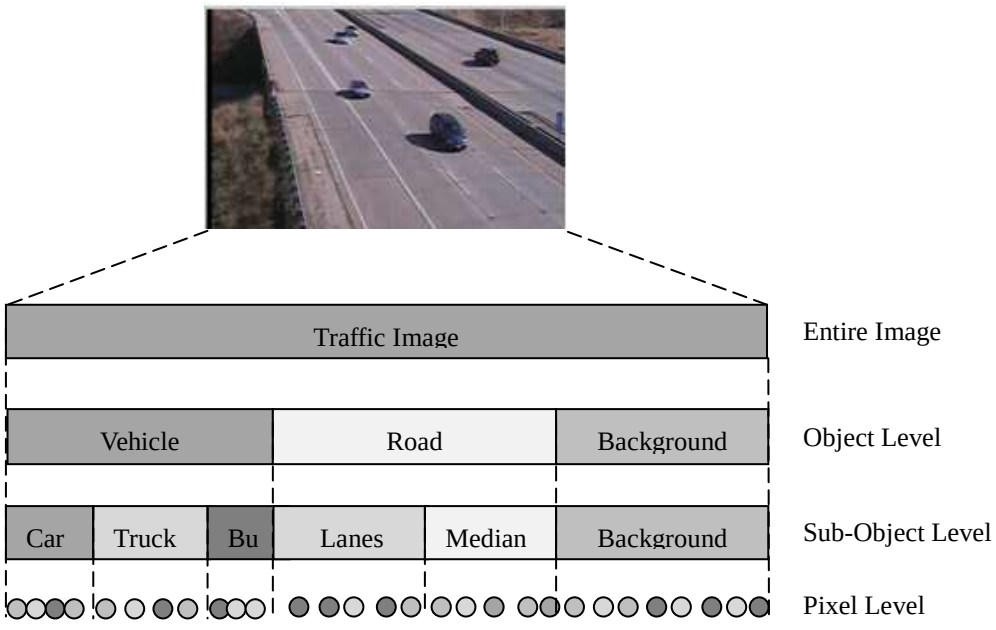

Figure 3.3: Image Hierarchy Structure

In contrast, the computer recognizes the image on the pixel level. The computer needs to learn some knowledge or rules to understand the object level, which is the bottom-up pattern recognition. Although there are so many image segmentation methods, there is still not an universal algorithm that fit to all different tasks due to the diversity and complexity of the image segmentation problems. One can only take the segmentation approach according to the specific issues. In this study, I apply the multi-scale segmentation and followed by feature extraction to conduct vehicle detection. Figure 3.4 shows the flowchart of image segmentation algorithm.

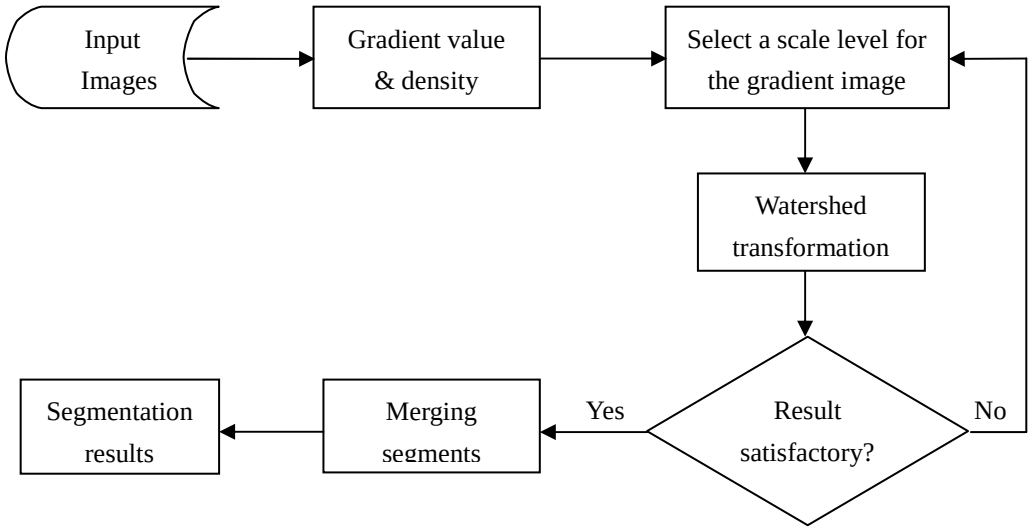

Figure 3.4 Image Segmentation Algorithm

A gradient map is generated first by calculating the gradient value and density of the image. The gradient of an image is the first order derivative of image in x and y directions.

$$\nabla f = \left(\frac{\partial f}{\partial x}, \frac{\partial f}{\partial y}\right) \tag{3.7}$$

Where,

$\frac{\partial f}{\partial x}$: the gradient in x direction

$\frac{\partial f}{\partial y}$: the gradient in y direction

The strength of intensity discontinuities is often to be used for identifying the edge locations of an image. A gradient magnitude operator can detect the amplitude edges at which pixels change their gray level suddenly. The gradient magnitude is defined in equation 3.8.

$$|\nabla f| = \sqrt{\left(\frac{\partial f}{\partial x}\right)^2 + \left(\frac{\partial f}{\partial y}\right)^2} \quad (3.8)$$

Following, the density function of gradients over the image could be computed in the form of a cumulative relative histogram. The density function means percentage of the pixels have gradient values less than or equal to the density value. Once the cumulative relative histogram has been calculated, it could be used along with the gradient map to determine the scale level to segment the image (Jung, C., 2003). Cumulative relative histogram can show the relative numbers of pixels at or below a particular gradient magnitude for a selected cumulative relative histogram level (scale level).

The morphological watershed algorithm is employed in the next step. Instead of working on an image itself, this algorithm is applied on its gradient image which was generated above. There are three types of points in the gradient image:

1) Points belonging to a regional minimum
2) Points at which a drop of water will certainly fall to a single minimum (Catchment basin or watershed of a regional minimum)

3) Points at which a drop of water will be equally likely to fall to more than one minimum (divide lines or watershed lines on the topographic surface)

This algorithm is to identify all the third type of points for segmentation (Beucher, S. and Bilodeau, M., 1994). Denote M_1, M_2, …, M_R as the sets of the coordinates of the points in the regional minima of the gradient image g(x,y). Let $C(M_i)$ be the coordinates of the points in the catchment basin associated with regional minimum M_i. The minimum and maximum gradient levels of g(x,y) are *min* and *max*. Define T[n] as the set of coordinates (s,t) for which g(s,t) < n, the topography in the gradient image increments from *min*+1 to *max*+1.

- $C_n(M_i)$ represents the point coordinates in the catchment basin associated with minimum M_i at stage n.

$$C_n(M_i) = C(M_i) \cap T[n]$$

- C[n] is the union of the catchment basin portions at stage n:

$$C[n] = \bigcup_{i=1}^{R} C_n(M_i) \text{ and } C[\max+1] = \bigcup_{i=1}^{R} C(M_i)$$

- Initialize C[min+1]=T[min+1]
- At each step n, assume C[n-1] has been constructed and the goal is to obtain C[n] from C[n-1]
- Define Q[n] as the connected components in T[n], for each $q \in Q[n]$, there are three possibilities

1) $q \cap C[n-1]$ is empty (q_1): A new minimum is encountered, q is incorporated into C[n-1] to form C[n]
2) $q \cap C[n-1]$ contains one connected component of C[n-1] (q_2), q is incorporated into

C[n-1] to form C[n]

3) $q \cap C[n-1]$ contains more than one connected components of C[n-1] (q_3): A ridge separating two or more catchment basins has been encountered. A dam has to be built within q to prevent overflow between the catchment basins

- Repeat the procedure until n=max+1

By suppressing weak edges to different levels, the algorithm can yield multi-scale segmentation results from finer to coarser segmentation. Scale Level values range from 0.0 (finest segmentation) to 100.0 (coarsest segmentation) and all pixels are assigned to one segmented region.

Over segmentation is the problem of watershed transformation algorithm. Merging is to aggregate small segments where over-segmentation may be occurred. The merge level parameter represents the threshold lambda value, which ranges from 0.0 to 100.0. The Lambda-Schedule algorithm was created by Robinson (2002). The algorithm iteratively merges adjacent segments based on a combination of spectral and spatial information. Merging proceeds if the algorithm finds a pair of adjacent regions, i and j, such that the merging cost $t_{i,j}$ is less than a defined threshold lambda value which shown in equation 3.9.

$$t_{i,j} = \frac{\frac{|O_i||O_j|}{|O_i|+|O_j|}|| u_i - u_j ||^2}{\text{length}(\partial(O_i,O_j))} \quad (3.9)$$

Where:

O_i : region i of the image, $|O_i|$ is the area of region i

u_i : the average value in region i and u_j is the average value in region j

$|| u_i - u_j ||$ is the Euclidean distance between the spectral values of regions i and j

length($\partial(O_i, O_j)$) : the length of the common boundary of O_i and O_j

Figure 3.6 shows the sample result of vehicle detection procedure. The process is initialized by the multi-scale segmentation technique, and figure 3.6b shows the result of multi-segmentation. The green lines in the image indicate the detected object contour.

3.3.2 Feature Extraction

A color image has multiple features such as the spectral, spatial, texture and color space feature. These features can be combined together by building rules for object detection. Rules building is based on human knowledge and reasoning about the object's specific characteristics. In terms of roadway, basically it is straight and long, and for vehicles, approximate have a rectangular shape etc. Each object can be defined by the meaningful rules according to its multiple features.

Each kind of feature consists of various attributes. For example, the spatial features have approximate 15 attributes to evaluate the object's shape in a variety of respects. The basic attributes can calculate the object's area, length, compact, rectangular fit and roundness etc. I tested various attributes, the significant features used in this study are described in detail as follows.

- Area (A_i): The actual number of pixels in the region (unit is pixel).
- Elongation: A shape measure indicates the ratio of the major axis length and the minor axis of the region.

$$E(i) = \frac{Max(L_i)}{Min(L_i)} \quad (3.10)$$

- Compact: A shape measure derived from the ratio of area and perimeter to describe the compactness of the region.

$$C(i) = \frac{\sqrt{4*A_i/\pi}}{c_i} \quad (3.11)$$

c_i is the perimeter that length around the boundary of the region.

- Roundness: A shape measure that compares the area of the object to the square of the length of the major axis of the object.

$$R(i) = \frac{4*A_i}{\pi*Max(L_i)^2} \quad (3.12)$$

- Tx range: Average data range of the pixels comprising the region.

$$Tx\_range(i) = \frac{\sum_{i=1}^{n} g_i}{n} \quad (3.13)$$

g_i is the pixel value in the region.

- Band ratio: The ratio between two bands, values range from -1.0 to 1.0.

$$BR(i) = \frac{B_2 - B_1}{B_2 + B_1 + eps} \quad (3.14)$$

Where, eps is a small number to avoid division by zero.

Combining these specific features together could build rules for object detection according to the object characteristics. For example, the rules to identify the roadway could be defined as follows:

- Objects with a area greater than 500 AND

- Objects with an elongation greater than 5 AND
- Objects with a compactness less than 0.15

In Figure 3.6c, the red objects represent the detected vehicles from the traffic image through feature extraction to remove the roadway as well as other background.

3.3.3 Vehicle Size Extraction

By masking the detected vehicles (Figure 3.6c) and the input traffic image (Figure 3.6a), the extracted vehicles could be obtained as depicted in Fig 3.6d. The image acquisition process can be regarded as a perspective transform from the 3D world space to the 2D image space. The individual vehicle is a 3D object projected on a 2D plane which was shown in Figure 3.6e by the red and yellow lines. The yellow lines represent the bottom plane with four vertexes A, B, C and D. In principle, the edge AB and CD are in parallel, as well as BC and AD. Note that the vehicle shadow is also extracted as part of the vehicle. The shadow will affect the accuracy of vehicle size. In order to remove the shadow and extract the vehicle size, I applied the accumulative histogram approach.

Image projection and accumulative histogram can be used to identify the vehicle's spatial feature. Figure 3.5 shows the approach of vehicle size extraction. I projected the vehicle (include the vehicle shadow) to the horizontal and vertical directions. I try to extract the vehicle bottom area ABCD. In Figure 3.5, the corner points A (V_1, H_1), B (V_b, H_2), C (V_3, H_2), D (V_2, H_1) are the vertices with their coordinates of the bottom area (yellow parallelogram).

The coordinates V_1, V_2, V_3, H_1 and H_2 can be derived from the projected histogram.

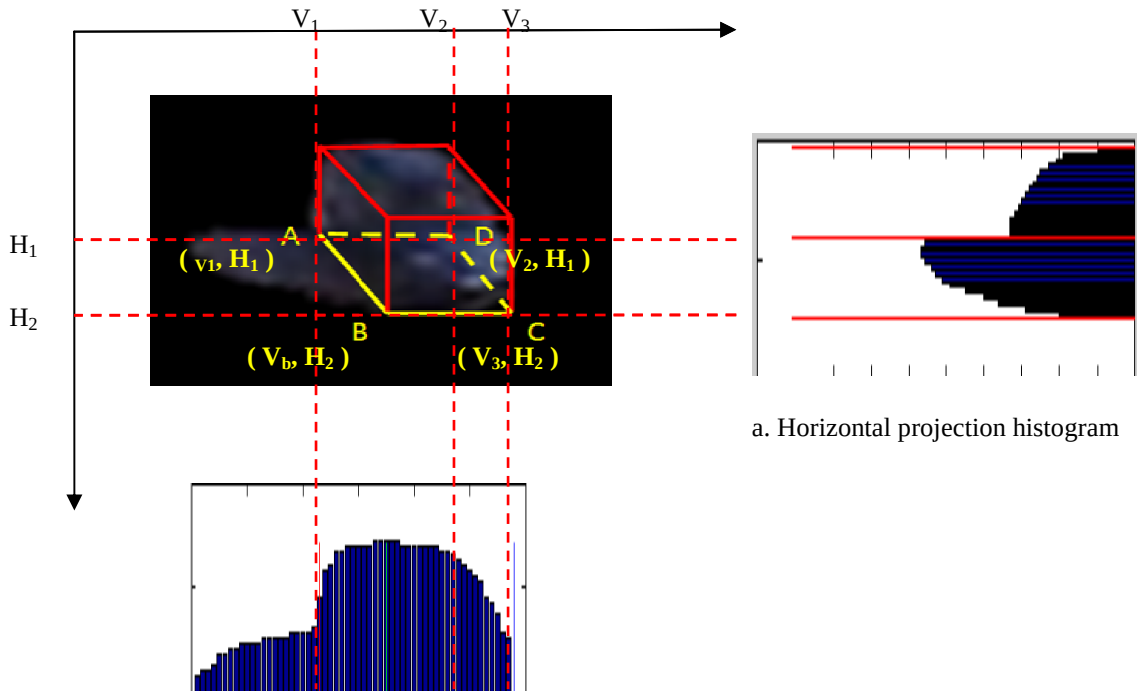

a. Horizontal projection histogram

b. Vertical projection histogram

Figure 3.5 Individual Vehicle Projection and Size Extraction

In the vertical projection histogram, V_1 and V_2 fall in the highest histogram group. They may not the maximum but significant higher than average histogram. Let MaxVertical represents the maximum histogram and set Tv = 0.8, which represents the vertical histogram ratio. V_1 and V_2 are corresponding to the first and last larger histogram than maximum histogram multiplying by 0.8. For V_3, it is corresponding to the length of the histogram figure.

Similarly, in the horizontal projection histogram, H_1 corresponds to the histogram which the first one larger than maximum histogram multiplying by 0.8. For H_2, it corresponds to the

length of the projection histogram. The coordinate V_b can be calculated based on the parallelogram feature: $V_b = V_1 + V_3 - V_2$. Then link the corner points for each vehicle in the image which produces the final vehicle size (bottom area) as depicted in Figure 3.6f.

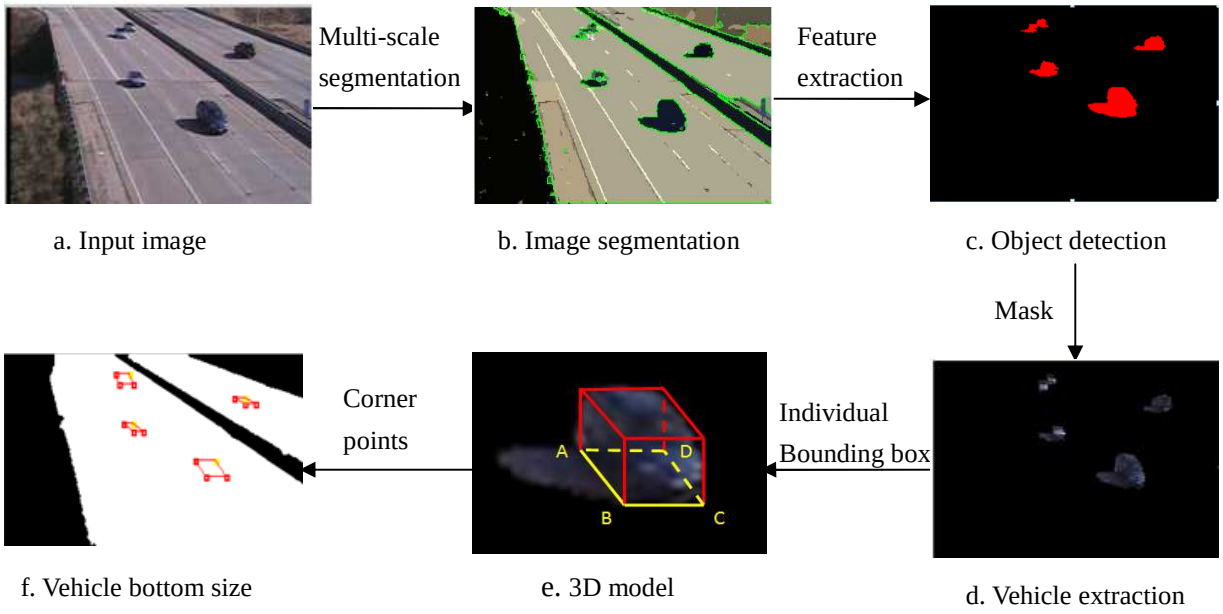

Figure 3.6 Vehicle Extraction Algorithm and Procedure

3.4 Projection Transformation

3.4.1 Perspective Projection vs. Orthographic Projection

As discussed previously, in order to measure the traffic parameters, general video-based traffic detection system requires the camera calibration to remove the inherent perspective effect of video images. The perspective effect relates the 3D points on the road (real world) coordinate system with 2D pixels on the image plane, depending on their distance from the

camera. This effect associates different information contents to different image pixels. Thus, road markings or objects of the same size appear smaller in the image as they move away from the camera view.

Traditional camera calibration requires field data (sample points) to calculate the camera height, angle and focus etc. This is inconvenient when there are lots of camera equipments are applied. In this section, I proposed a projective transformation method to remove the inherent perspective effect when camera parameters are unavailable. The roadway assumptions define a general highway scene, where the ground plane is flat, the road boundaries are parallel with constant width, the horizontal and vertical road curvature change slowly, which was shown in the Figure3.7:

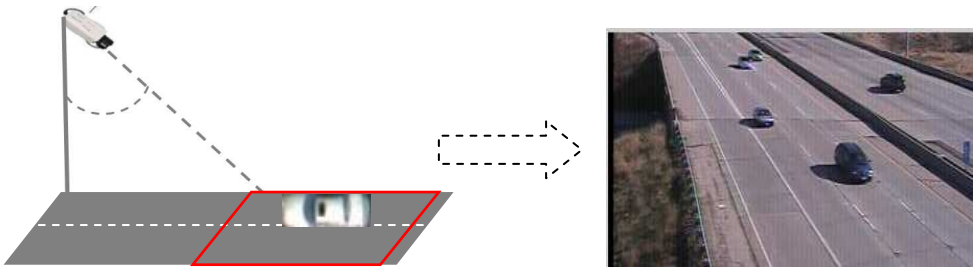

Figure 3.7 Perspective Projection

The inverse perspective mapping aims at inverting the perspective effect, forcing homogeneous distribution of information within the image plane. To remove the perspective effect it is essential to know the image acquisition structure with respect to the road coordinates (camera position, orientation etc.) and the road geometry (Tan, Sovira, et al.,

2006). The re-mapped views transforms the perspective projection to an orthographic projection (a form of parallel projection) corresponding to the parallel roadway boundaries and vertical size scale (Figure 3.8).

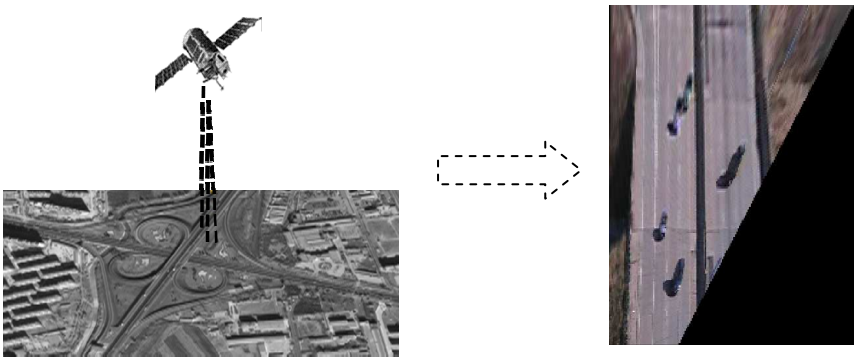

Figure 3.8 Orthographic Projection

3.4.2 Projection Transformation

A projective transformation holds between the scene coordinate and the image coordinate when the scene is a plane. The relationship between the road plane and the image plane could be represented by a 3*3 homography matrix.

$$\begin{pmatrix} x' \\ y' \\ 1 \end{pmatrix} = H_{3*3} \begin{pmatrix} x \\ y \\ 1 \end{pmatrix} = \begin{pmatrix} a_{11} & a_{12} & a_{13} \\ a_{21} & a_{22} & a_{23} \\ a_{31} & a_{32} & a_{33} \end{pmatrix} \begin{pmatrix} x \\ y \\ 1 \end{pmatrix} \quad (3.15)$$

Where,

x’, y’: Road plane coordinate

x, y: Image plane coordinate

H_{3*3}: A 3*3 homography matrix

a_{ij}: The parameters in the homography matrix which conduct different image rotation, scale and reflection changes

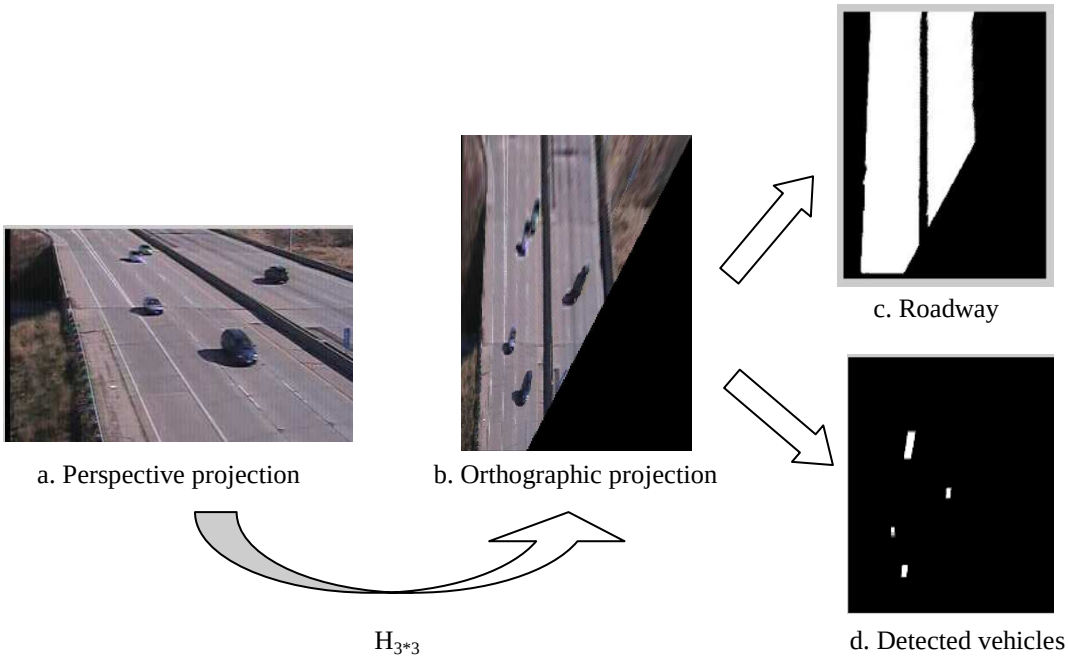

Figure 3.9 Projection Transformation

Figure 3.9 shows the projective transformation procedure. The image under perspective projection (a) was mapped to the image under orthographic projection (b) via a homography matrix. The transformation is necessary to calibrate the image distortion caused by the camera perspective projection. For example, the left and right sides of the roadway segments have been calibrated to parallel and have the same width in Figure 3.9 b.

In MATLAB, conduct pattern search and global optimization to adjust the parameters in the matrix. The calibration rules are, 1) make the roadway boundaries parallel and 2) the vehicles

have the same size scale. Once the transformation has been achieved, we can specify the roadway region and vehicle size. Figure 3.9c and 3.9d indicate the roadway region and detected vehicles respectively. We can compute the bidirectional roadway distance and the total vehicle length based on the divided images. And further, the traffic space occupancy can be derived.

3.5 Estimation of Traffic Occupancy

Various traffic parameters could estimate the traffic states, such as the traffic flow, speed, density and occupancy. In this study, traffic space occupancy is used as the measurement. Traditional traffic occupancy is usually defined with respect to point detector (loop detector) and it is averaged over time. In this research, the vehicles were extracted from the roadway segments and thus, it is average over space.

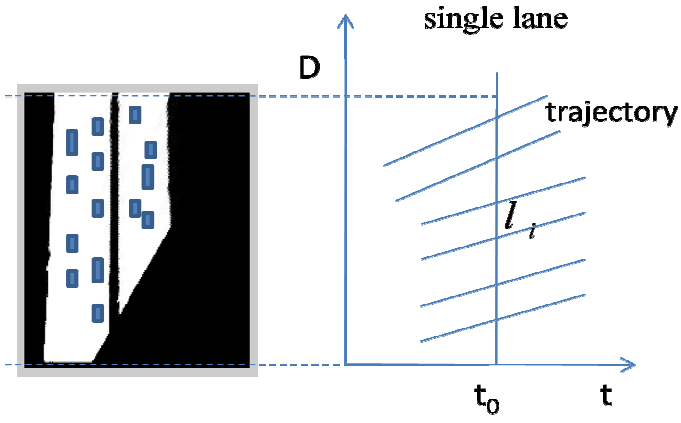

Figure 3.10 Space Occupancy Estimation

Consider the roadway segment as shown in Figure 3.10, at time t_0 with n vehicles passing through it. Let D be the roadway segment distance, and l_i denotes the length of the i^{th} vehicle. The time space diagram indicates the vehicle trajectories from a single lane (the right lane of the roadway right side). There are three vehicles on this lane. The lean solid lines indicate the vehicle trajectories, the different slope represents vehicles have different speed at time t_0.

The space occupancy is defined as the ratio of the sum of the vehicle length and the roadway distance multiply the number of lanes. It can be calculated as follows:

$$O_S = \frac{1}{\sum_{a=1}^{m} \tilde{D}_a} \sum_{i=1}^{n} \tilde{l}_i \tag{3.16}$$

Where,

$\tilde{D}$: Pseudo roadway segment length

a: the ith lane

m: number of lanes

$\tilde{l}_i$: Pseudo length of the ith vehicle

n: Number of vehicles

Note that the roadway segment length $\tilde{D}$ and the vehicle length $\tilde{l}_i$ in the equation only have relative values. The units of the values are pixels measured from the image, not from the real world. To obtain the actual distance, the image scale corresponding to the real world is required to map the distance from the camera image to the real world.

According to the traffic occupancy, we can provide the traffic congestion status. Table 3.1 shows the congestion level from the light traffic flow to the congestion status. To determine the model performance, I will compare with loop detector data collected from the same roadway segments for model validation and evaluation.

Traffic State	Light	Moderate	Congestion
Space Occupancy	Below 10%	10-25%	More than 25%

Table 3.1 Traffic Congestion Estimation Level

CHAPTER 4 EXPERIMENTAL DESIGN AND VALIDATION

4.1 Experimental Data Description

The Wisconsin Department of Transportation (WisDOT) has deployed CCTV system and published stationary images through 511 website to provide real time traffic information. The cameras are installed along major freeways and intersections, help to detect congestion segments and traffic incidents. In addition, the image data can provide traveler information to driver and motorists enable emergency dispatchers. The traffic images were updated every three minutes at 352*260 pixel resolution, and the image data can be downloaded freely from the WisDOT 511 web site.

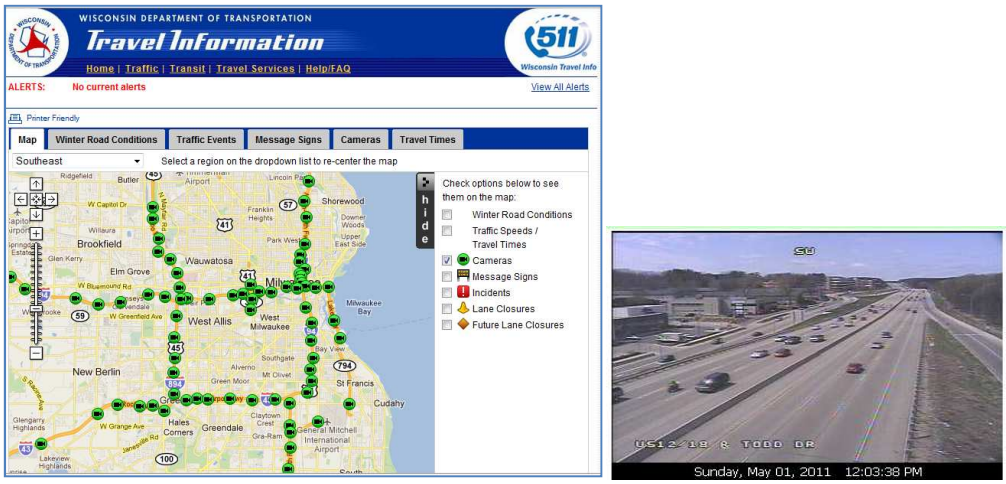

Figure 4.1 Traffic Cameras Map in Milwaukee, WI

Figure 4.1 shows the traffic camera locations in Milwaukee, Wisconsin (*Source from: http://www.511wi.gov/Web/Default.aspx*). These wayside cameras were installed along major

highway and usually placed on top of 45 foot poles. The cameras can be remotely controlled to pan, tilt and zoom. Video data could be fed to the local traffic operations center to assist operators in monitoring the traffic status and emergency events. The CCTV stationary images used in this study were collected from I-894 freeway corridor in Milwaukee, Wisconsin.

4.2 Model Calibration

The proposed model has been calibrated for image segmentation, feature extraction and projection transformation to achieve the optimal performance. Five representative individual images collected from I-894 freeway corridor were used to calibrate the model parameters.

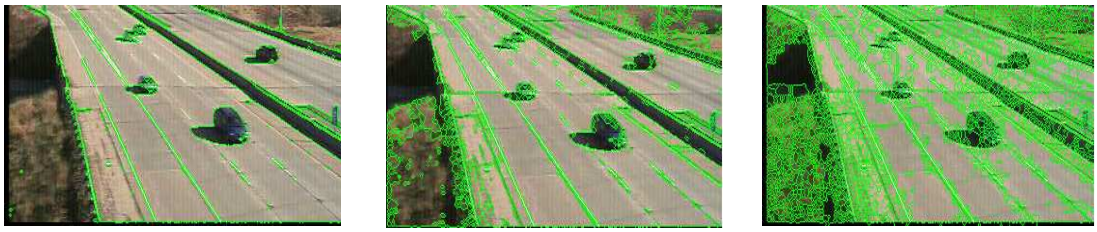

a. Scale Level=80 b. Scale Level= 65 c. Scale Level= 30

Coarse Fine

Figure 4.2 Segmentation Results under Different Scale Levels

The multi-scale segmentation algorithm takes scale parameters for the dissimilitude between the adjacent pixels and yield meaningful objects considering the homogeneity criteria. In Figure 4.2, from a to c, shows the segmentation results under different scale parameters. Small scale level generates result with small regions and much fine, while large scale parameter gives coarse partitions. Different scale parameters has been tested and obtained the

optimum scale level 65 for the experimental data.

Due to the over segmentation, image merge is performed after the multi-scale segmentation. In Figure 4.3, from a to c, shows the merge results under different levels. Figure 4.3a is the image segmentation under scale 65 without merging. Merge level 90 could result in an optimal result.

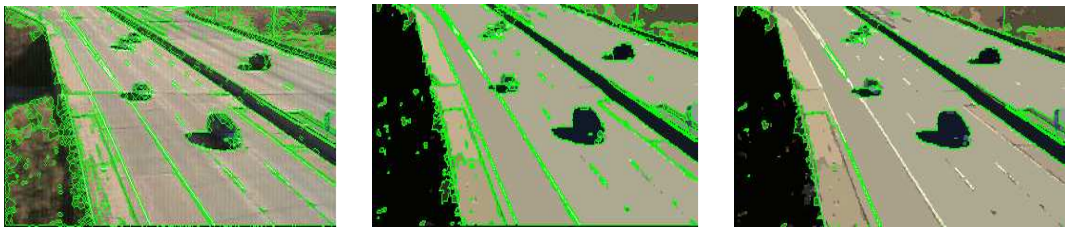

a. Merge level=0 b. Merge level= 50 c. Merge level= 90

Figure 4.3 Merge Results under Different Levels

While the image was segmented into several objects, criteria could be developed according to the object's features to extract vehicles from the image as the following.

- Area< TA
- Elongation< TE
- Std band> TSB
- Compact> TC
- Saturation> TS

Area criterion can be used to effectively remove the roadway and median. Consider the features of the lane marks and road boundary, their shapes are long and narrow, so I select the elongation as the second feature. Other features, std band, compact and saturation can be used

to remove the residual objects.

The rules were built according to the object's features to extract two vehicles from the test image. Table 4.1 shows the features, measure and extraction results. The area is the first feature used to identify the roadway since the roadway usually occupies large area in the traffic image. The extraction results 1, 2 and 3 indicate that the area feature is very significant to identify the road area. When the area reduces from 13277.52 pixels to 241.53 pixels (measure column), the roadway and median have been removed from the image. Only two vehicles, some lane marks and road boundary still exist in the image (the red color region represents the objects waiting to be identified. When the objects have been identified, they will be removed and the color turns to black).

Consider the features of the lane marks and road boundary, their shapes are long and narrow, so I select the elongation as the second feature. The result shows that it is very useful to identify the lane marks and road boundary. Comparing with the extraction result 3, most of the lane marks and road boundary have been removed, only few small patches exist in the extraction result 4. I tested other features, std band, compact and saturation are used to remove the residual objects and extract two vehicles. According to the features and measures in Table 2, I build following rules to extract the vehicles. If Area< 241.53, Elongation< 3.89, Std band> 13.24, Compact>0.15 and Saturation>0.02, then the object belongs to the vehicle.

Table 4.1 Features Extraction Results

Feature	Measure	Extraction Result
Area	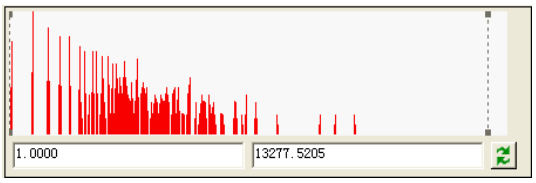	 1
	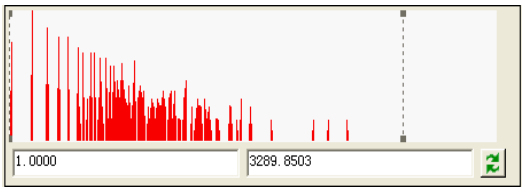	 2
	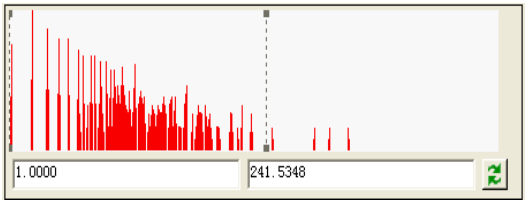	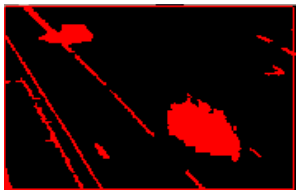 3
Elongation	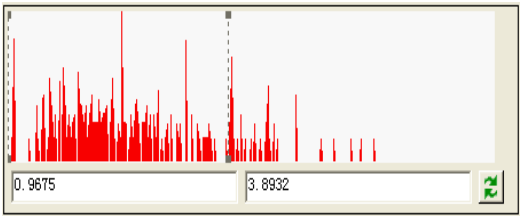	 4
Std band	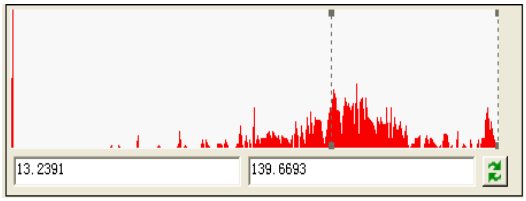	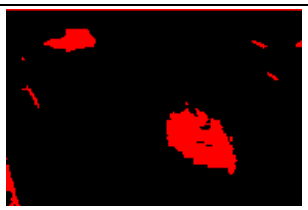 5
Compact	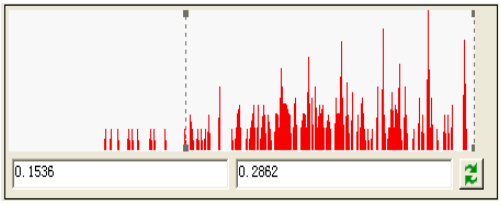	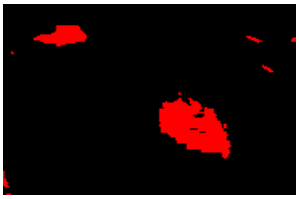 6
Saturation	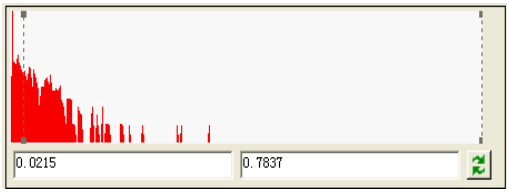	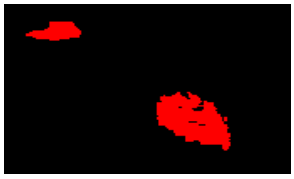 7

Table 4.2 presents the detection results of the five individual images and the quantitative assessment for different traffic scenes. Overall, slight performance drop can be observed with increased number vehicles appear in the detection region.

Table 4.2 Individual Image Analysis

Image	Vehicle Detection	Features and Measures	Detection Results	No. of Vehicles	Precision
	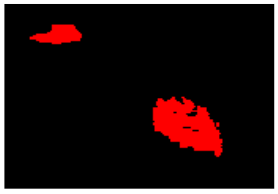	Area< 241.53 Elongation< 3.89 Std band> 13.24 Compact>0.15 Saturation>0.02	2	2	100%
		Area< 2522 Elongation< 4.9 Compact>0.14 Saturation>0.01	6	6	100%
		Area< 1248.18 Elongation< 5.61 Std band>2.5 Tx variance>418.3 Band ratio [-0.12, 0.4] Tx range<158.5	10	11	91%
	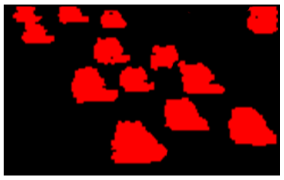	Area< 417.96 Elongation< 4.08 Band ratio [-0.04, 0.28] Compact>0.16 Roundness>0.17 Intensity [0.03, 1]	12	14	86%
	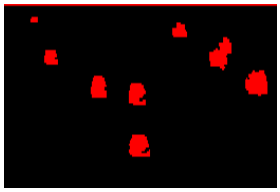	Area< 500 Elongation< 5 Band ratio [-0.04, 0.28] Compact>0.15	8	10	80%

The first image has been used to illustrate the image processing procedure. The second image was captured on the same road segment. The six vehicles can be detected, but their shadows cannot be effectively separated from the vehicles. The third and fourth images were captured on the same road segment and show a three-lane highway with more vehicles. The vehicles are close to each other and some vehicles can't be detected correctly. They link together and were recognized to one vehicle in the final result.

In terms of the multi-feature extraction, more features are required when vehicle increases (image 3 and 4). The features, area, elongation and compact are significant to identify the roadway and median. To recognize the lane mark and roadside background, the feature band ratio, std band, saturation and texture variation etc. are useful. However, these features are not always sensitive, and the measures will vary for different images. More effective features should be built according to the vehicle's characteristics in the future work.

To calibrate the projection transformation, the parameters in the transformation matrix were tested in MATLB to identify their functions. There are nine parameters which perform different image rotate, reflection and scale changes. When the matrix is a 3*3 unit matrix which presents in equation 4.1, the original image has not any changes.

$$\begin{pmatrix} a_{11} & a_{12} & a_{13} \\ a_{21} & a_{22} & a_{23} \\ a_{31} & a_{32} & a_{33} \end{pmatrix} = \begin{pmatrix} 1 & 0 & 0 \\ 0 & 1 & 0 \\ 0 & 0 & 1 \end{pmatrix} \qquad (4.1)$$

We change only one parameter each time and keep other parameters as shown in the unit matrix to illustrate the parameters functions. For each parameter, we have tested both of the positive and negative values, the results are summarized in Table 4.3. In this research, to perform a transformation from perspective projection to orthographic projection, a_{22}, a_{23} and a_{33} are significant parameters.

Table 4.3 Parameter Functions in Transformation Matrix

<table>
<tr><td colspan="3"> 
Original image</td></tr>
<tr><td>Parameter</td><td>Positive value</td><td>Negative value</td></tr>
<tr><td>a_{11}</td><td> 
Horizontal stretch
(a_{11}=2)</td><td> 
Horizontal reflection/mirror image
(a_{11}= -1)</td></tr>
<tr><td>a_{12}</td><td> 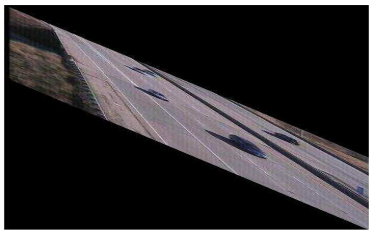
Horizontal clockwise rotation around the center line (a_{12}=1)</td><td> 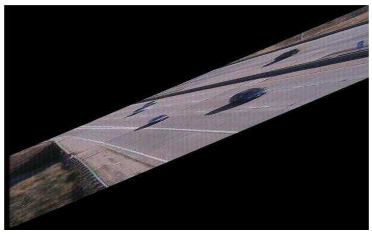
Horizontal anticlockwise rotation around the center line (a_{12}= -1)</td></tr>
<tr><td></td><td></td><td></td></tr>
</table>

a_{13}	 Image geometric distortion (a_{13}=0.005)	 Image geometric distortion (a_{13}= -0.002)
a_{21}	 Anticlockwise rotation around the image center point (a_{21}=2)	 Clockwise rotation around the image center point (a_{21}= -1.5)
a_{22}	 Vertical rotation (a_{22}=5)	 Vertical reflection/mirror image (a_{22}= -2)
a_{23}	 Focus close to the object (a_{23}= 0.01)	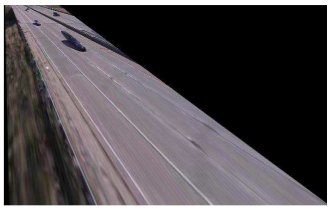 Focus far away from the object (a_{23}= -0.005)
a_{31} & a_{32}	Image translation parameters, no geometric changes	
a_{33}	 Image zoom out (a_{33}=3)	 Zoom out & vertical reflection (a_{33}= -3)

The model parameters in terms of the image processing and projection transformation have been summarized in Table 4.4 according to the model calibration discussed above.

Table 4.4 Calibrated Parameters

Image processing	Parameter	Value
Image segmentation	Segment scale	65
	Merge scale	90
Feature extraction	Area	< 500
	Elongation	<5
	Compact	>0.15
	Band ratio	[-0.04, 0.28]
	Tx range	<150
Transformation matrix (I-894, Lincoln Ave)	$H_{3*3} = \begin{pmatrix} 1 & 0 & 0 \\ 0 & 6 & 0.025 \\ 0 & 0 & 2 \end{pmatrix}$	

4.3 Experimental Results Analysis

The stationary traffic images used for experimental design were downloaded by an automatic program and organized by location. The images were captured on Oct 27, 2009 (Tuesday), from 7:30 am to 5:00 pm, at I-894 Lincoln Ave in Milwaukee, WI. In all, there are 165 images. The model and algorithms were implemented in MATLAB. The space occupancy results of

I-894 Lincoln Ave were shown in Figure 4.4. Note that the top figure shows the northbound occupancy (between red lines in the images) and the bottom figure shows the southbound occupancy (between yellow lines in the images).

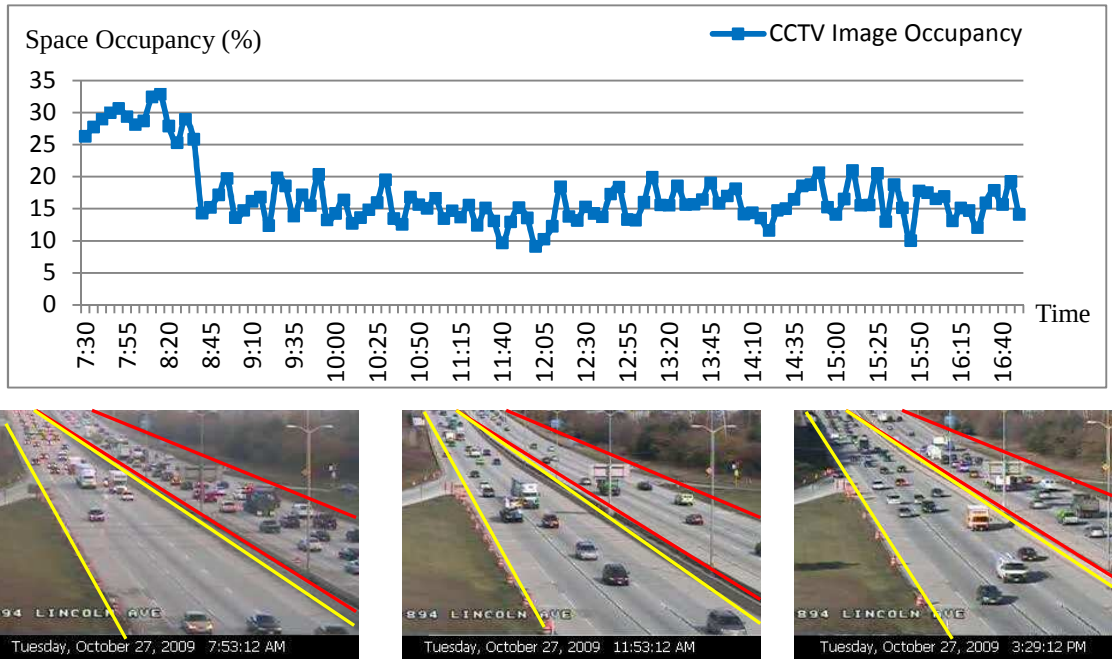

29.39% /17.06% (7:55AM) 13.6%/12.69% (11:53AM) 20.55%/21.08% (3:29PM)

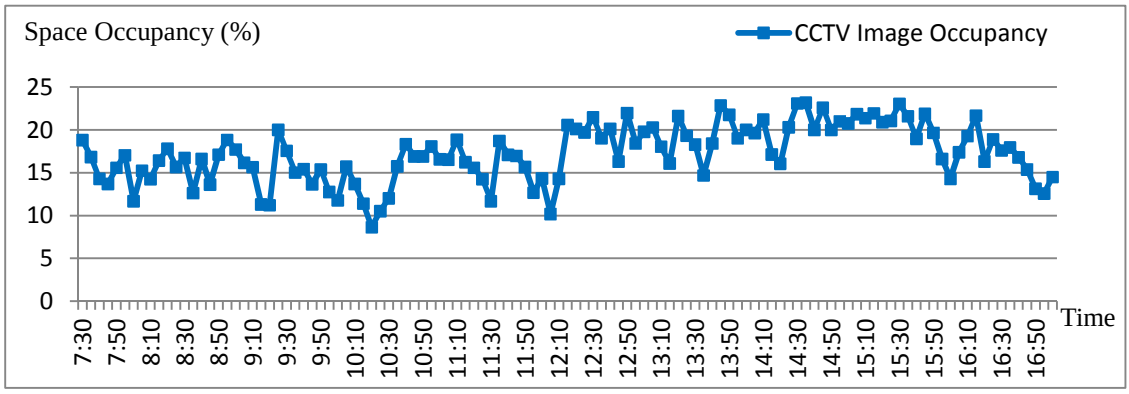

Figure 4.4 Space Occupancy &Image Data of I-894 Lincoln Ave

In the figure, the X axis shows the time from 7:30 AM to 17:00 PM, and Y axis represents the space occupancy, and the unit is percentage. The results could catch the trend of the traffic flow change in the day time. For the northbound, the average occupancies were basically less than 20%. But during the peak hours, from 7:30 to 8:30, the space occupancy could reach more than 30%. After the peak hour, the traffic flow descended and the occupancy waved between 10% and 20%. It shows a light traffic status during the period of noon time. The traffic flow increased rapidly in the afternoon from 20% to 25% during 3:00 PM to 5:00 PM which indicated a little congestion. This is the evening peak hour which is a common traffic pattern on the urban freeway.

In terms of the southbound, the occupancies were less than 25%. No significant peak hour or traffic congestion on this direction. Three representative images were shown under the figure. The first image was captured at 7:55AM which shows the space occupancies of NB and SB were 29.39% and 17.06% respectively. It is obvious the congestion status shown from the NB in the image (between red lines). The second image was captured at 11:53AM and the space occupancies were 13.6% and 12.69% at that time. That represents a light traffic status on both directions. The third image shows a moderate traffic condition which captured at 3:29PM, the space occupancies were 20.55% and 21.08% on NB and SB respectively. The estimated space occupancy from the stationary images could provide reasonable results for the real-time traffic state detection. In the following contexts, we will compare the experimental results with field loop detector data to validate the performance of the proposed model.

4.4 Model Validation

4.4.1 Time Occupancy vs. Space Occupancy

The traffic occupancy which obtained in this study is the space occupancy. We will compare the results with the loop detector data to validate the precision. However, the loop detector measurement is the time occupancy. This section will descript the relationship between the space occupancy and time occupancy.

The space occupancy is defined as the total vehicle length divided by the roadway distance.

$$O_S = \frac{\sum_{i=1}^{m} l_i}{L} = \frac{\frac{1}{m}\sum_{i=1}^{m} l_i}{\frac{1}{m}L} = \frac{m}{L}\frac{\sum_{i=1}^{m} l_i}{m} = k(A)\bar{l} \qquad (4.2)$$

Where,

O_s is the space occupancy,

l_i is the i^{th} vehicle length,

L is the roadway distance,

m is the number of vehicles.

$K(A)$ is the density of the roadway region A,

$\bar{l} = \frac{\sum_{i=1}^{m} l_i}{m}$ is the arithmetic mean of vehicle length.

The time occupancy is commonly measured by loop detectors, defined as the percentage of time that vehicles spend atop a loop detector. Such a definition is made evident by illustrating each trajectory with two parallel lines tracing the vehicle's front and rear (as seen by a detector) and this is exemplified in Figure 4.5. The time occupancy in the region *A*, O_T can be taken as the fraction of the region's area covered by the shaded strips in the figure (Hall, F. L., 1996).

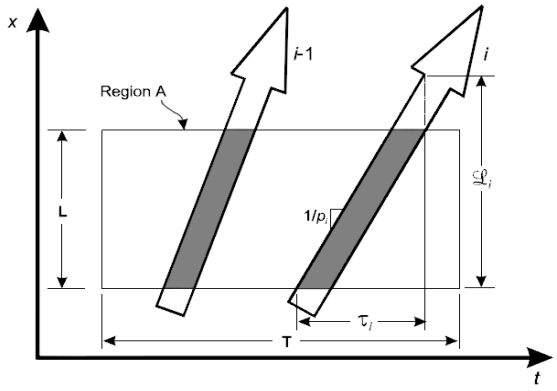

Figure 4.5 Trajectories of Vehicle Fronts and Rears in the Time-space Diagram

The *L* is assumed to be the length of road visible to the loop detector, the so-called detection zone. The *T* is interval of time over which the detector measurements. The time each i^{th} vehicle spends atop the detector is denoted as t_i. Thus, if *m* vehicles pass the detector during time *T*, the time occupancy is

$$O_T = \frac{\sum_{i=1}^{m} t_i}{T} = \frac{\frac{1}{m}\sum_{i=1}^{m} t_i}{\frac{1}{m}T} = \frac{m}{T}\frac{\sum_{i=1}^{m} t_i}{m} \tag{4.3}$$

Note that *m/T* in equation (4.4) is the traffic flow *q(A)* which is the number of vehicles passing a reference point per unit of time, and is measured in vehicles per hour. If l_i is the length of vehicle *i*, and v_i is the speed, therefore,

$$O_T = \frac{m}{T}\frac{\sum_{i=1}^{m} t_i}{m} = q(A)\frac{\sum_{i=1}^{m}(l_i/v_i)}{m} = k(A)\frac{v_S}{m}\sum_{i=1}^{m}(l_i/v_i) \quad (4.4)$$

Where *K(A)* is the density and v_S is the space mean speed.

Space mean speed is given in equation 4.5:

$$v_s = m/\sum_{i=1}^{m}\frac{1}{v_i} \quad (4.5)$$

Where:

v_s: The space mean speed

m: The number of vehicles passing the roadway segment

v_i: The observed speed of the i^{th} vehicle

Let $\tau_i = 1/v_i$,

$$O_T = k(A)\frac{1}{m}\frac{m}{\sum_{i=1}^{m}\frac{1}{v_i}}\sum_{i=1}^{m}(l_i/v_i) = k(A)\left[\frac{\sum_{i=1}^{m}\tau_i l_i}{\sum_{i=1}^{m}\tau_i}\right] \quad (4.6)$$

Where the term in brackets is the pace-based mean vehicle length, in which faster vehicle has smaller weights, while slow-moving vehicles have larger weights. If all vehicles travel at the same speed, both quantities are equal. Otherwise, they are not equal.

Figure 4.6 illustrates the effects of slow and fast vehicles for calculating the space and time occupancy. According to the definition of space and time occupancy, the horizontal strip represents the loop detector and the vertical strip indicates the CCTV snapshot. Faster vehicles are more likely to be captured by loop detectors and slower vehicle are more likely to be captured by stationary images. As a result, given the same density, the average vehicle lengths will be larger than longer vehicles generally travels slower than smaller vehicles. This sometimes outweighs the impact of the averaging effect difference. During congestion when speed becomes synchronized, such effects can be reduced and the averaging effects can kick in.

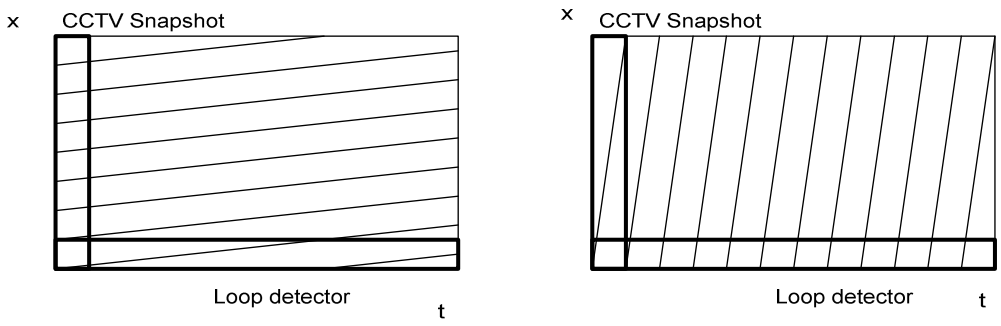

a. Slow vehicles b. Fast vehicles

Figure 4.6 Trajectories of Slow and Fast Vehicles in the Time-space Diagram

The relationship between the space and time occupancy could be concluded as follows:

- Space occupancy is a more accurate measurement for density which is only affected by the average vehicle length. And the time occupancy is affected by both speed distribution and vehicle length distribution.

- Both methods have some systematic errors, e.g. faster vehicles are more likely to be detected by snapshot, rather than loop detector. As a result, time occupancy becomes smaller than the space occupancy.
- Meanwhile, another effect can potentially cause time occupancy to be larger than space occupancy is when slow moving heavy vehicles appear, it will increase the weighted average of the pace-based vehicle length causing the time occupancy to be larger.
- In reality, the systematic caused by speed variations outweighs the impact of vehicle length variations, hence the time occupancy is usually smaller than space occupancy detected by CCTV snapshots.

In general, coefficient between the time and space occupancy can be determined by 1) speed variations, 2) vehicle compositions. Apparently, the former one has more impact based on our validation results.

4.4.2 Occupancy Comparison

The proposed model needs to be validated to illustrate the traffic detection ability. The validation is based on the loop detector data collected at the same locations and same time. For loop detector data, there are 3 detectors record the traffic occupancy of different lanes on I-894 freeway. The loop detector data provides the occupancy records every 5 minutes. Figure 4.7 shows the original time occupancy from loop detector data on northbound (source from Tops lab database). The red, blue and green curves represent three detectors' data located at

different lanes. It records one day 24 hour data which shows a peak hour from 7:00AM to 8:30AM and another peak hour during 3:00 PM to 5:00 PM. From 9:00AM to 3:00PM, the traffic flow descended and the occupancy waved between 10% and 20%. In the night time, there are few traffic and the average occupancy will below 5%.

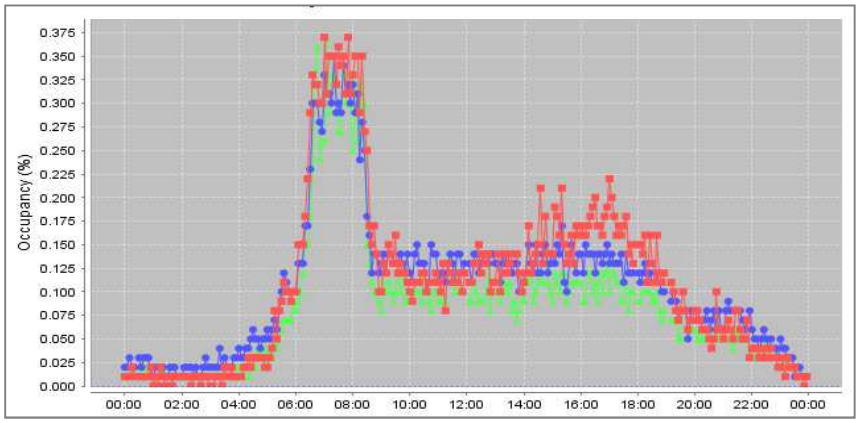

Figure 4.7 Time Occupancy Data from Loop Detector

(I-894 Lincoln Ave. Northbound, Oct 27/2009, 0:00AM-12:00PM)

We average the original loop detector data to compare with the estimated space occupancy. Note that the space occupancy focuses on the day time traffic flow from 7:30AM to 5:00PM. In Figure 4.8, the blue curve indicates the average time occupancy and the interval between two red dash lines is the corresponding interval we try to compare with the estimated space occupancy from CCTV images.

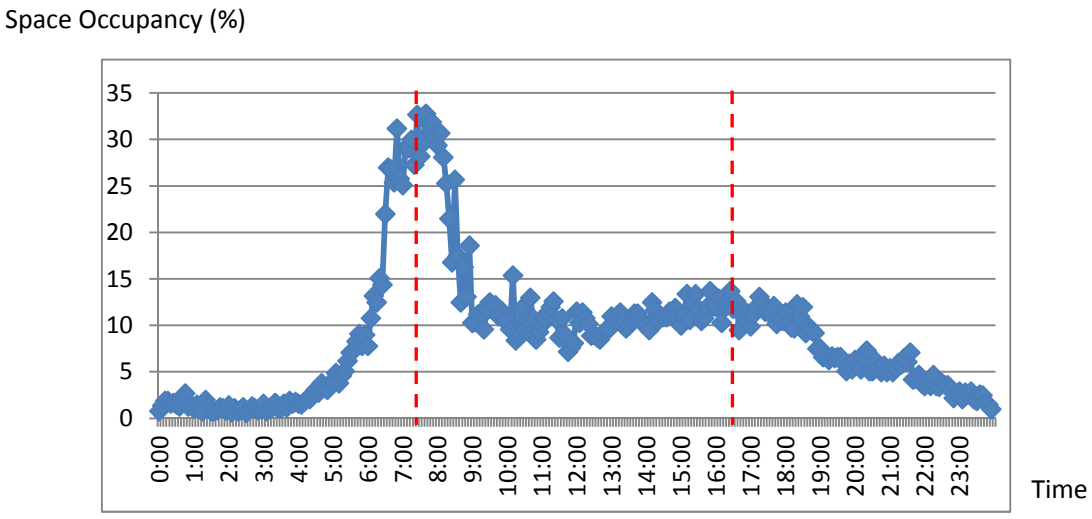

Figure 4.8 Average occupancy from original loop detector data

Figure 4.9 shows the comparison of loop detector occupancy (green curve) with CCTV image occupancy (red curve). As discussed above, under congestion condition, loop detector occupancy is close to the CCTV image occupancy due to the small vehicle speed variation. Figure 4.9a shows the northbound comparison. During peak hour 7:30 to 8:30, the green curve and red curve are very closed. After the peak hour, the red curve lies above the green one which indicates the CCTV image occupancy is greater than loop detector occupancy. Figure 4.9b represents the southbound comparison. No significant peak hour or congestion traffic on this roadway direction. The red curve always lies above the green one which indicates the CCTV image occupancy is greater than loop detector occupancy. The results are consistent with the relationship analysis previously. The traffic occupancy and the difference between loop detector data are provided in Appendix table A-2.

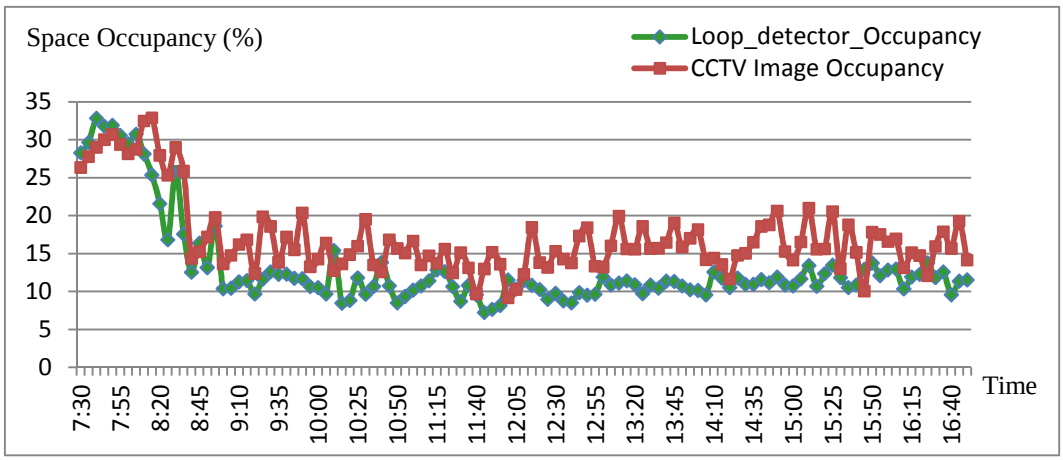

a. Northbound

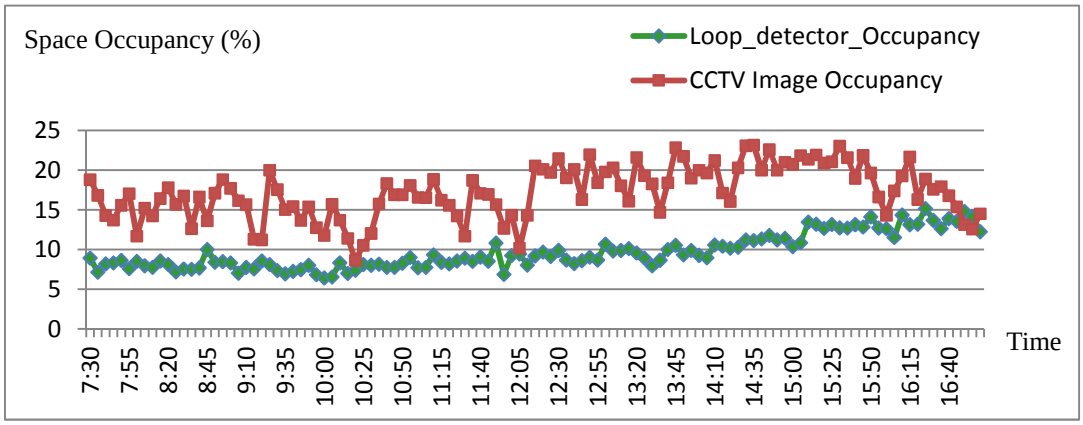

b. Southbound

Figure 4.9 Occupancy Comparison

The mean absolute error (MAE) is introduced to measure how close between the eventual outcomes. The mean absolute error is given as follows:

$$MAE = \frac{1}{n}\sum_{i=1}^{n} |O_C - O_L| \quad (4.8)$$

Where,

O_C is the estimated space occupancy

O_L is the loop detector occupancy

The mean absolute error are 4.51% and 7.62% for two roadway directions respectively which show that the proposed model can provide a reasonable performance over long time duration.

4.5 Chapter Summary

In this chapter, data acquisition, model calibration and model validation were described in detail. The traffic images captured from different freeway segments in Milwaukee were selected to calibrate the model parameters. The model validation was conducted using field loop detector data to demonstrate the performance of the proposed model. The experimental data was collected from I-894 Lincoln Ave. in Milwaukee, WI. This freeway corridor often suffers from a daily recurrent congestion during both AM and PM peak hours, and makes it a good site to exam the model performance under both free flow and congested conditions.

The experimental results show that the space occupancy estimated from the traffic stationary images could catch the trend of the traffic flow change in the day time as well as the congestion during AM and PM peak hours. Comparing with the loop detector data, basically, the estimated space occupancy is greater than the time occupancy. The mean absolute error (MAE) is introduced to analyze the accuracy of experimental results quantitatively. The accuracy measured by MAE are 4.51% and 7.62% for two roadway directions respectively, which show that the proposed model could provide reasonable traffic variables to detect the freeway traffic status.

CHAPTER 5 MODEL EVALUATION

5.1 Traffic Data Description

The proposed model consists of three modules: roadway detection module, vehicle extraction module and projection transformation module. Each module is comprised of many computer vision and image processing algorithms. All algorithms are implemented using MATLAB. The model is calibrated and validated using the traffic images captured from Lincoln Ave. on I-894 freeway corridor. The robustness of the algorithm and model would be evaluated with the traffic images from different locations along I-894 corridor. The locations and characteristics of the data will be described in this section. The evaluation results and sensitivity analysis will also be described.

The traffic image data captured from four sites on I-894 freeway are used to evaluate the model performance. These sites were selected because they locate close to each other. We expected that the traffic flow patterns are consistent along these roadway segments. Data was taken from 60th St. to 92nd St. on I-894 corridor and the time from 7:30 AM to 6:00 PM on September 27, 2009 (Tuesday). The total distance of this corridor is about 2.1 miles including four sites 60th St., 76th St., 84th St. and 92nd St. (Figure 5.1).The adaptability of the model under different traffic situations, illumination conditions and geometric roadway is also examined. The relationship between the estimated space occupancy and loop detector measurement is discussed in the following context.

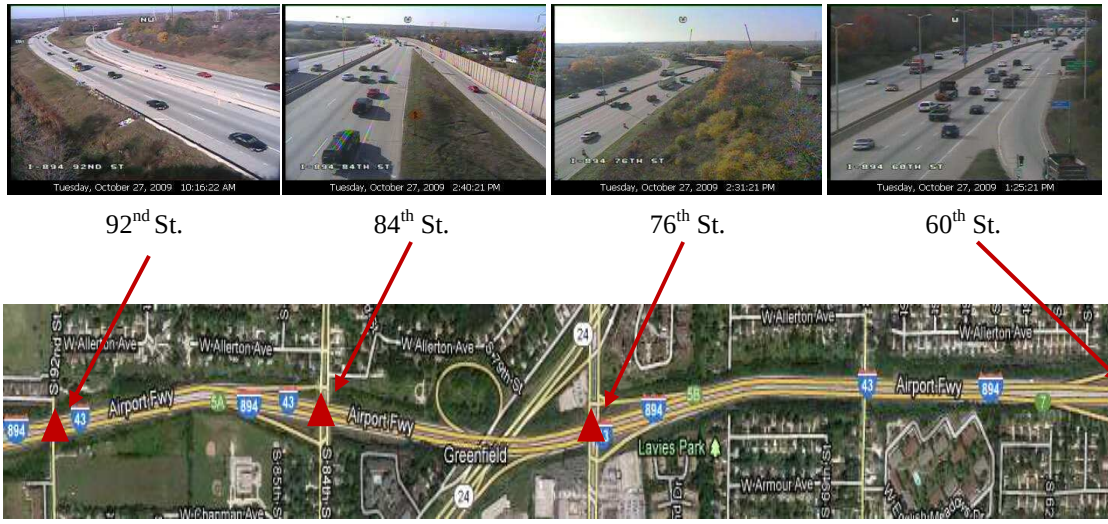

Figure 5.1 Camera Sites and Traffic Images on Freeway I-894 Corridor

5.2 Model Evaluation Results and Analysis

5.1.1 60th Street

The traffic images at this site captured from the intersection of 60th St. and I-894 freeway. Both directions of the roadway segments have three lanes and an on-ramp on the right direction. The traffic images were collected from 7:30 AM to 5:30 PM and the average interval between successive images is 3 minutes. Figure 5.2 is the sample of image processing results of each module. Figure (a) shows the original traffic scene captured at this site. Figure (b) shows the detected roadway area. Figure (c) is the detection region cropped from the original image. Figure (d) displays the vehicles extracted from the left and right side of the roadway segment. Figure (e) shows the result of the vehicle bottom area. Figure (f) presents the projection transformation result of the roadway and the extracted vehicles respectively.

a.Original Image

b.Detected Roadway

c. Detection Region

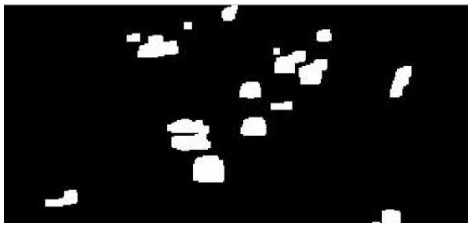

d.Vehicle Extraction

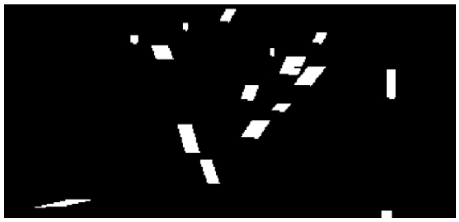

e. Vehicle Bottom Area

f. Roadway and Vehicle Projection Transformation

Figure 5.2 Sample of the Image Processing Results (60th St.)

A total of 201 traffic still images are successfully performed in MATLAB. The traffic occupancy and the difference between loop detector data are provided in Appendix table A-3. Figure 5.3 shows the occupancy comparison between the estimated results and the loop detector data. In the figure, the X axis shows the time from 7:30 AM to 17:30 PM, and Y axis shows the space occupancy, the unit is percentage. The green curve represents the estimated occupancy and the red one is the field loop detector data.

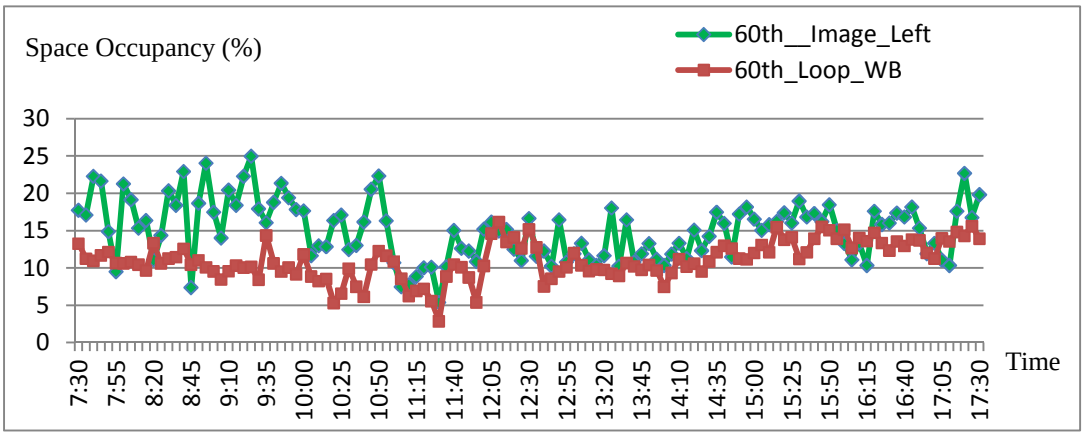

a. Traffic Occupancy of Westbound

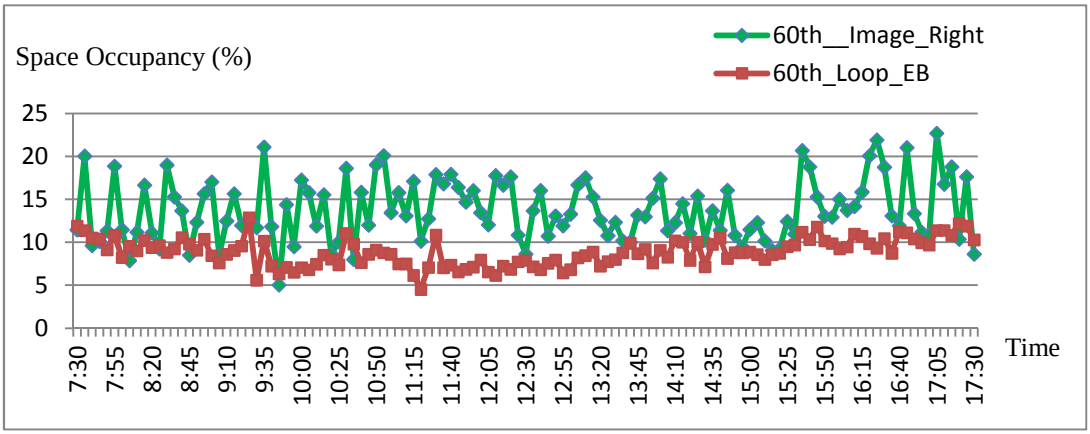

b. Traffic Occupancy of Eastbound

Figure 5.3 Occupancy Comparison (60th Street)

For the left side of the roadway which is the westbound, the estimated occupancies range

from 5.41% to 25% between 7:30 AM and 5 PM. For the right side of the roadway, the eastbound, estimated occupancies ranged from 5.06% to 22.72%. The traffic conditions in both directions were light or moderate for most of the time. There are not significant peak hours or traffic congestion on this roadway segment. The estimated traffic status could catch the trend of the traffic flow pattern derived from loop detector. Overall, the space occupancy is greater than the occupancy collected from loop detector. The mean absolute errors (MAE) for westbound is 4.56%, and 5.12% on eastbound. The proposed model can estimate the traffic situation appropriately for this roadway segment.

5.1.2 76th Street

Both directions of the roadway segments at the intersection of 76th St. and I-894 freeway have three lanes and the left side has an on-ramp. The traffic images were collected from 7:30 AM to 18:00 PM and the time interval between successive images is 3 minutes. A total of 210 traffic still images are successfully performed by the model. Traffic occupancy and congestion status were estimated based on the traffic images.

Figure 5.4 is the sample of image processing results from each module. Figure (a) shows the original traffic scene captured at this segment. Figure (b) shows the detected roadway segment area. Figure (c) is the detection region of the image. Figure (d) displays the vehicles extracted from the left and right side of the roadway. Figure (e) shows the result of the vehicle bottom area. Figure (f) presents the projection transformation results of the roadway and the extracted vehicles respectively.

a. Original Image

b.Detected Roadway

c. Detection Region

d.Vehicle Extraction

e.Vehicle Bottom Area

f. Roadway and Vehicle Projection Transformation

Figure 5.4 Sample of the Image Processing Results (76th St.)

The traffic occupancy and the difference between loop detector data are provided in Appendix table A-4. Figure 5.5 shows the occupancy comparison between the estimated results and the loop detector data. In the figure, the X axis shows the time from 7:30 AM to 6:00 PM, and Y axis shows the space occupancy, the unit is percentage. The green curve represents the estimated occupancy and the red one is the field loop detector data.

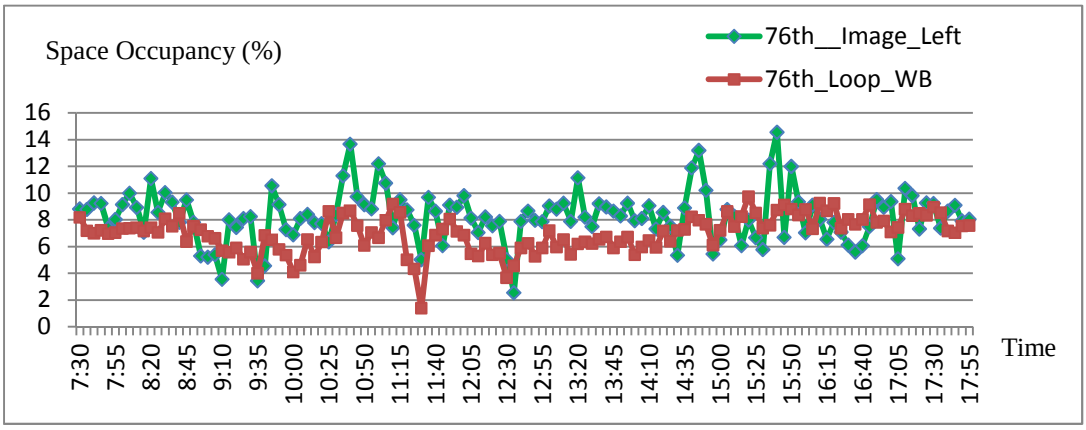

a. Traffic Occupancy of Westbound

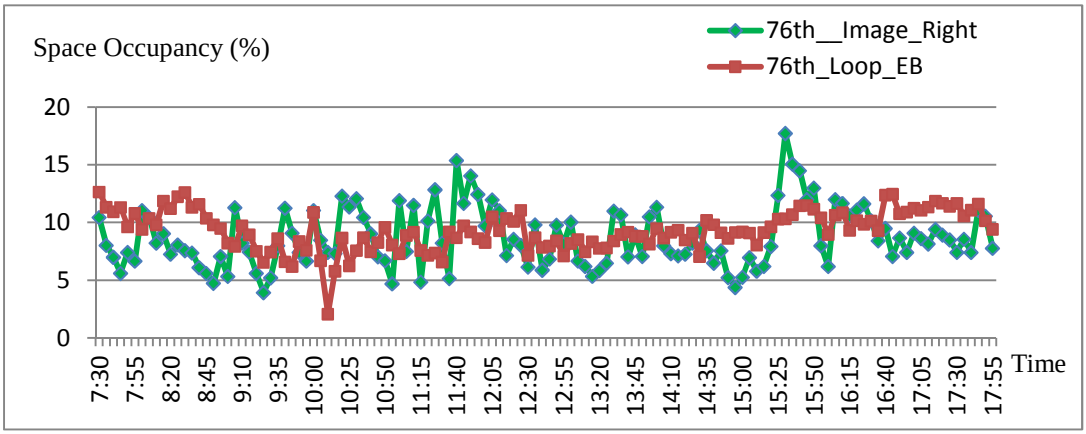

b. Traffic Occupancy of Eastbound

Figure 5.5 Occupancy Comparison (76th Street)

The estimated occupancies of the left side (westbound) of the roadway segment range from 2.56% to 14.56% between 7:30 AM and 6 PM. For the right side of the roadway, the eastbound, estimated occupancies ranged from 3.94% to 17.73%. There is not significant peak hour or traffic congestion on both roadway directions. The traffic status on this roadway segment is light or moderate in the day time. The estimated traffic status is consistent with the trend of the traffic data derived from the loop detector. The mean absolute errors (MAE) for westbound and eastbound comparing with loop detector data are 2.07% and 2.53% respectively.

5.1.3 84th Street

The camera at this site was located at the intersection of 84th St. and I-894 freeway. The geometry of this segment is three main lanes on each direction, and there is an auxiliary lane and on ramp on the right side. The left side of the roadway segment appeared much shorter than the right one since the camera view focused on the right side of the roadway. The traffic images were collected from 7:30 AM to 6:00 PM and the time interval between two successive images is 3 minutes.

Figure 5.6 shows the sample of image processing results of each module. Figure (a) is the original traffic image captured at this location. Figure (b) presents the detected roadway segment. Figure (c) is the detection region cropped from the original image. Figure (d) displays the vehicles extracted from the roadway segment. Figure (e) shows the result of the vehicle bottom area. Figure (f) presents the projection transformation result of the roadway and the extracted vehicles respectively. A total of 211 traffic still images were successfully performed by the model.

a.Original Image

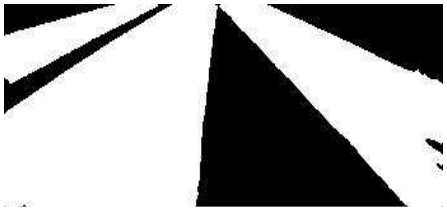

b.Detected Roadway

c. Detection Region

d.Vehicle Extraction

e.Vehicle Bottom Area

f. Roadway and Vehicle Projection Transformation

Figure 5.6 Sample of the Image Processing Results (84th St.)

Traffic occupancy and congestion status could be estimated based on the proposed model. The traffic occupancy and the difference between loop detector data are summarized in Appendix table A-5. Figure 5.7 presents the occupancy comparison between the estimated results and the loop detector data. In the figure, the X axis shows the time from 7:30 AM to 6:00 PM, and Y axis shows the space occupancy, the unit is percentage. The green curve represents the estimated occupancy and the red one is the field loop detector data.

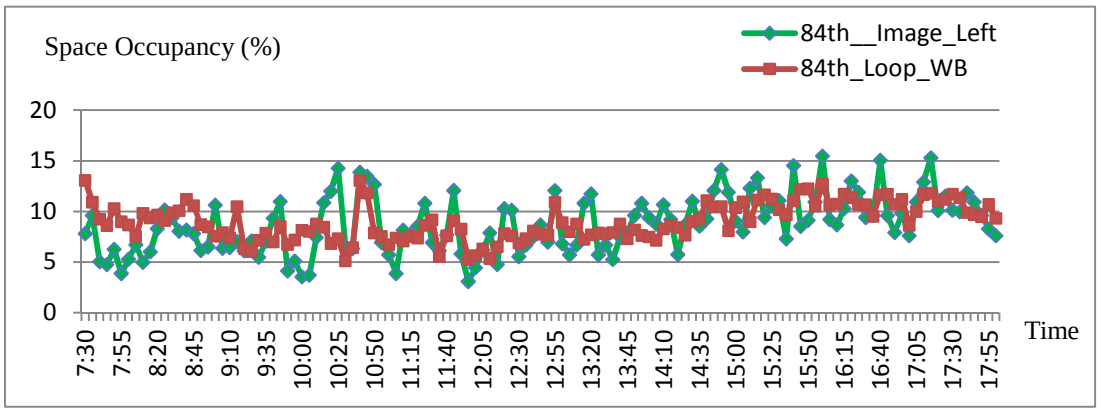

a. Traffic Occupancy of Westbound

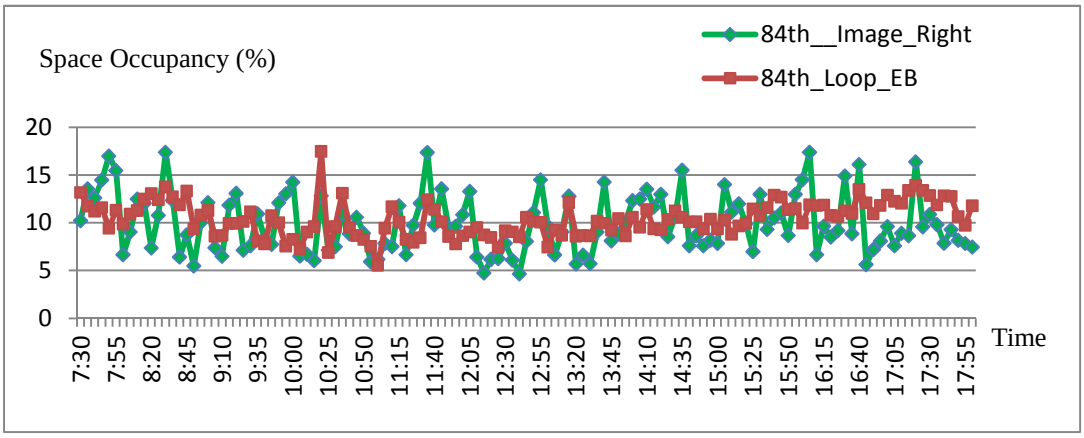

b. Traffic Occupancy of Eastbound

Figure 5.7 Occupancy Comparison (84th Street)

The figure shows that the estimated occupancies range from 3.08% to 15.47% between 7:30

AM and 6:00 PM for the left side of the roadway which is the westbound. In terms of the right side of the roadway, the estimated occupancies ranged from 4.67% to 17.4%. The traffic flow in both directions shows a light or moderate for most of the time. There is not significant traffic congestion state on this roadway segment during the day time. The estimated traffic condition is close to the traffic flow status derived from the loop detector. The mean absolute error (MAE) of westbound is 2.05%, and eastbound is 2.65%.

5.1.4 92nd Street

The roadway segment at 92nd street divided into two road branches. Both directions of the roadway have three lanes. A total of 211 traffic still images were collected from 7:30 AM to 6:00 PM. Figure 5.8 is the sample of image processing results from each module. Figure (a) shows the original traffic scene captured at this site. Figure (b) shows the detected roadway segment. Figure (c) is the detection region image. Figure (d) displays the vehicles extracted from the roadway segment. Figure (e) shows the result of the vehicle bottom area. Figure (f) presents the projection transformation result of the roadway and the extracted vehicles respectively. The traffic occupancy and congestion status could be estimated based on the traffic images.

The traffic occupancy and the difference between loop detector data are summarized in Appendix table A-6. Figure 5.9 presents the occupancy comparison between the estimated results and the loop detector data. In the figure, the X axis represents the time from 7:30 AM to 6:00 PM, and Y axis shows the space occupancy which the unit is percentage. The green curve represents the estimated occupancy and the red one is the field loop detector data.

a.Original Image

b.Detected Roadway

c. Detection Region

d.Vehicle Extraction

e.Vehicle Bottom Area

f. Roadway and Vehicle Projection Transformation

Figure 5.8 Sample of the Image Processing Results (92nd St.)

The figure shows that the estimated occupancies range from 2.83% to 15.4% between 7:30 AM and 6:00 PM for the left side of the roadway which is the westbound. In terms of the right side of the roadway, the estimated occupancies ranged from 2.6% to 19.35%. The traffic flow in both directions shows a light or moderate for most of the time. No significant traffic peak hour or congestion occurred on this roadway segment. The estimated traffic condition is consistent with the traffic flow data derived from the loop detector. The mean absolute errors (MAE) for westbound is 3.62% and for eastbound is 3.79%.

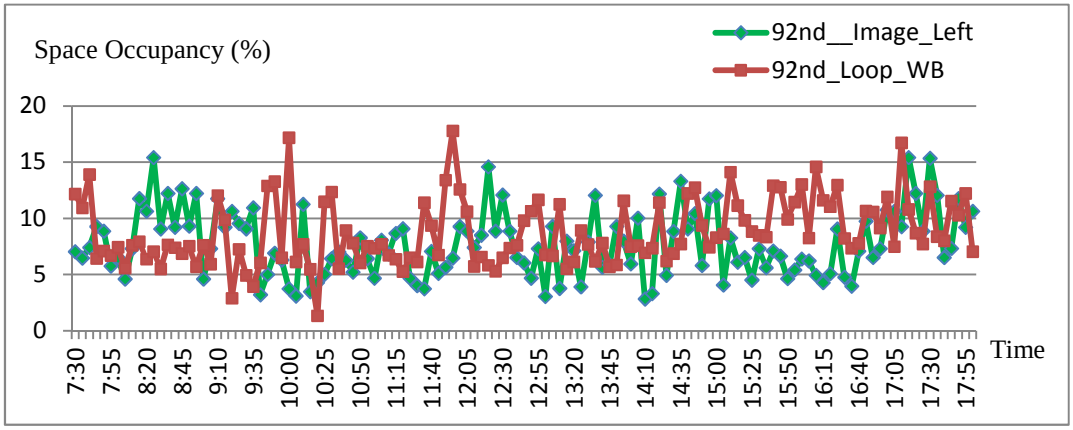

a. Traffic Occupancy of Westbound

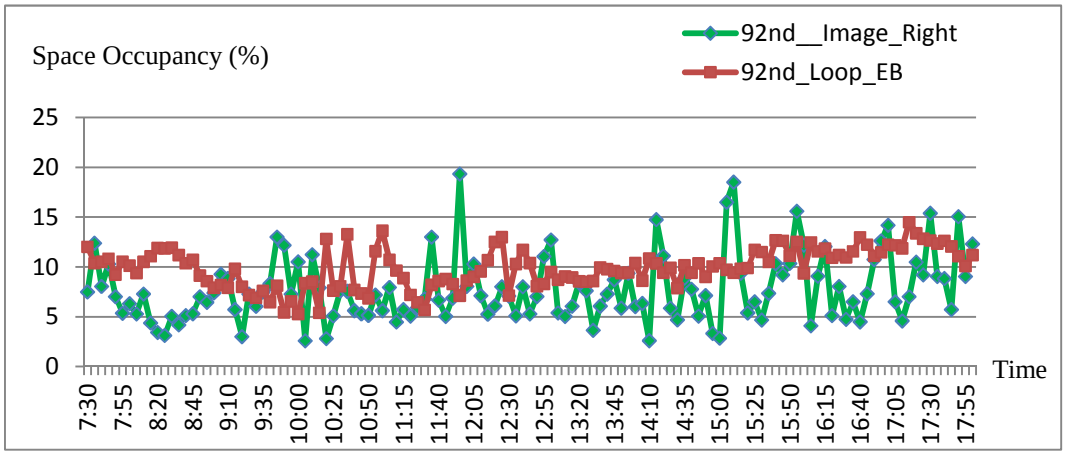

b. Traffic Occupancy of Eastbound

Figure 5.9 Occupancy Comparison (92nd Street)

5.3 Sensitivity Analysis

This chapter discusses the evaluation results of the proposed model applied to the traffic image data captured from four different locations on highway I-894 freeway corridor in Wisconsin. Estimated space occupancies and traffic conditions are reasonable and consistent with the records from the loop detector data. Overall, the methodology and model performed well. However, there are several factors and parameter settings would impact the model performance.

The proposed traffic detection model is consisted of three major modules. The most critical factors corresponding to each module are object shadow, vehicle occlusion and roadway geometry. When deploying the model to the real time traffic data, their influence are quite important for effective calibrating, tuning and maintaining the methodology. So far, there are still not perfect solutions to solve such image processing problems like object shadow. I shall conduct a qualitative analysis based on the image processing samples.

- Object shadow

Object shadow is the common limitation that associated with image processing. The shadows in the traffic image can be cast by buildings, trees and vehicles. The shadows will also be varied due to the illumination changes during the day time. We can handle part of this problem by extracting the vehicle bottom area. However, if under a strong illumination with significant shadows in the image, it is hard to remove the shadow as the long shadows will link together closed vehicles.

In Figure 5.10, from a to d, shows the shadow influence for vehicle separation. The red circle includes five vehicles which could be segmented correctly in the final results. But in the yellow circle, two vehicles link together due to the shadow and were recognized into one vehicle finally. In figure c and d, the detection result is longer and wider obviously comparing with the original vehicles.

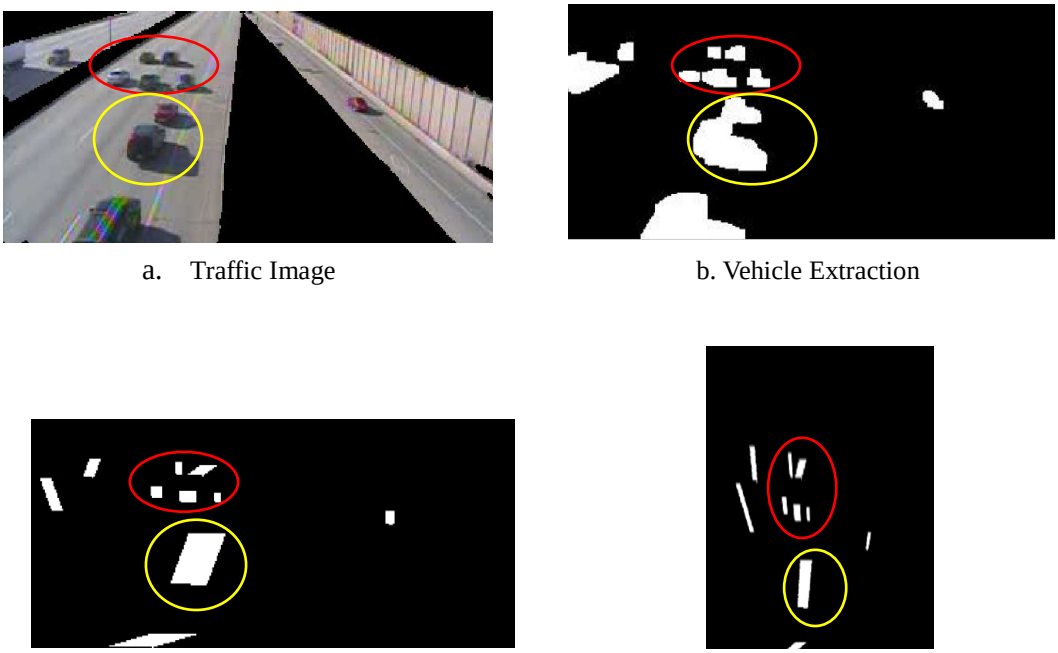

a. Traffic Image

b. Vehicle Extraction

c. Vehicle Bottom Area

d. Vehicle Projection Transformation

Figure 5.10 Object Shadow

- Vehicle occlusion

The accuracy of the proposed method mostly depends on the vehicle extraction quality. In order to extract the vehicles, several features are investigated including the vehicle shape, size, color and texture etc. Even the vehicle recognition could be accomplished successfully, the occluded vehicles may disturb the detection results.

Figure 5.11 indicated the vehicle occlusion impact. Two groups of occluded vehicles are labeled in the image by red and yellow circles respectively. In figure b, the vehicles could be extracted from the traffic image. However, they could not be divided due to occlusion. There are six vehicles labeled in figure a, but there are only three vehicles in figure b, c and d. The detected vehicles are larger obviously comparing with the original vehicles.

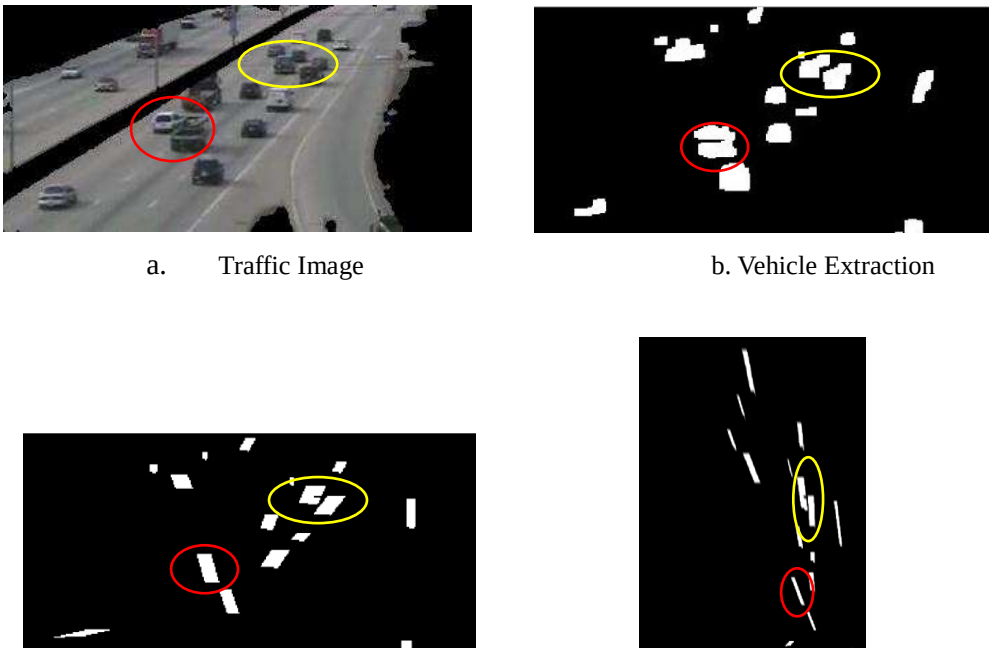

a. Traffic Image

b. Vehicle Extraction

c. Vehicle Bottom Area

d. Vehicle Projection Transformation

Figure 5.11 Vehicle Occlusion

- Roadway geometry

Roadway geometry especially the horizontal curve can affect the roadway projection transformation. Figure 5.12 shows a curved segment with divisions. The guideline of projection transformation is to convert the roadway segment into parallel if it is straight and symmetry. But if the roadway segment has curve or complex construction such as the division

or branch, the projection transformation may result in distortion.

a. Original Image b. Image Mask c. Projection Transformation

Figure 5.12 Roadway Geometry

The sensitivity analysis reveals that the model performance is sensitive to these factors. Further improvements are required to optimize the model algorithms.

CHAPTER 6 CONCLUSION AND FUTURE WORK

6.1 Summary of Research

The primary motivation of this research is to develop a novel traffic state detection model using the online stationary images. These traffic stationary images clipped from CCTV video data and published via DOT/511 website. The proposed model concentrates on stationary images instead of the successive video data to determine the traffic status. It could estimate the traffic space occupancy and make qualitative analysis on current traffic condition such as the light traffic or traffic congestion. The thesis consists of six chapters.

Chapter 1 introduces the ITS progress, the background of the video-based traffic detection and 511 traveler information project. Problem statement, the objectives and scope of research are also presented in this chapter.

Chapter 2 is the literature review providing the information of the previous studies using traffic video stream data to detect the traffic information. The generic image segmentation methods are also reviewed in this section, especially the algorithms for roadway and object detection.

The methodology and model architecture are given in Chapter 3. The model has three major modules including roadway detection module, vehicle detection module and projection transformation module. When the roadway and vehicles were identified, the projection

transformation will be applied to convert the traffic images from perspective projection into orthographic (parallel) projection. In order to improve the computational speed, the model will only process the detection regions instead of the entire image. The traffic space occupancy could be estimated based on the roadway length and total vehicle length. Finally, the traffic congestion status could be determined.

Chapter 4 presents the experimental design and model validation. The traffic image data acquisition and data processing procedure are described in detail in this part. The model calibration is divided into three parts, the calibration of multi-scale segmentation thresholds, the calibration of vehicle features extraction and projection transformation parameters calibration. Then experimental data were collected from I-894 Lincoln Ave. on September 27, 2009 in Milwaukee, Wisconsin.

To ensure the model performance, it is necessary to evaluate the detection algorithm under various roadway environments. In Chapter 5, the evaluation criteria and sensitive analysis are presented based on four different roadway segments on I-894 freeway corridor. The experimental results of the proposed model are analyzed and the measurement of the effectiveness is evaluated. The results indicate a reliable performance of the proposed model.

6.2 Conclusions

Video-based traffic surveillance is deployed broadly by Department of Transportation. However, most of the traffic video data are used for traffic monitor and could not provide

traffic flow measurements. The stationary traffic images which are available online would be a kind of new data source for traffic quantitative analysis. The primary contribution of this study is the development of a novel traffic detection model utilizing these stationary image data. The proposed model could provide an effective solution to detect traffic occupancy and congestion status. Traffic space occupancy is used as a reliable measurement for traffic quantitative analysis and congestion detection.

The adaptability was evaluated under different traffic status and illumination conditions using traffic images taken from four sites from 7:30 AM to 6:00 PM. Estimation of space occupancy depicted the traffic conditions reasonably. The proposed model successfully performed the traffic data taken from 60th St., 76th St., 84th St. and 92nd St. on freeway I-894 corridor where the roadway geometry and traffic flow conditions are different. The evaluation results indicated that the estimated occupancy is consistent with the records collected from the loop detector data at the same time and locations.

This research could contribute to both academic and industry fields. From an academic standpoint, I proposed a traffic detection model using the new data source which is available freely from the internet. A complete suite of algorithms for roadway detection, vehicle extraction and projection transformation have been developed. I provided a way to measure space occupancy which could not be measured directly in the field. The projection transformation method could eliminate the perspective distortion while the camera calibration parameters are unknown.

In terms of the application benefits in a practical perspective, the study addresses the problem of how to utilize the internet traffic data more efficiently for quantitative traffic state analysis. It could be a complement of loop detector data with quality issues (usually 20-30% bad data) and store longer for historical traffic study. The performance of the methodology could assist traffic manager to watching numerous monitors and reduce the human burden.

6.3 Future Work

Some improvements could be achieved based on the current traffic detection model. The short term future work for this study will focus on the proposed algorithms to optimize and improve the robustness of the model performance.

- Roadway detection algorithm

Existing roadway detection methods are primarily based on the image binary and mathematical morphology. As discussed in the sensitivity analysis, the traffic congestion or significant shadows are common limitations for image processing. The roadway detection and vehicle extraction from these situations either failed or contained a lot of noise. To increase the model robustness, a dynamic roadway boundary and median detection algorithm should be considered in the further study.

- Vehicle multiple feature investigation

The accuracy of the proposed method mostly depends on the vehicle extraction quality. Image processing is quite sensitive to the impacts of vehicle shadow and occlusion which could be an enhancement to the existing algorithm. The image texture feature will be useful in the vehicle segmentation. The integration of current work should be investigated more microscopic or macroscopic texture characteristics of vehicles.

- Projection transformation optimization

When conduct the projection transformation, we assume fixed camera position and angle with respect to the road in current research, no significant vertical deviation, zoom in or rotation. If the camera zoomed in for incidents, assume such changes are logged or identifiable. However, camera movements will often impact the field of view. In the future work, we will consider the projection transformation under camera zoom in or rotation situations.

At the application side of this research, a long term future work will consider the following research directions.

- Extending to arterial traffic dada

A benefit of the still traffic image is that it could be a complement of traffic data source where the other detector data is not available or has quality issues. Most of loop detectors were installed on the highways. For arterial and local streets, there are not such traditional loop detector data for quantitative traffic analysis. Comparing with the freeway mainline segments, the arterial and local streets are more complex as there are traffic signals and

control signs. There are also bike lanes, pedestrian pavement and bus stations for the roadway construction. Nowadays, more and more CCTV cameras were installed on the urban major arterials and intersection to monitor the traffic status. These image data could be collected and used to detect the arterial traffic flow patterns in the future work.

- Traffic incidents detection

It is possible to detect the traffic incidents taking advantages of the CCTV traffic image data which are distributed broadly. If the traffic occupancy is very high or congestion occurred during non peak hours, the traffic manager should pay attention to the special roadway segment. This would be helpful to assist traffic management or police to response quickly with abnormal traffic conditions.

- Detecting traffic on network level combining with remote sensing image

Due to the data source limitations, remote sensing images are not considered as a reliable input in this research. The research focused on each location separately and only tested four roadway segments. When high frequency and resolution RS data is available, fusion of the two data sources can possibly be implemented. The expansion of the proposed model combining with the growing remote sensing technologies could detect the traffic pattern on the network level.

REFERENCES

Badenas, J. M. Bober, F. Pla (2001), Segmenting traffic scenes from grey level and motion information, Pattern Analysis and Applications 4, 28–38.

Badenas, J., Sanchiz, J.M. and Pla, F. (2001), Motion-based segmentation and region tracking in image sequences, Pattern Recognition 34, 661–670.

Bensrhair, M., Bertozzi, A., Broggi, P., Mich´e, S. Mousset, and Toulminet, G. (2001), A cooperative approach to vision-based vehicle detection, in Proceedings of IEEE International Conference on Intelligent Transportation Systems, pp. 209–214.

Bertozzi, M. and Broggi, A. (1998), A parallel real-time stereo vision system for generic obstacle and lane detection, IEEE Transaction Image Processing 7 (1).

Beucher, S. and Bilodeau, M. (1994), Road segmentation and obstacle detection by a fast watershed transform, Proceedings of IEEE Intelligent Vehicles 94, 296–301.

Beymer, D., McLauchlan, P., Coifman B. and Malik, J. (1997), A real time computer vision system for measuring traffic parameters, in Proceedings of the IEEE Conference on Computer Vision and Pattern Recognition, pp. 495-501.

Bose B. and Grimson, E. (2004), Improving object classification in far-field video, In proceedings of the 2004 IEEE Computer Society Conference on Computer Vision and Pattern Recognition.

Broggi (1995), Parallel and local feature extraction: a real-time approach to road boundary detection, IEEE Transaction on Image Processing 4 (2), 217–223.

Buch, N., Orwell, J. and Velastin, S.A. (2010), Urban Road User Detection and Classification using 3D Wire Frame Models, IET Computer Vision Journal, 4(2) IET, June, pp. 105-116.

Bullock, Darcy, Garrett Jr. James, Hendrickson, Chris (1993), A neural network for image-based vehicle detection, Transportation Research Part C: Emerging Technologies, Volume 1, Issue 3, September, Pages 235-247

Cheung, S.C. and Kamath, C. (2004), Robust techniques for background subtraction in urban traffic video, Proceedings of SPIE, Volume 5308, pp. 881-892.

Chi, Hongbo, Lu, Chenxi, Zhao, Fang and Shen, David L. (2009), Vehicle Detection from Satellite Images, Journal of the Transportation Research Board, No. 2105, pp. 109-117.

Cho, Young (2006), Estimating velocity fields on a freeway from low resolution video, Diss. University of California, Berkeley, 3253808.

Coifmana, Benjamin, Beymerb, David, McLauchlanb, Philip and Malikb, Jitendra (1998.), A real-time computer vision system for vehicle tracking and traffic surveillance, Transportation Research Part C, 271-288.

Dailey, Daniel J. and Li, Li, (2000), Algorithm for Estimating Mean Traffic Speed with Uncalibrated Cameras, Journal of the Transportation Research Board, No. 1719, pp. 27-32.

Fathy, M. and Siyal, M.Y. (1998), A window-based image processing technique for quantitative and qualitative analysis of road traffic parameters, IEEE Transactions on Vehicular Technology 47 (4).

Fathy, M., Siyal, M.Y. (1995), An image detection technique based on morphological edge detection and background differencing for real-time traffic analysis, Pattern Recognition

Letters, Volume 16, Issue 12, Pages 1321-1330.

Fung, G., Yung, N. and Pang, G. (2003), Camera calibration from road lane markings, Opt. Eng., 42(10), 2967-2977.

Gonzalez, Rafael C. and Woods, Richard E. (2002), Digital Image Processing, 2nd Edition, Prentice Hall.

Gupte, S., Masoud, O., Martin, R.F.K., Papanikolopoulos, N.P. (2004), Detection and classification of vehicles, Intelligent Transportation Systems, IEEE Transactions on Volume: 3 , Issue: 1, Page(s): 37 – 47.

Hall, F. L. (1996), Traffic stream characteristics, In Gartner, N. Messer, C. and Rathi, A. editors, Traffic Flow Theory, US Federal Highway Administration.

Hickman, Angel, M., Mirchandani, P. and Chandnani, D. (2003), Methods of analyzing traffic imagery collected from aerial platforms, IEEE Transactions on Intelligent Transportation Systems, 4(2), pp. 99-107.

Jin, Xiaoying & Davis, Curt H. (2007), Vehicle detection from high-resolution satellite imagery using morphological shared-weight neural networks. Image Vision Comput., 25(9): 1422-143.

Jung, Claudio Rosito (2003), Multi-scale image segmentation using wavelets and watersheds, IEEE Symp, Computer Graphics and Image Processing, pp.278–284.

Jung, Y.K. and Ho, Y.S. (2001), A feature-based vehicle tracking system in congested traffic video sequences, Springer, Berlin, pp.190–197.

Kang, Wen-Xiong, Yang, Qing-Qiang, Liang, Run-Peng (2009), The Comparative Research

on Image Segmentation Algorithms, First International Workshop on Education Technology and Computer Science.

Kanhere, N.K and Birchfield, S.T. (2008), Real-Time Incremental Segmentation and Tracking of Vehicles at Low Camera Angles Using Stable Features, Intelligent Transportation Systems, IEEE Transactions on Volume: 9 , Issue: 1, Page(s): 148 – 160.

Kanhere, Neeraj K., Birchfield, Stanley T. and Sarasua, Wayne A. (2008), Automatic Camera Calibration Using Pattern Detection for Vision-Based Speed Sensing, Journal of the Transportation Research Board, No. 2086, pp. 30–39.

Kastrinaki, V., Zervakis, M., Kalaitzakis, K. (2003), A survey of video processing techniques for traffic applications, Image and Vision Computing, 21, 359–381.

Kim, J.B., Park, H.S., Park, M.H. and Kim, H.J. (2001), A real-time region-based motion segmentation using adaptive thresholding and K-means clustering, Springer, Berlin, pp. 213–224.

Kim, Z. and Malik, J. (2003), Fast vehicle detection with probabilistic feature groping and its application to vehicle tracking, in Proceedings of the 9th IEEE International Conference on Computer Vision, 1, pp. 524-531.

Klausmann, P., Kroschel, K. and Willersinn, D. (1999), Performance prediction of vehicle detection algorithms, Pattern Recognition 32, 2063–2065.

Kluge, K. and Lakshmanan, S. (1995), A deformable-template approach to lane detection, IEEE Proceedings of Intelligent Vehicles 95, 54–59.

Koller, D., Daniilidis, K. and Nagel, H. (1993), Model-based object tracking in monocular image sequences of road traffic scenes, International Journal Computer Vision 10, 257–281.

Kreucher, C. and Lakshmanan, S. (1999), A lane extraction algorithm that uses frequency domain features, IEEE Transactions on Robotics and Automation 15 (2).

Lee, W. and Ran, B. (2006), Real-Time Background Generation and Update Using Online CCTV Video. Proceedings of Applications of Advanced Technologies in Transportation (AATT), June 2006.

Lee, Woochul (2006), Developing an image sensor system (ISENS) for real-time traffic surveillance using online CCTV videos, Diss. University of Wisconsin-Madison, 3234695.

Liu, Ping (2004), A survey on threshold selection of image segmentation, Journal of Image and Graphics, pp.86–92.

Malinovskiy, Yegor, Wu, Yao-Jan and Wang, Yinhai (2009), Video-Based Vehicle Detection and Tracking Using Spatiotemporal Maps, Journal of the Transportation Research Board, No.2121, pp. 81-89.

O'Kelly, Morton, Matisziw, Timothy, Li, Ron, Merry, Carolyn, Niu, Xutong (2005), Identifying truck correspondence in multi-frame imagery, Transportation Research Part C: Emerging Technologies, Volume 13, Issue 1, Pages 1-17

Otsu, N., (1979). A threshold selection method from gray-level histograms, IEEE Trans. Sys., Man., Cyber. 9 (1): 62–66

Palubinskas, G., Kurz F. and Reinartz, P. (2010), Model based traffic congestion detection in optical remote sensing imagery, Eur. Transp. Res. Rev. 2:85–92.

Paragios, N. and Deriche, R. (2000), Geodesic active contours and level sets for the detection and tracking of moving objects, IEEE Transactions on Pattern Analysis and Machine Intelligence 22 (3), 266–280.

Pumrin, Suree (2002), A framework for dynamically measuring mean vehicle speed using un-calibrated cameras, Diss. University of Washington, 3072126.

Robinson, D. J., Redding, N. J., and Crisp, D. J. (2002), Implementation of a fast algorithm for segmenting SAR imagery, Scientific and Technical Report, Australia: Defense Science and Technology Organization.

Schoepflin, Todd N. and Dailey, Daniel J. (2003), Correlation Technique for Estimating Traffic Speed from Cameras, Journal of the Transportation Research Board, No. 1 1855, 66-73.

Schoepflin, Todd Nelson (2003), Algorithms for estimating mean vehicle speed using un-calibrated traffic management cameras, Diss. University of Washington, 3111129.

Stauffer, C. and Grimson, W. (2000), Learning patterns of activity using real-time tracking, IEEE Transactions on Pattern Analysis and Machine Intelligence, 22, pp. 747-757.

Sullivan, G.D., Baker, K.D., Worrall, A.D., Attwood, C.I. and Remagnino, P.M. (1997), Model-based vehicle detection and classification using orthographic approximations, Image and Vision Computing 15, 649–654.

Tan, Sovira, Dale, Jason L., Anderson, Andrew and Johnston, Alan (2006), Inverse perspective mapping and optic flow: A calibration method and a quantitative analysis. Image Vision Comput., 24(2): 153-165.

Techmer, A. (2001), Real-time motion based vehicle segmentation in traffic lanes, Springer, Berlin, pp. 202–207.

Wang, J. and Miller, R. (2005), Overtaking vehicle detection using dynamic and quasi-static background modeling, in Proceeding of IEEE Computer Society Conference on Computer Vision and Pattern Recognition, 3, pp.64-71.

Wang, Qiaoping (1998), One image segmentation technique based on wavelet analysis in the context of texture, Data Collection and Processing, vol.13, pp.1216.

Wang, Y., Shen, D. and Teoh, E.K. (1994), Lane detection using spline model, Pattern Recognition Letters 21, 677–689.

Yu, X., Beucher, S. and Bilodeu, M. (1992), Road tracking, lane segmentation and obstacle recognition by mathematical morphology, Proceedings of IEEE Intelligent Vehicles 92, 166–170.

Yuille, A.L. and Coughlan, J.M. (2000), Fundamental limits of Bayesian inference: order parameters and phase transitions for road tracking, IEEE Pattern Analysis and Machine Intelligence 22 (2), 160–173.

Zhang, Guohui, Avery, Ryan P. and Wang, Yinhai (2007), Video-Based Vehicle Detection and Classification System for Real-Time Traffic Data Collection Using Uncalibrated Video Cameras, Journal of the Transportation Research Board, No. 1993, pp. 138-147.

Zhang, Xu, Forshaw, M.R.B. (1997), A parallel algorithm to extract information about the motion of road traffic using image analysis , Transportation Research Part C: Emerging

Technologies, Volume 5, Issue 2, Pages 141-152

APPENDIX:

Table A-1 Traffic Monitor Cameras Online in U.S. States

State	Cameras statewide	Update (min)	Website
Alabama	158	Video	http://alitsweb.dot.state.al.us/its/
Alaska	55	10	http://511.alaska.gov/alaska511/mappingcomponent
Arizona	230	5	http://www.az511.com/adot/files/cameras/
Arkansas	-	-	Under construction
California	1,365	Video	http://quickmap.dot.ca.gov/
Colorado	384 & 48 Videos	10	http://www.cotrip.org/device.htm
Connecticut	280	3 sec	http://www.ct.gov/dot/cwp/view.asp?a=2354&Q=290242&dotNav=|
Delaware	150	Video	http://www.deldot.gov/traffic/map.ejs
Florida	-	-	http://www.fl511.com/Cameras.aspx
Georgia	Over 500	2	http://www.georgia-navigator.com/traffic/cam.php
Hawaii	-	-	Under construction
Idaho	147 & 46 videos	15	http://lb.511.idaho.gov/idlb/
Illinois	-	-	Under construction
Indiana	115	5	http://www.in.gov/indot/2420.htm
Iowa	176	5	http://lb.511ia.org/ialb/
Kansas	33 statewide & 28 in Wichita Metro	2	http://511.ksdot.org/KanRoadPublic/Default.aspx
Kentucky	150	1	http://511.ky.gov/kylb/
Louisiana	140	5	http://lb.511la.org/lalbweb/cameras/routeselect.jsf?view=state&text=m&textOnly=false
Maine	27	5	http://www.511maine.gov/cameras.htm
Maryland	-	-	http://www.md511.org/traffic.aspx?showCameras=true
Massachusetts	-	10 sec	http://www.mass511.com/preferences.sws
Michigan	-	-	http://mdotnetpublic.state.mi.us/drive/default.aspx
Minnesota	500 in Minneapolis and 60 in Duluth,	1	http://hb.511mn.org/main.jsf

	Rochester and St. Cloud.		
Mississippi	379	5 sec	http://www.mdottraffic.com/
Missouri	-	-	http://maps.modot.mo.gov/timi/
Montana	-	-	http://www.mdt.mt.gov/travinfo/weather/rwis_google.shtml
Nebraska	160	3-30	http://www.511.nebraska.gov/atis/html/index.html
Nevada	385 statewide (20 in Reno & 8 in Elko area)	-	http://www.nevadadot.com/Traveler_Info/Traffic_Cameras/Traffic_Cameras.aspx http://bugatti.nvfast.org/PMMS/CCTVs.aspx
New Hampshire	44	-	Do not publish online
New Jersey	-	1-2	http://www.511nj.org/cameras.aspx?default=NJ%20Turnpike%20Tour
New Mexico	89	10 sec	http://nmroads.com/
New York	-	30-60 sec	http://www.511ny.org/mapview.aspx?custommap=true&layers=cctv
North Carolina	-	-	Under construction
North Dakota	39 (32 DOT owned, 7 leased to LiveView)	10	http://www.dot.nd.gov/travel-info-v2/
Ohio	350	5 sec	http://www.dot.state.oh.us/districts/D02/TrafficCameras/Pages/default.aspx
Oklahoma	-	Video	http://www.oktraffic.org/map.php?location=statewide#
Oregon	310	2	http://www.tripcheck.com/Pages/CamerasEntry.asp
Pennsylvania	662 (647 are public facing)	3 sec	http://www.511pa.com/Traffic.aspx?ShowCameras=true
Rhode Island	115	20 sec	http://www.tmc.dot.ri.gov/camcenter/camcentermapview.aspx#
South Carolina	348	5	http://206.74.144.28/getting/cams/index.asp
South Dakota	-	-	Under construction
Tennessee	425	5	http://ww2.tdot.state.tn.us/tsw/smartmap.htm
Texas	-	2 sec	http://www.dot.state.tx.us/travel/traffic_cameras.htm

Utah	over 900	3-5	http://www.utahcommuterlink.com/
Vermont	24	5	http://511.vermont.gov/main.jsf
Virginia	-	Video	http://www.511virginia.org/
Washington	850	1.5-30	http://www.wsdot.com/traffic/Cameras/default.aspx
West Virginia	25	Video	Http://www.wv511.org
Wisconsin	203	3	http://www.511wi.gov/Web/map.aspx?region=southwest
Wyoming	104	3-10	http://map.wyoroad.info/hi.html?cp=1&co=0&al=0

Table A-2 Traffic Data of Lincoln Avenue (Unit: %)

	NB			SB		
Time	Estimated Occupancy	Loop Detector Occupancy	Error	Estimated Occupancy	Loop Detector Occupancy	Error
7:30	26.34	28.27	1.93	18.82	8.97	9.85
7:35	27.78	29.65	1.87	16.85	7.15	9.69
7:40	28.99	32.84	3.85	14.30	8.20	6.10
7:45	30.01	31.79	1.78	13.72	8.35	5.37
7:50	30.69	31.92	1.23	15.60	8.66	6.95
7:55	29.39	30.57	1.18	17.06	7.60	9.46
8:00	28.15	29.48	1.33	11.70	8.53	3.17
8:05	28.73	30.75	2.02	15.26	7.99	7.27
8:10	32.49	28.13	4.36	14.28	7.77	6.51
8:15	32.91	25.36	7.55	16.45	8.56	7.88
8:20	27.94	21.58	6.36	17.82	8.15	9.67
8:25	25.34	16.82	8.52	15.70	7.21	8.49
8:30	28.99	25.73	3.26	16.76	7.57	9.19
8:35	25.87	17.56	8.31	12.65	7.54	5.10
8:40	14.34	12.53	1.81	16.63	7.71	8.92
8:45	15.24	16.38	1.14	13.63	10.02	3.61
8:50	17.20	13.15	4.05	17.13	8.42	8.71
8:55	19.75	18.64	1.11	18.85	8.49	10.36
9:00	13.65	10.37	3.28	17.73	8.34	9.39
9:05	14.76	10.44	4.32	16.18	7.05	9.13
9:10	16.19	11.28	4.91	15.68	7.78	7.90
9:15	16.83	11.46	5.37	11.35	7.59	3.74
9:20	12.38	9.66	2.72	11.23	8.56	2.67

9:25	19.84	11.63	8.21	20.02	8.12	11.90
9:30	18.57	12.57	6.00	17.58	7.37	10.21
9:35	13.86	12.24	1.62	15.05	6.97	8.08
9:40	17.20	12.28	4.92	15.43	7.27	8.17
9:45	15.50	11.73	3.77	13.67	7.40	6.27
9:50	20.37	11.69	8.68	15.39	8.03	7.36
9:55	13.27	10.65	2.62	12.77	6.85	5.92
10:00	14.29	10.53	3.76	11.79	6.43	5.36
10:05	16.40	9.68	6.72	15.73	6.56	9.18
10:10	12.75	15.42	2.67	13.72	8.35	5.37
10:15	13.65	8.47	5.18	11.42	7.02	4.40
10:20	14.87	8.82	6.05	8.66	7.40	1.26
10:25	15.98	11.80	4.18	10.55	8.13	2.41
10:30	19.52	9.62	9.90	12.05	8.03	4.01
10:35	13.49	10.67	2.82	15.78	8.19	7.59
10:40	12.59	13.83	1.24	18.35	7.77	10.58
10:45	16.83	10.75	6.08	16.93	7.79	9.15
10:50	15.66	8.50	7.16	16.93	8.30	8.63
10:55	15.08	9.36	5.72	18.09	9.01	9.08
11:00	16.67	10.17	6.50	16.59	7.72	8.87
11:05	13.49	10.75	2.74	17.55	8.78	8.77
11:10	14.71	11.40	3.31	18.86	9.36	9.50
11:15	13.70	12.85	0.85	16.25	8.40	7.85
11:20	15.61	12.64	2.97	15.60	8.20	7.40
11:25	12.43	10.65	1.78	14.27	8.58	5.70
11:30	15.13	8.70	6.43	11.70	8.92	2.78
11:35	13.12	10.80	2.32	18.73	8.52	10.21
11:40	9.68	9.57	0.11	17.10	9.08	8.02
11:45	12.96	7.23	5.73	16.98	8.54	8.43
11:50	15.19	7.65	7.54	15.69	10.84	4.85
11:55	13.60	8.14	5.46	12.69	6.89	5.80
12:00	9.15	11.52	2.37	14.36	9.25	5.11
12:05	10.26	10.30	0.04	10.20	9.45	0.75
12:10	12.28	11.47	0.81	14.32	8.06	6.26
12:15	18.47	10.82	7.65	20.58	9.21	11.37
12:20	13.81	10.25	3.56	20.13	9.70	10.43
12:25	13.17	8.96	4.21	19.73	9.14	10.59
12:30	15.32	9.74	5.58	21.48	9.92	11.55
12:35	14.27	8.75	5.52	19.05	8.68	10.37
12:40	13.76	8.51	5.25	20.13	8.25	11.88
12:45	17.32	9.86	7.46	16.32	8.62	7.70
12:50	18.41	9.52	8.89	21.99	9.05	12.94
12:55	13.33	9.63	3.70	18.43	8.70	9.73

13:00	13.23	11.92	1.31	19.80	10.69	9.11
13:05	16.03	10.85	5.18	20.31	9.83	10.47
13:10	19.95	11.13	8.82	18.06	9.91	8.15
13:15	15.61	11.40	4.21	16.11	10.13	5.97
13:20	15.56	10.92	4.64	21.63	9.58	12.06
13:25	18.57	9.74	8.83	19.33	8.93	10.40
13:30	15.66	10.86	4.80	18.30	7.96	10.35
13:35	15.71	10.42	5.29	14.70	8.68	6.03
13:40	16.46	11.38	5.08	18.43	10.03	8.40
13:45	19.05	11.32	7.73	22.86	10.54	12.32
13:50	15.87	10.75	5.12	21.78	9.36	12.42
13:55	17.02	10.21	6.81	19.03	9.92	9.11
14:00	18.15	10.16	7.99	20.02	9.28	10.74
14:05	14.18	9.54	4.64	19.66	8.99	10.67
14:10	14.39	12.57	1.82	21.23	10.59	10.65
14:15	13.57	11.76	1.81	17.15	10.44	6.70
14:20	11.64	10.53	1.11	16.08	10.19	5.89
14:25	14.76	11.80	2.96	20.32	10.31	10.01
14:30	15.03	10.93	4.10	23.11	11.22	11.88
14:35	16.50	10.95	5.55	23.19	11.17	12.02
14:40	18.57	11.57	7.00	20.02	11.34	8.68
14:45	18.78	11.14	7.64	22.61	11.79	10.82
14:50	20.63	11.90	8.73	20.01	11.24	8.76
14:55	15.27	10.85	4.42	21.02	11.45	9.57
15:00	14.13	10.73	3.40	20.76	10.39	10.37
15:05	16.53	11.65	4.88	21.86	10.87	11.00
15:10	21.01	13.42	7.59	21.39	13.48	7.91
15:15	15.56	10.68	4.88	21.95	13.20	8.75
15:20	15.61	12.35	3.26	20.92	12.68	8.24
15:25	20.55	13.46	7.09	21.08	13.17	7.91
15:30	13.02	11.83	1.19	23.05	12.75	10.30
15:35	18.78	10.52	8.26	21.60	12.72	8.88
15:40	15.16	10.86	4.30	18.99	13.16	5.83
15:45	10.05	12.93	2.88	21.89	12.84	9.05
15:50	17.82	13.75	4.07	19.68	14.14	5.53
15:55	17.53	12.10	5.43	16.63	12.74	3.89
16:00	16.57	12.83	3.74	14.32	12.63	1.68
16:05	16.93	12.96	3.97	17.40	11.55	5.86
16:10	13.12	10.34	2.78	19.29	14.37	4.92
16:15	15.13	11.93	3.20	21.69	13.15	8.54
16:20	14.75	12.27	2.48	16.33	13.22	3.11
16:25	12.06	13.75	1.69	18.90	15.20	3.70
16:30	15.94	11.82	4.12	17.62	13.70	3.92

16:35	17.89	12.60	5.29	17.96	12.65	5.31
16:40	15.68	9.57	6.11	16.80	13.92	2.88
16:45	19.28	11.35	7.93	15.39	13.57	1.82
16:50	14.13	11.52	2.61	13.16	14.81	1.65
MAE			4.51			7.62

Table A-3 Traffic Data of 60th Street (Unit: %)

	WB			EB		
Time	Estimated Occupancy	Loop Detector Occupancy	Error	Estimated Occupancy	Loop Detector Occupancy	Error
7:30	17.78	13.29	4.49	11.48	11.90	0.42
7:35	17.13	11.27	5.86	20.05	11.38	8.67
7:40	22.31	10.98	11.33	9.64	10.53	0.89
7:45	21.67	11.73	9.94	10.12	10.41	0.29
7:50	14.91	12.17	2.74	11.36	9.15	2.21
7:55	9.54	10.69	1.15	18.89	10.84	8.05
8:00	21.30	10.66	10.64	11.48	8.24	3.24
8:05	19.17	10.83	8.34	7.90	9.57	1.67
8:10	15.37	10.48	4.89	11.21	9.03	2.18
8:15	16.39	9.68	6.71	16.67	10.23	6.44
8:20	11.12	13.36	2.24	11.12	9.41	1.71
8:25	14.40	10.64	3.76	9.26	9.65	0.39
8:30	20.37	11.29	9.08	19.01	8.84	10.17
8:35	18.43	11.48	6.95	15.31	9.24	6.07
8:40	22.96	12.60	10.36	13.70	10.57	3.13
8:45	7.41	10.48	3.07	8.52	9.83	1.31
8:50	18.70	11.05	7.65	12.35	9.10	3.25
8:55	24.07	10.12	13.95	15.68	10.39	5.29
9:00	17.50	9.58	7.92	17.05	8.46	8.59
9:05	14.05	8.48	5.57	8.52	7.62	0.90
9:10	20.46	9.59	10.87	12.50	8.63	3.87
9:15	18.43	10.36	8.07	15.68	9.08	6.60
9:20	22.31	10.08	12.23	11.98	9.58	2.40
9:25	25.00	10.17	14.83	12.47	12.90	0.43
9:30	17.96	8.45	9.51	11.73	5.62	6.11
9:35	16.10	14.39	1.71	21.10	10.17	10.93
9:40	18.82	10.64	8.18	11.85	7.26	4.59
9:45	21.39	9.55	11.84	5.06	6.34	1.28
9:50	19.44	10.08	9.36	14.40	7.10	7.30
9:55	17.87	9.18	8.69	9.51	6.53	2.98

10:00	17.69	11.84	5.85	17.28	7.09	10.19
10:05	11.67	8.88	2.79	15.80	6.82	8.98
10:10	13.00	8.27	4.73	11.90	7.47	4.43
10:15	12.87	8.57	4.30	15.56	8.54	7.02
10:20	16.39	5.33	11.06	8.64	8.05	0.59
10:25	17.13	6.59	10.54	10.07	7.41	2.66
10:30	12.50	9.95	2.55	18.64	11.05	7.59
10:35	13.06	7.52	5.54	8.02	9.83	1.81
10:40	16.20	6.16	10.04	15.84	7.64	8.20
10:45	20.58	10.50	10.08	12.01	8.64	3.37
10:50	22.37	12.30	10.07	19.05	9.12	9.93
10:55	16.35	11.67	4.68	20.12	8.79	11.33
11:00	10.74	10.89	0.15	13.46	8.64	4.82
11:05	7.50	8.59	1.09	15.80	7.50	8.30
11:10	7.78	6.27	1.51	13.09	7.51	5.58
11:15	8.90	6.97	1.93	17.13	6.18	10.95
11:20	10.05	7.24	2.81	10.16	4.53	5.63
11:25	10.15	5.60	4.55	12.75	7.09	5.66
11:30	5.41	2.89	2.52	17.91	10.87	7.04
11:35	10.20	8.90	1.30	16.84	7.07	9.77
11:40	15.07	10.50	4.57	17.95	7.37	10.58
11:45	12.65	10.13	2.52	16.42	6.57	9.85
11:50	12.30	8.75	3.55	14.69	6.87	7.82
11:55	10.89	5.41	5.48	16.05	7.13	8.92
12:00	15.22	10.30	4.92	13.46	7.97	5.49
12:05	16.19	14.65	1.54	12.05	6.56	5.49
12:10	15.00	16.19	1.19	17.78	6.16	11.62
12:15	15.20	13.50	1.70	16.67	7.25	9.42
12:20	12.53	14.13	1.60	17.65	6.87	10.78
12:25	11.02	12.65	1.63	10.86	7.75	3.11
12:30	16.67	15.22	1.45	8.64	7.91	0.73
12:35	11.60	12.80	1.20	13.70	7.18	6.52
12:40	12.30	7.57	4.73	16.05	6.84	9.21
12:45	10.28	8.58	1.70	10.74	7.58	3.16
12:50	16.48	9.56	6.92	13.09	7.95	5.14
12:55	10.83	10.12	0.71	11.94	6.47	5.47
13:00	11.94	12.02	0.08	13.30	6.83	6.47
13:05	13.33	10.39	2.94	16.70	8.23	8.47
13:10	11.10	9.63	1.47	17.52	8.49	9.03
13:15	10.37	9.83	0.54	15.30	8.88	6.42
13:20	11.67	9.77	1.90	12.59	7.24	5.35
13:25	18.06	9.26	8.80	10.80	7.78	3.02
13:30	10.28	8.98	1.30	12.35	8.02	4.33

13:35	16.48	10.68	5.80	10.21	8.79	1.42
13:40	10.83	10.25	0.58	10.03	9.94	0.09
13:45	11.94	9.80	2.14	13.19	8.71	4.48
13:50	13.30	10.43	2.87	13.00	9.20	3.80
13:55	11.20	9.69	1.51	15.16	7.60	7.56
14:00	10.37	7.49	2.88	17.41	9.10	8.31
14:05	11.90	9.37	2.53	11.37	8.29	3.08
14:10	13.35	11.20	2.15	12.30	10.21	2.09
14:15	11.31	10.22	1.09	14.52	10.03	4.49
14:20	15.10	10.60	4.50	11.05	7.92	3.13
14:25	12.35	9.55	2.80	15.42	10.07	5.35
14:30	14.27	10.91	3.36	10.28	7.16	3.12
14:35	17.50	12.14	5.36	13.69	9.78	3.91
14:40	16.00	13.00	3.00	11.41	10.50	0.91
14:45	11.50	12.65	1.15	16.09	8.15	7.94
14:50	17.25	11.30	5.95	10.83	8.81	2.02
14:55	18.20	11.18	7.02	9.50	8.79	0.71
15:00	16.58	12.04	4.54	11.49	8.88	2.61
15:05	15.07	13.12	1.95	12.31	8.59	3.72
15:10	15.83	12.13	3.70	10.18	8.02	2.16
15:15	16.27	15.50	0.77	9.08	8.58	0.50
15:20	17.41	13.82	3.59	9.27	8.75	0.52
15:25	16.05	14.15	1.90	12.47	9.53	2.94
15:30	19.00	11.23	7.77	10.98	9.70	1.28
15:35	16.85	12.13	4.72	20.71	11.21	9.50
15:40	17.35	13.95	3.40	18.79	10.34	8.45
15:45	16.25	15.55	0.70	15.30	11.82	3.48
15:50	18.50	15.09	3.41	13.05	10.18	2.87
15:55	15.07	13.94	1.13	12.95	9.88	3.07
16:00	13.30	15.16	1.86	15.04	9.27	5.77
16:05	11.11	12.71	1.60	13.75	9.47	4.28
16:10	13.37	14.05	0.68	14.20	10.98	3.22
16:15	10.37	13.63	3.26	15.87	10.71	5.16
16:20	17.65	14.75	2.90	20.09	9.85	10.24
16:25	15.86	13.38	2.48	21.94	9.32	12.62
16:30	16.05	12.37	3.68	18.77	10.45	8.32
16:35	17.40	13.58	3.82	13.09	8.74	4.35
16:40	16.85	12.98	3.87	11.95	11.23	0.72
16:45	18.20	13.84	4.36	21.04	11.13	9.91
16:50	15.37	13.73	1.64	13.35	10.42	2.93
16:55	11.94	12.04	0.10	11.20	9.98	1.22
17:00	13.35	11.29	2.06	10.86	9.69	1.17
17:05	11.10	14.01	3.91	22.72	11.41	11.31

17:10	10.37	13.58	3.21	16.79	11.40	5.39
17:15	17.65	14.84	2.81	18.80	10.83	7.97
17:20	22.72	14.33	8.39	10.37	12.20	1.83
17:25	16.79	15.62	1.17	17.65	11.90	5.75
17:30	19.85	13.94	5.91	8.64	10.31	1.67
MAE			4.56			5.12

Table A-4 Traffic Data of 76th Street (Unit: %)

	WB			EB		
Time	Estimated Occupancy	Loop Detector Occupancy	Error	Estimated Occupancy	Loop Detector Occupancy	Error
7:30	8.82	8.19	0.63	10.45	12.66	2.21
7:35	8.78	7.19	1.59	8.03	11.34	3.31
7:40	9.27	7.01	2.26	7.00	10.95	3.95
7:45	9.23	7.22	2.01	5.61	11.33	5.72
7:50	7.38	6.97	0.41	7.42	9.63	2.21
7:55	8.04	7.05	0.99	6.67	10.81	4.14
8:00	9.15	7.36	1.79	11.06	9.42	1.64
8:05	10.00	7.38	2.62	10.45	10.38	0.07
8:10	8.93	7.43	1.50	8.23	9.82	1.59
8:15	7.09	7.18	0.09	9.05	11.88	2.83
8:20	11.10	7.43	3.67	7.27	11.22	3.95
8:25	8.56	7.07	1.49	8.06	12.26	4.20
8:30	10.05	8.08	1.97	7.58	12.62	5.04
8:35	9.33	7.53	1.80	7.38	11.34	3.96
8:40	7.82	8.50	0.68	6.11	11.60	5.49
8:45	9.50	6.38	3.12	5.60	10.38	4.78
8:50	7.82	7.53	0.29	4.75	9.82	5.07
8:55	5.31	7.27	1.96	7.08	9.50	2.42
9:00	5.22	6.78	1.56	5.34	8.23	2.89
9:05	5.40	6.62	1.22	11.30	7.94	3.36
9:10	3.56	5.70	2.14	8.24	9.74	1.50
9:15	8.02	5.58	2.44	7.45	8.95	1.50
9:20	7.45	5.90	1.55	5.61	7.53	1.92
9:25	8.10	5.06	3.04	3.94	6.55	2.61
9:30	8.25	5.60	2.65	5.22	7.45	2.23
9:35	3.45	4.01	0.56	8.00	8.62	0.62
9:40	4.56	6.85	2.29	11.26	6.61	4.65
9:45	10.56	6.52	4.04	9.09	6.20	2.89
9:50	9.15	5.80	3.35	7.42	8.37	0.95

9:55	7.28	5.37	1.91	6.67	7.61	0.94
10:00	6.89	4.10	2.79	11.06	10.89	0.17
10:05	8.10	4.62	3.48	8.48	6.71	1.77
10:10	8.42	6.54	1.88	7.42	2.08	5.34
10:15	7.80	5.23	2.57	7.33	5.80	1.53
10:20	7.72	6.35	1.37	12.30	8.67	3.63
10:25	6.37	8.65	2.28	11.37	6.27	5.10
10:30	8.39	6.67	1.72	12.08	7.58	4.50
10:35	11.30	8.51	2.79	10.45	8.70	1.75
10:40	13.67	8.70	4.97	9.03	7.48	1.55
10:45	9.74	7.57	2.17	7.05	8.28	1.23
10:50	9.15	6.09	3.06	6.70	9.60	2.90
10:55	8.82	7.07	1.75	4.70	8.07	3.37
11:00	12.20	6.67	5.53	11.91	7.31	4.60
11:05	10.75	7.98	2.77	7.50	8.90	1.40
11:10	7.42	9.18	1.76	11.50	9.19	2.31
11:15	9.51	8.57	0.94	4.85	7.59	2.74
11:20	8.76	5.02	3.74	10.15	7.18	2.97
11:25	7.60	4.34	3.26	12.85	7.37	5.48
11:30	5.03	1.40	3.63	8.24	6.59	1.65
11:35	9.69	6.07	3.62	5.15	9.22	4.07
11:40	8.65	6.87	1.78	15.39	8.69	6.70
11:45	6.07	7.32	1.25	11.67	9.73	1.94
11:50	9.12	8.07	1.05	14.05	9.20	4.85
11:55	8.95	7.14	1.81	12.45	8.62	3.83
12:00	9.82	6.87	2.95	9.72	8.29	1.43
12:05	8.14	5.46	2.68	11.98	10.50	1.48
12:10	7.06	5.30	1.76	11.04	9.30	1.74
12:15	8.22	6.26	1.96	7.15	10.36	3.21
12:20	7.56	5.39	2.17	8.56	10.11	1.55
12:25	7.89	5.52	2.37	8.04	11.08	3.04
12:30	5.05	3.68	1.37	6.15	7.16	1.01
12:35	2.56	4.57	2.01	9.82	8.70	1.12
12:40	7.89	5.90	1.99	5.89	7.86	1.97
12:45	8.67	6.25	2.42	6.84	7.98	1.14
12:50	7.96	5.28	2.68	9.79	8.43	1.36
12:55	7.87	5.91	1.96	8.15	7.11	1.04
13:00	9.05	7.20	1.85	10.05	8.20	1.85
13:05	8.80	5.97	2.83	6.68	8.53	1.85
13:10	9.25	6.53	2.72	6.21	7.48	1.27
13:15	7.89	5.42	2.47	5.35	8.34	2.99
13:20	11.15	6.21	4.94	5.85	7.77	1.92
13:25	8.21	6.36	1.85	6.48	7.82	1.34

13:30	7.50	6.23	1.27	11.01	8.41	2.60
13:35	9.22	6.56	2.66	10.67	8.98	1.69
13:40	8.96	6.73	2.23	7.04	9.19	2.15
13:45	8.67	5.90	2.77	8.95	8.84	0.11
13:50	8.29	6.37	1.92	7.08	8.82	1.74
13:55	9.25	6.72	2.53	10.50	8.15	2.35
14:00	7.94	5.39	2.55	11.34	9.50	1.84
14:05	8.10	5.98	2.12	8.00	8.68	0.68
14:10	9.07	6.47	2.60	7.33	9.18	1.85
14:15	7.33	5.94	1.39	7.12	9.35	2.23
14:20	8.56	7.17	1.39	7.27	8.50	1.23
14:25	7.53	6.41	1.12	8.24	9.10	0.86
14:30	5.35	7.21	1.86	9.35	7.07	2.28
14:35	8.90	7.29	1.61	7.58	10.20	2.62
14:40	11.89	8.24	3.65	6.50	9.83	3.33
14:45	13.20	7.98	5.22	7.56	9.13	1.57
14:50	10.21	7.68	2.53	5.24	8.65	3.41
14:55	5.45	6.12	0.67	4.39	9.16	4.77
15:00	6.50	7.23	0.73	5.27	9.20	3.93
15:05	8.79	8.63	0.16	6.97	9.11	2.14
15:10	8.27	7.50	0.77	5.80	8.05	2.25
15:15	6.08	8.25	2.17	6.21	9.15	2.94
15:20	8.00	9.73	1.73	7.94	9.64	1.70
15:25	6.67	8.53	1.86	12.37	10.32	2.05
15:30	5.78	7.39	1.61	17.73	10.34	7.39
15:35	12.20	7.61	4.59	15.07	10.70	4.37
15:40	14.56	8.74	5.82	14.50	11.46	3.04
15:45	6.70	9.13	2.43	12.00	11.49	0.51
15:50	12.00	8.82	3.18	13.00	11.18	1.82
15:55	9.35	8.37	0.98	8.00	10.42	2.42
16:00	7.04	8.78	1.74	6.20	8.97	2.77
16:05	9.12	7.33	1.79	12.00	10.66	1.34
16:10	8.05	9.27	1.22	11.67	10.87	0.80
16:15	6.56	8.68	2.12	10.59	9.33	1.26
16:20	7.82	9.23	1.41	11.09	10.17	0.92
16:25	7.09	7.38	0.29	11.63	9.87	1.76
16:30	6.12	8.04	1.92	10.16	10.14	0.02
16:35	5.60	7.67	2.07	8.42	9.31	0.89
16:40	6.07	8.04	1.97	9.50	12.39	2.89
16:45	7.50	9.15	1.65	7.08	12.47	5.39
16:50	9.53	7.82	1.71	8.67	10.77	2.10
16:55	8.94	7.93	1.01	7.42	10.92	3.50
17:00	9.37	7.09	2.28	9.09	11.25	2.16

17:05	5.10	7.44	2.34	8.63	11.07	2.44
17:10	10.37	8.80	1.57	8.16	11.35	3.19
17:15	9.82	8.32	1.50	9.42	11.88	2.46
17:20	7.33	8.49	1.16	8.93	11.68	2.75
17:25	9.27	8.35	0.92	8.50	11.42	2.92
17:30	9.23	8.96	0.27	7.42	11.67	4.25
17:35	7.38	8.54	1.16	8.57	10.59	2.02
17:40	8.67	7.18	1.49	7.42	11.09	3.67
17:45	9.10	7.04	2.06	11.05	11.63	0.58
17:50	7.93	7.55	0.38	10.56	10.16	0.40
17:55	8.05	7.58	0.47	7.78	9.42	1.64
MAE			2.07			2.53

Table A-5 Traffic Data of 84th Street (Unit: %)

	WB			EB		
Time	Estimated Occupancy	Loop Detector Occupancy	Error	Estimated Occupancy	Loop Detector Occupancy	Error
7:30	7.80	13.06	5.26	10.24	13.20	2.96
7:35	9.60	10.91	1.31	13.57	11.75	1.82
7:40	5.04	9.23	4.19	12.62	11.23	1.39
7:45	4.75	8.61	3.86	14.50	11.62	2.88
7:50	6.27	10.28	4.01	17.00	9.44	7.56
7:55	3.87	8.99	5.12	15.50	11.35	4.15
8:00	5.27	8.67	3.40	6.67	9.90	3.23
8:05	6.70	7.54	0.84	9.05	10.94	1.89
8:10	4.98	9.82	4.84	12.50	11.31	1.19
8:15	6.00	9.37	3.37	12.05	12.52	0.47
8:20	8.30	9.65	1.35	7.38	13.07	5.69
8:25	10.15	9.09	1.06	10.80	12.42	1.62
8:30	9.38	9.89	0.51	17.40	13.79	3.61
8:35	8.05	10.07	2.02	12.38	12.75	0.37
8:40	8.17	11.19	3.02	6.43	11.90	5.47
8:45	7.80	10.58	2.78	8.76	13.35	4.59
8:50	6.14	8.69	2.55	5.50	9.39	3.89
8:55	6.50	8.47	1.97	10.07	10.84	0.77
9:00	10.62	7.54	3.08	12.14	11.31	0.83
9:05	6.36	7.92	1.56	7.40	8.60	1.20
9:10	6.43	7.38	0.95	6.50	8.70	2.20
9:15	7.01	10.47	3.46	11.86	9.96	1.90
9:20	6.10	6.36	0.26	13.10	9.97	3.13

9:25	7.07	6.05	1.02	7.14	10.16	3.02
9:30	5.47	7.14	1.67	7.62	11.19	3.57
9:35	7.06	7.85	0.79	10.95	8.11	2.84
9:40	9.33	6.98	2.35	8.33	7.81	0.52
9:45	10.97	8.50	2.47	7.76	10.77	3.01
9:50	4.13	6.72	2.59	12.10	10.05	2.05
9:55	5.10	7.18	2.08	13.05	7.57	5.48
10:00	3.53	8.15	4.62	14.27	8.28	5.99
10:05	3.71	8.02	4.31	6.53	7.31	0.78
10:10	7.43	8.78	1.35	6.71	9.05	2.34
10:15	10.86	8.44	2.42	6.06	9.63	3.57
10:20	12.00	6.83	5.17	12.85	17.50	4.65
10:25	14.27	7.30	6.97	7.15	6.92	0.23
10:30	6.53	5.11	1.42	7.52	9.63	2.11
10:35	6.33	6.42	0.09	10.95	13.13	2.18
10:40	13.87	13.05	0.82	8.87	9.53	0.66
10:45	13.47	11.83	1.64	10.60	8.69	1.91
10:50	12.67	7.87	4.80	8.93	8.28	0.65
10:55	6.93	7.52	0.59	5.95	7.57	1.62
11:00	5.71	6.72	1.01	6.19	5.56	0.63
11:05	3.86	7.38	3.52	7.86	9.45	1.59
11:10	8.16	7.08	1.08	7.53	11.70	4.17
11:15	7.74	7.52	0.22	11.80	10.10	1.70
11:20	8.53	7.36	1.17	6.67	8.29	1.62
11:25	10.80	8.64	2.16	9.76	7.98	1.78
11:30	6.93	9.18	2.25	12.06	8.46	3.60
11:35	6.13	5.54	0.59	17.38	12.45	4.93
11:40	7.67	7.60	0.07	9.80	11.42	1.62
11:45	12.07	9.09	2.98	13.57	10.15	3.42
11:50	5.80	8.25	2.45	9.50	8.59	0.91
11:55	3.08	5.26	2.18	9.65	7.80	1.85
12:00	4.43	5.64	1.21	10.87	8.67	2.20
12:05	6.19	6.31	0.12	13.30	9.06	4.24
12:10	7.87	5.35	2.52	6.43	9.53	3.10
12:15	4.76	6.50	1.74	4.76	8.75	3.99
12:20	10.27	7.82	2.45	6.19	8.49	2.30
12:25	10.13	7.59	2.54	6.27	7.44	1.17
12:30	5.53	6.88	1.35	7.87	9.18	1.31
12:35	6.67	7.30	0.63	6.12	9.07	2.95
12:40	7.50	8.07	0.57	4.67	8.55	3.88
12:45	8.67	7.73	0.94	8.07	10.59	2.52
12:50	6.97	7.66	0.69	11.09	10.18	0.91
12:55	12.06	10.90	1.16	14.52	10.08	4.44

13:00	6.80	8.90	2.10	9.70	7.48	2.22
13:05	5.71	7.99	2.28	6.66	9.26	2.60
13:10	6.67	8.78	2.11	9.05	8.72	0.33
13:15	10.80	7.23	3.57	12.80	12.13	0.67
13:20	11.73	7.69	4.04	5.71	8.62	2.91
13:25	5.71	7.87	2.16	6.65	8.68	2.03
13:30	6.67	7.78	1.11	5.73	8.66	2.93
13:35	5.24	7.93	2.69	9.05	10.21	1.16
13:40	7.47	8.78	1.31	14.29	9.98	4.31
13:45	7.87	7.31	0.56	8.13	9.26	1.13
13:50	9.60	8.18	1.42	8.87	10.47	1.60
13:55	10.80	7.63	3.17	10.10	8.63	1.47
14:00	9.38	7.48	1.90	12.35	10.61	1.74
14:05	8.75	7.15	1.60	12.50	9.54	2.96
14:10	10.67	8.27	2.40	13.53	11.42	2.11
14:15	9.20	8.60	0.60	11.67	9.40	2.27
14:20	5.74	8.42	2.68	13.00	9.27	3.73
14:25	8.67	7.66	1.01	8.56	10.37	1.81
14:30	11.00	9.02	1.98	10.64	11.29	0.65
14:35	8.53	9.27	0.74	15.53	10.60	4.93
14:40	9.27	11.07	1.80	7.62	10.11	2.49
14:45	12.07	10.44	1.63	8.67	10.13	1.46
14:50	14.13	10.48	3.65	7.60	9.40	1.80
14:55	11.90	8.08	3.82	8.20	10.40	2.20
15:00	9.05	10.37	1.32	7.86	9.40	1.54
15:05	7.98	10.94	2.96	14.03	10.31	3.72
15:10	12.29	8.97	3.32	11.12	8.80	2.32
15:15	13.32	11.13	2.19	12.00	9.69	2.31
15:20	9.39	11.65	2.26	9.90	9.97	0.07
15:25	10.53	11.23	0.70	7.00	11.49	4.49
15:30	11.07	10.17	0.90	13.00	10.75	2.25
15:35	7.29	9.68	2.39	9.33	11.61	2.28
15:40	14.53	11.07	3.46	10.53	12.93	2.40
15:45	8.52	12.19	3.67	11.07	12.71	1.64
15:50	9.12	12.24	3.12	8.68	11.41	2.73
15:55	10.93	10.54	0.39	13.00	11.50	1.50
16:00	15.47	12.72	2.75	14.53	9.98	4.55
16:05	9.20	10.66	1.46	17.40	11.90	5.50
16:10	8.67	10.74	2.07	6.68	11.82	5.14
16:15	10.27	11.72	1.45	9.67	11.89	2.22
16:20	13.01	11.34	1.67	8.51	10.80	2.29
16:25	11.90	10.68	1.22	9.20	10.69	1.49
16:30	9.41	10.67	1.26	14.93	11.29	3.64

16:35	9.60	9.51	0.09	8.87	10.99	2.12
16:40	15.05	11.66	3.39	16.13	13.52	2.61
16:45	9.58	11.71	2.13	5.65	12.12	6.47
16:50	7.90	10.70	2.80	7.20	10.96	3.76
16:55	9.82	11.19	1.37	8.10	11.84	3.74
17:00	7.60	8.64	1.04	9.62	12.93	3.31
17:05	10.93	9.99	0.94	7.60	12.28	4.68
17:10	12.90	11.67	1.23	8.93	12.05	3.12
17:15	15.29	11.80	3.49	8.67	13.41	4.74
17:20	10.09	10.96	0.87	16.40	13.95	2.45
17:25	11.52	11.20	0.32	9.60	13.41	3.81
17:30	10.12	11.72	1.60	10.89	12.87	1.98
17:35	9.96	11.34	1.38	9.83	11.89	2.06
17:40	11.84	9.89	1.95	7.87	12.84	4.97
17:45	10.93	9.68	1.25	9.30	12.79	3.49
17:50	9.60	9.49	0.11	8.17	10.68	2.51
17:55	8.27	10.71	2.44	7.85	9.76	1.91
18:00	7.60	9.31	1.71	7.47	11.81	4.34
MAE			2.05			2.65

Table A-6 Traffic Data of 92nd Street (Unit: %)

	WB			EB		
Time	Estimated Occupancy	Loop Detector Occupancy	Error	Estimated Occupancy	Loop Detector Occupancy	Error
7:30	7.03	12.16	5.13	7.50	12.03	4.53
7:35	6.46	10.92	4.46	12.40	10.38	2.02
7:40	7.40	13.90	6.50	8.05	10.53	2.48
7:45	9.27	6.42	2.85	10.31	10.84	0.53
7:50	8.85	7.09	1.76	7.02	9.24	2.22
7:55	5.75	6.70	0.95	5.37	10.53	5.16
8:00	6.51	7.43	0.92	6.32	10.15	3.83
8:05	4.60	5.57	0.97	5.29	9.39	4.10
8:10	7.30	7.61	0.31	7.30	10.54	3.24
8:15	11.75	7.92	3.83	4.38	11.09	6.71
8:20	10.63	6.37	4.26	3.44	11.91	8.47
8:25	15.40	7.03	8.37	3.13	11.88	8.75
8:30	9.05	5.50	3.55	5.06	11.94	6.88
8:35	12.22	7.65	4.57	4.19	11.21	7.02
8:40	9.21	7.39	1.82	5.12	10.38	5.26
8:45	12.63	6.87	5.76	5.31	10.73	5.42

8:50	9.30	7.53	1.77	7.02	9.15	2.13
8:55	12.22	5.70	6.52	6.46	8.59	2.13
9:00	4.60	7.61	3.01	7.40	7.93	0.53
9:05	7.30	5.92	1.38	9.27	8.19	1.08
9:10	11.75	12.03	0.28	8.85	7.93	1.02
9:15	9.21	9.87	0.66	5.73	9.82	4.09
9:20	10.63	2.89	7.74	3.02	8.02	5.00
9:25	9.54	7.25	2.29	7.29	7.18	0.89
9:30	9.07	4.93	4.14	6.05	6.91	0.86
9:35	10.93	3.93	7.00	7.50	7.60	1.10
9:40	3.20	6.04	2.84	8.33	6.49	1.84
9:45	5.00	12.89	7.89	13.02	8.14	4.88
9:50	6.90	13.27	6.37	12.19	5.46	6.73
9:55	6.29	6.50	0.21	7.29	6.56	0.73
10:00	3.73	17.17	13.44	10.52	5.29	5.23
10:05	3.09	6.13	3.04	2.60	8.38	5.78
10:10	11.25	7.69	3.56	11.25	8.53	2.72
10:15	3.47	5.47	2.00	7.92	5.41	2.51
10:20	4.27	1.33	2.94	2.81	12.83	10.02
10:25	5.01	11.47	6.46	5.10	7.63	2.53
10:30	6.42	12.34	5.92	7.60	8.07	2.44
10:35	7.00	5.52	1.48	7.56	13.29	5.73
10:40	6.27	8.93	2.66	5.63	7.71	2.08
10:45	5.21	7.80	2.59	5.31	7.35	2.04
10:50	8.27	6.03	2.24	5.15	6.87	1.72
10:55	6.42	7.52	1.10	7.20	11.60	4.40
11:00	4.67	7.34	2.67	5.63	13.64	8.01
11:05	8.06	7.70	0.36	7.96	10.73	2.77
11:10	6.83	6.71	0.12	4.48	9.65	5.17
11:15	8.67	6.36	2.31	5.73	8.90	3.17
11:20	9.07	5.27	3.80	5.08	7.21	2.13
11:25	4.67	6.50	1.83	5.94	6.47	1.87
11:30	4.02	6.12	2.10	6.81	5.70	1.11
11:35	3.73	11.39	7.66	13.02	8.22	4.80
11:40	7.06	9.35	2.29	6.67	8.60	1.93
11:45	5.10	6.74	1.64	5.05	8.79	3.74
11:50	5.65	13.40	7.75	6.88	8.30	2.02
11:55	6.46	17.78	11.32	19.35	7.13	12.22
12:00	9.27	12.57	3.30	8.06	8.65	0.59
12:05	8.85	10.60	1.75	10.31	9.02	1.29
12:10	7.40	5.73	1.67	7.13	9.57	2.44
12:15	8.50	6.57	1.93	5.27	10.70	5.43
12:20	14.58	5.82	8.76	6.09	12.52	6.43

12:25	8.85	5.30	3.55	8.03	13.01	4.98
12:30	12.08	6.50	5.58	7.09	7.14	1.05
12:35	8.85	7.36	1.49	5.10	10.31	5.21
12:40	6.51	7.61	1.10	8.02	11.72	3.70
12:45	6.04	9.80	3.76	5.29	10.40	5.11
12:50	4.68	10.64	5.96	7.04	8.09	1.05
12:55	7.30	11.64	4.34	11.06	8.30	2.76
13:00	3.04	6.75	3.71	12.73	9.51	3.22
13:05	9.28	6.67	2.61	5.40	8.74	3.34
13:10	3.77	11.25	7.48	5.05	9.06	4.01
13:15	7.97	5.51	2.46	6.07	8.95	2.88
13:20	7.12	6.12	1.00	8.41	8.58	1.17
13:25	3.91	8.93	5.02	7.62	8.52	1.90
13:30	7.90	7.67	0.23	3.65	8.60	4.95
13:35	12.04	6.17	5.87	6.08	9.97	3.89
13:40	5.64	7.80	2.16	7.30	9.79	2.49
13:45	5.87	5.69	0.18	8.73	9.61	1.88
13:50	9.28	5.85	3.43	5.87	9.41	3.54
13:55	7.97	11.56	3.59	9.37	9.46	0.09
14:00	5.94	7.49	1.55	6.03	10.40	4.37
14:05	10.03	7.57	2.46	6.35	8.64	2.29
14:10	2.83	6.93	4.10	2.61	10.87	8.26
14:15	3.30	7.35	4.05	14.76	10.37	4.39
14:20	12.17	11.40	0.77	11.12	9.44	1.68
14:25	4.93	6.19	1.26	5.87	9.92	4.05
14:30	8.84	6.87	1.97	4.70	7.90	3.20
14:35	13.30	7.71	5.59	8.89	10.18	1.29
14:40	9.06	12.22	3.16	7.78	9.43	1.65
14:45	10.43	12.73	2.30	5.08	10.39	5.31
14:50	5.80	9.37	3.57	7.14	9.02	1.88
14:55	11.74	7.43	4.31	3.33	10.07	6.74
15:00	12.03	8.29	3.74	2.86	10.38	7.52
15:05	4.06	8.61	4.55	16.51	9.73	6.78
15:10	8.26	14.11	5.85	18.52	9.43	9.09
15:15	6.09	11.13	5.04	9.37	9.84	2.53
15:20	6.51	9.82	3.31	5.40	9.91	4.51
15:25	4.51	8.82	4.31	6.51	11.72	5.21
15:30	7.30	8.49	1.19	4.68	11.51	6.83
15:35	5.60	8.33	2.73	7.36	10.51	3.15
15:40	7.10	12.91	5.81	10.35	12.69	2.34
15:45	6.64	12.77	6.13	9.21	12.64	3.43
15:50	4.63	9.90	5.27	10.36	11.14	0.78
15:55	5.40	11.45	6.05	15.60	12.54	3.06

16:00	6.38	13.01	6.63	12.20	9.38	2.82
16:05	6.22	8.24	2.02	4.10	12.48	8.38
16:10	4.93	14.58	9.65	9.08	11.57	2.49
16:15	4.28	11.60	7.32	12.06	11.85	1.21
16:20	5.07	11.03	5.96	5.12	10.93	5.81
16:25	9.05	12.95	3.90	8.05	11.20	3.15
16:30	4.76	8.21	3.45	4.76	10.97	6.21
16:35	3.97	7.35	3.38	6.51	11.58	5.07
16:40	7.08	7.78	0.70	4.50	12.99	8.49
16:45	9.74	10.66	0.92	7.32	12.25	4.93
16:50	6.51	10.58	4.07	10.75	11.13	0.88
16:55	7.30	9.14	1.84	12.63	11.48	1.15
17:00	10.75	11.90	1.15	14.20	12.25	1.95
17:05	10.63	7.48	3.15	6.51	12.19	5.68
17:10	9.25	16.72	7.47	4.60	11.89	7.29
17:15	15.40	10.80	4.60	7.02	14.50	7.48
17:20	12.22	8.69	3.53	10.50	13.40	2.90
17:25	8.85	7.72	1.13	9.21	12.84	3.63
17:30	15.34	12.82	2.52	15.40	12.67	2.73
17:35	12.04	8.37	3.67	9.05	12.37	3.32
17:40	6.51	8.01	1.50	8.85	12.63	3.78
17:45	7.32	11.54	4.22	5.73	12.07	6.34
17:50	11.77	10.28	1.49	15.06	11.09	3.97
17:55	9.20	12.21	3.01	9.06	10.11	1.05
18:00	10.63	7.04	3.59	12.32	11.20	1.12
MAE			3.62			3.79